METHODOLOGY FOR ASSESSING THE POTENTIAL IMPACT OF

URBAN DEVELOPMENT ON URBAN RUNOFF AND THE RELATIVE

EFFICIENCY OF RUNOFF CONTROL ALTERNATIVES

by

Guy Leclerc

B.A.   College Andre-Grasset de Montreal (1965)

B.Sc.A. Ecole Polytechnique de Montreal (1969)

S.M.   Massachusetts Institute of Technology (1972)

C.E.   Massachusetts Institute of Technology (1972)

Submitted in partial fulfillment of the
requirements for the degree of

DOCTOR OF PHILOSOPHY

at the

Massachusetts Institute of Technolocy

(June 1973)

VOL. I

Signature of Author . . . .
                        Department of Civil Engineering, June 1973

Certified by . . . .
                                                        Thesis Supervisor

Accepted by . . . .
              Chairman, Departmental Committee on Graduate Students

Abstract

METHODOLOGY FOR ASSESSING THE POTENTIAL IMPACT OF
URBAN DEVELOPMENT ON URBAN RUNOFF AND THE RELATIVE
EFFICIENCY OF RUNOFF CONTROL ALTERNATIVES

by

Guy Leclerc

Submitted to the Department of Civil Engineering in
June 1973, in partial fulfillment of the requirements
for the degree of Doctor of Philosophy.

This study describes a methodology developed to assess
the potential impact of urban development on urban runoff and to
measure the relative efficiency of runoff control alternatives.

The methodology utilizes runoff frequency curves, derived
at different stages of development of the urban catchment. Com-
parisons of these curves completely quantify the impact of urban
development and/or the efficiency of a control structure.

Runoff frequency curves are derived directly from the rain-
fall process. The method of solution utilizes a stochastic model
of the rainfall process and a deterministic model of the catchment.
The rainfall model describes the rainfall exterior and the rainfall
interior and preserves the Intensity-Duration-Frequency curves of
the historical rainfall sample. The catchment model developed with
the kinematic wave equations is a modular model; detailed and
simplified configurations of the prototype catchment has been
successfully developed.

Filter theory is used to estimate the parameters of the
infiltration model from observations of the rainfall and of the
runoff.

The method of solution, referred to as stochastic/deter-
ministic simulation, incorporates the stochastic rainfall model,
the deterministic catchment model, and the results of the infil-
tration estimator. Results obtained show that the solution pro-
cedure and the methodology developed are practical and are recom-
mended for urban drainage analysis.

Thesis Supervisor: John Christian Schaake, Jr.
                          Associate Professor Civil Engineering

Acknowledgements

The author wants to thank his wife Lucie for her active presence during his graduate studies. She deserves much credit for my success at M.I.T. My love goes to her and my son Eric. The author is very grateful to his parents for all they have done for him.

The author also wants to express his great appreciation and thanks for the interest, guidance, and patience of his advisor and supervisor, Prof. John C. Schaake Jr. The interest of Professors D.H. Marks and Eric VanMarcke was greatly appreciated. The timely comments of Prof. Eagleson and his analytical derivation of $T_E(Q_{max})$ were very important to the methodology presented in this work. Dr. Brendan M. Harley of Resources Analysis Inc. provided many practical comments on runoff control alternatives.

The scholarship, awarded by the Ministère des Richesses Naturelles, Gouv. de Quebec, made it financially possible for the author to attend M.I.T.

The drawings of the figures were done by my brother-in-law, Mr. Andre Brodeur. His professional contribution was greatly appreciated.

The author thanks Ms. Erika Babcock for her patience and her expert typing of this report.

Finally, the author is grateful to all those at M.I.T. who contributed the climate for successful graduate studies.

TABLE OF CONTENTS

List of Principal Symbols

The list that follows provides a brief description of the principal symbols used in the text. Symbols which have been used in a special way have not been included in this list but are defined in the text wherever they are used. In some cases a single notation has been used to represent more than one quantity; the particular definition which applies at any point in the text should be clear from the context in which it is used.

A	Area of the catchment (acres, sq. mi.)
$A(x,t)$	Cross-section of the flow (ft^2)
AVGTIM	A given critical time
D	Pipe diameter (ft)
DMAX	Maximum depth of rain during AVGTIM
E	Vector of Estimation error
$\mathbb{E}$	Error covariance matrix of $\hat{\psi}_*$
F	Known vector in the filter model
$F_X(x)$	Cumulative probability distribution
H1, H2,	Transformation matrices
I	Identity matrix
$I(t)$	A vector of rainfall intensities
L	Filter model
L_x	Length of segment x
N	Number of years in the sample

N	Noise function (Chapter 5)
$\mathbb{N}$	Covariance of the noise function
P	Precipitation intensities
Q	Runoff variable
$Q(x,t)$	Discharge (cfs)
Q_p, Q_{max}	Peak discharge
QTH	Flow threshold (cfs)
S, S_o	Slope of a segment
T	Time period
$T_E(\cdot), T_M(\cdot)$	Recurrence interval
V	Maximum runoff variable during T
$V(QTH)$	Exceedance volume (ft^3)
$WIDTH1(\cdot)$	Multiplier of the lateral inflow
$WIDTH2(\cdot)$	Multiplier of the upstream inflow
d	Total storm depth (in)
$f_X(x)$	Probability density function of X
f_o	Initial infiltration rate (in/hr)
f_c	Rate of infiltration when soil is saturated (in/hr)
$\bar{i}_o, \bar{i}_e$	Averaged rainfall intensities (in/hr)
k	Decay parameter of the infiltration model $min.^{-1}$
m	Rank of an observation
m_x	Parameter of the kinematic wave equations (for segment x)
n	Manning's roughness coefficient
$q(x,t)$	Lateral inflow to a segment

t	Time coordinate
t_r, t_{re}	Storm duration (hr)
t_x	Time of concentration of segment x
x	Space coordinate
z	Horizontal component of the slope of the banks of the channel
Σ_X	Covariance matrix of X
Θ	Vector of rainfall random variables
α_x	Parameter of the kinematic wave equations (for segment x)
β	Parameter of the distribution of point rainfall intensities (hr/in)
λ	Parameter of the distribution of the storm duration hr^{-1}
μ_X	Mean of X
ψ	Spatially averaged infiltration function
ψ_*	Parameter of ψ
$\hat{\psi}_*$	Estimate of ψ_*
$\phi(t)$	Instantaneous rates of infiltration
σ_x	Variance of x
τ	Time between storms (hr)
$\varepsilon\{\ \}$	Expectation of $\{\ \}$
$\ln(x)$	Natural logarithm of x

LIST OF TABLES

List of Figures

CHAPTER I

INTRODUCTION

Storm runoff from urban or natural catchments is a stochastic process. Each observed runoff event constitutes a sample function of this process. Because runoff is spatially distributed throughout the catchment the process is multivariate.

Storm runoff as a stochastic process occurs as the output from a deterministic physical system. This system receives input from two other multivariate stochastic processes: rainfall and the initial soil moisture condition.

Certain runoff characteristics (e.g. the peak runoff rate at a particular location) are important physical measures that aid in assessing the performance of hydrologic systems. In this study, the variable V is used to denote any such runoff characteristics. Variable V is a scalar function of a stochastic process. Each sample function (storm event) leads to an observation of V. The ensemble of sample functions that defines the stochastic process also defines the probability density function (PDF) $f_V(v)$. One of the contributions of this study is the presentation of a theoretically sound and practically useful procedure for deriving $f_V(v)$ in cases where V has not been or cannot be measured. These procedures may be used to assess the impacts of urban development and to evaluate alternative management and investment schemes to control

these impacts.

The need to recognize storm runoff as a multivariate stochastic process arises because urban drainage practice, on the basis of over-simplified hydrologic techniques, has contributed to undesirable hydrologic impacts. These techniques are over-simplified because they fail to recognize important multivariate and stochastic characteristics of storm runoff. For example, downstream impacts of upstream activities too often are not considered. Even when they are, it usually is not in terms of impacts on $f_V(v)$ but in terms of the impact of some design storm events. Another oversimplification is that design storms usually are erroneously assumed to possess certain statistical properties, such as being a T-yr event, whereas such properties may only be attributed to scalar variables such as V. Finally, there is no way at present to judge whether a control alternative(such as detention storage space) in one subcatchment could compensate for desirable impacts on $f_V(v)$ caused by urban development in another subcatchment.

1.1 Summary of the Proposed Methodology

Variable V could be any physical, chemical, biological or other measure of performance of a hydrologic system. Since storm runoff is a stochastic process, V is a random variable, having a PDF, $f_V(v)$, and a cumulative distribution function (CDF), $F_V(v)$. Variable V may be a property of individual storm events or a property of the set of events that occur in a period of time, for example,

any one year. This investigation is concerned with the estimation of $F_V(v)$ and with the estimation of the mean recurrence interval $T_E(V)$ between events that equal or exceed V.

The proposed methodology begins with a stochastic process model of rainfall and antecedent soil moisture conditions. Any appropriately simple or detailed model can be used. Next a deterministic mathematical model of the physical system is needed to transform the rainfall into runoff and to compute the variable, V.

Computationally, V may be regarded as a function of the rainfall and soil moisture stochastic processes. With sufficiently simple models, analytical techniques may be used to approximate $T_E(V)$ [Eagleson, 1972]. An example analytical solution will be presented in Chapter 7. In principle there are many possible solution procedures to derive $T_E(V)$. Some of these are considered briefly in Appendix B. In practice, the solution procedure likely to be most useful in the immediate future is stochastic simulation of the rainfall events and determinstic simulation of catchment response to these events. This procedure followed throughout most of this investigation is referred to herein as stochastic/deterministic simulation.

1.2 Literature Review

Few applications have been reported in the literature of the use of a stochastic rainfall model in conjunction with a catchment model to derive runoff frequency distributions. In one of these,

Perkins [1970] presented a procedure for computing frequency curves of flood stages in a flood plain. His method includes a rainfall model, a catchment model, and a flood plain model. In the flood plain model, the unsteady flow equations for open-channel flow in one-dimension are solved; the catchment model represents the runoff process in terms of the movement of a kinematic wave and the rainfall model follows the ideas suggested by Grace and Eagleson, [1967].

Flemming and Franz [1971] compared four methods for deriving flood frequency curves for small watersheds. The four methods are: (a) Simulation using HSP, (b) Regional flood frequency analysis, (c) Potter's method, and (d) Rational Method. In a test of eleven watersheds, the simulation approach proved superior to the other methods.

Eagleson, [1972] derived analytically the flood frequency curve of some natural catchments in Connecticut, using the kinematic wave routing model; he found that the analytic expressions for the cumulative distribution, $F_V(v)$, reproduced well the essential features of the observed curves. Leclerc and Schaake [1972] derived, by stochastic simulation, the flood frequency curve for a small hypothetical catchment using the kinematic wave routing model. They concluded that the approach is feasible and reliable, and that future work should be devoted to improve the computational efficiency of the procedure developed. A study of the relation between Eagleson's analytical solution and the simulation approach followed by Leclerc and Schaake led to a better understanding of the theoretical basis

for the derivation of flood frequency curves from rainfall [Leclerc and Schaake, forthcoming].

1.3 Description of the Chapters.

The report is divided into 8 chapters and several appendices. The first chapter is this introduction. The second chapter presents the probabilistic concepts pertinent to this proposed methodology. The third chapter discusses the physical characteristics of rainfall, reviews several rainfall models and describes the rainfall model used in this study. The fourth chapter develops a procedure for modelling urban catchments and illustrates the procedure for Gray Haven, Md. a 23 acre urban catchment. In Chapter 5 some preliminary ideas on how filter theory might be used to identify the parameters of the infiltration process are suggested. The rainfall model and routing model were used together to produce estimated runoff frequency curves for two runoff statistics for Gray Haven. These results appear in Chapter 6. Applications of runoff frequency curves to estimate the impact of urbanization on the runoff and/or to assess the effectiveness of control alternatives are presented in Chapter 7.

The conclusions and an assessment of future research needs are given in the final chapter.

CHAPTER II

THEORETICAL BASIS FOR THE DERIVATION OF RUNOFF

FREQUENCY DISTRIBUTIONS

Mathematically, the problem investigated in this study is to find the cumulative distribution function (CDF), $F_V(v)$ of the maximum value V of the runoff variable Q which occurs as a stochastic process during the period of time T. During T (e.g. one year) numerous individual events occur. During each the runoff variable Q may be observed. Variable V is the maximum value of Q during T. It also is given that Q is a function of the vector Θ (i.e. $Q = Q(\Theta)$) of rainfall and antecedent moisture variables. The mathematical relationship $Q(\Theta)$ between Θ and Q is equivalent to a mathematical model of catchment response to rainfall and soil moisture conditions. The rainfall and soil moisture variables that comprise Θ also occur as a multivariate stochastic process during T.

The following theoretical basis for estimating $F_V(v)$ applies to any runoff variable Q, to any catchment model $Q(\Theta)$ and to any set of variables which comprise Θ. The theory also applies to a wide range of stochastic processes by which Θ may occur.

Runoff variable Q may represent any of several quantities such as the peak runoff rate or the volume of storage capacity required to prevent runoff outflow in excess of a given runoff rate.

The procedure to derive $F_V(v)$ follows two separate steps. The first is to find $F_Q(q)$ and the second is to determine $F_V(v)$ from $F_Q(q)$. The CDF of $Q(\Theta)$ depends on the first-order joint density function, $f(\Theta_1, \ldots, \Theta_m)$ of the elements of Θ according to the relation [Benjamin and Cornell, 1970, pp.110-114].

$$F_Q(q) = \int \cdots \int_{R(q)} f(\Theta_1, \ldots, \Theta_m) \, d\Theta_1 \ldots d\Theta_m \qquad (2-1)$$

where $R(q)$ is the region where the vector Θ leads to values of Q that are less than or equal to q. Eagleson [1972] applied Eq. (2-1) to derive analytically an expression for $F_Q(q)$ for the special case where Q is the peak runoff rate, Θ is comprised of two rainfall variables (storm duration and average storm intensity) and $R(q)$ is determined on the basis of a kinematic wave model, $Q(\Theta)$, of catchment response to rainfall. A few possible computational methods to solve Eq. (2-1) are presented below in Appendix B.

In practice, the joint density function $f(\Theta)$ may vary from month to month. During month i let the joint density function be represented by $f_i(\Theta)$. It follows that $F_Q(q)$ must similarly vary from month to month. Let $F_{Q_i}(q)$ denote the CDF of q during month i. In the case where T is one year, the total period is comprised of 12 sub-periods. During each month, Eq. (2-1) applies to the events that occur during that month.

The CDF $F_Q(q)$ is a conditional distribution. It is conditional on a rainfall event having occurred and having produced the vector Θ for that event. Given that an event occurred, $F_Q(q)$ is the

probability that $Q(\Theta)$ will be less than q (prior to the computation of $Q(\Theta)$).

During the interval T a random number of rainfall events will occur. Each will give a value of $Q(\Theta)$. The largest of these will be V. The distribution $F_V(v)$ depends in part on the distribution of the number of events during T as well as on $F_Q(q)$.

A theoretical relationship between $F_Q(q)$ and $F_V(v)$ exists for the case where the time between events, τ, is an exponentially distributed random variable.

$$f(\tau) = \alpha e^{-\alpha \tau} \tag{2-2}$$

The probability that exactly n events will occur during T is, then, Poisson

$$p(n) = \frac{e^{-\alpha T} (\alpha T)^n}{n!} \tag{2-3}$$

The probability that the maximum value of Q is less than V, given the occurrence of n events is

$$F_{V|n}(v|n) = F_Q(q)^n \tag{2-4}$$

provided that the events occur independently. In the case where there is an important degree of serial dependence the proper relation is

$$F_{V|n}(v|n) = F_{Q_1}(q_1) \, F_{Q_2|q_1}(q_2|q_1) \ldots F_{Q_m|q_1 \ldots q_{m-1}}(q_m|q_1 \ldots q_{m-1}) \tag{2-5}$$

Eqs. (2-3) and (2-4) may be combined by the relation

$$F_V(v) = \sum_n F_{V|n}(v|n)\, p(n) \tag{2-6}$$

to give

$$F_V(v) = \exp\{-\alpha T(1-F_Q(v))\} \tag{2-7}$$

In the case where $F_Q(q)$ and $p(n)$ vary seasonally, Eq. (2-7) becomes

$$F_V(v) = \exp\{-\sum_i \alpha_i T_i (1-F_{Q_i}(v))\} \tag{2-8}$$

In cases where the mean time between storms is not exactly exponentially distributed, Eq. (2-8) may still give a good approximation. In such cases, the term $\alpha_i T_i$ is equal to the mean rate of occurrence of storm events (average number of events during T_i).

The mean recurrence interval, T_M, between annual maximum events that exceed v is

$$T_M(V) = \frac{1}{F_V(v)} \tag{2-9}$$

This, in turn, may be used to estimate the mean recurrence internal, T_E, between individual events of the partial duration series of all events above some minimum threshold value of V. The relation between $T_M(V)$ and $T_E(V)$ according to Chow [1964] is

$$T_E(V) = 1/[\ln T_M - \ln(T_M - 1)] \tag{2-10}$$

The next chapter discusses one possible model of the occurrence

-26-

of rainfall as a stochastic process. That chapter is concerned with a number of issues that implicitly influence the first order joint density function $f(\Theta)$.

Chapter 4 addresses the computation of $Q(\Theta)$. The issue is to find the computationally most efficient model of $Q(\Theta)$ that adequately represents the catchment response to Θ .

Chapter 5 is concerned with a procedure for measuring- during individual storms - the values of the infiltration parameters that are elements of Θ . By using these techniques to estimate infiltration parameters for a number of storm events it should be possible to estimate the joint density function of the elements of Θ related to the infiltration process.

Finally, in Chapter 6, the principles presented in the present chapter are applied to a real urban catchment gaged by the Hopkins Storm Drainage Research Project.

CHAPTER 3

STOCHASTIC RAINFALL MODEL

A model of rainfall as a stochastic process is needed to
derive $F_V(v)$. This model would account for the stochastic occurrence
of individual storm events and for the occurrence of rainfall given
that an event has occurred. The appropriate model would represent
only those rainfall characteristics essential to the estimation of
$F_V(v)$

3.1 Physical Occurrence of Rainfall

Rainfall occurs when moist-warm air is cooled through lifting
mechanisms; four major processes are commonly distinguished
[McKay, 1970]

Horizontal convergence where wind fields act to concentrate

the inflow of air in certain areas, thus forcing the air

to rise.

Orographic lifting when air is forced upwards by topo-

graphic barriers

Convection resulting when warm air becomes more buoyant

than the surrounding air

Weather frontal systems which separate large masses of

air having significantly different physical properties.

The first process is a localized phenomenon and the second

is a regional one, possibly significant even for small topographic barriers. The last two processes usually govern the characteristics of the rainfall in the central and eastern parts of Canada and the United States. The convective storms, generally called thunderstorms, are often short and intense whereas the frontal storms- with the exception of hurricanes (tropical storms)- are usually long and moderate, even light, events that occur on a regional scale. Many variations are undoubtedly observed in these general trends, variations which can cause serious floodings; for instance a quasi-stationary frontal system continuously fed by moist air causes long and relatively large rainfall intensities (thus large total precipitation depth) on the area where it is localized.

3.2 Rainfall Model Literature Review

The general objective of a rainfall model is the description of the rainfall process in simple terms to economically preserve the characteristics of the rainfall needed to achieve the resolution desired in the runoff hydrographs or in the runoff frequency curves.

3.2.1 Models of Point Rainfall Events

Pattison [1966] developed a Markov chain model that simulates hourly point precipitation; the wet periods (with precipitation) are modeled with a first order Markov chain and the dry periods with a sixth-order chain; Pattison's approach requires a large transition matrix (mxn) where m is the order of the Markov

chain and n the number of discrete states. The transition probabilities are derived from an observed rainfall record. Any transition that did not occur historically will not appear in the simulated rainfall record. This rainfall model accounts for both the storm interior and storm exterior and generates hourly blockshaped rainfall.

Grace and Eagleson [1967] developed a model to synthesize storm rainfall events in which storm interiors are stochastically generated at a 10 minute time step. The stochasticity of the climatological storm exterior variables is represented by their first order joint density functions. The time between storms (τ) and the storm duration t_r were fitted to a Weibull (3-parameters) probability function. The storm total depth was found to be independent of τ but not of t_r, where a linear trend was observed. Consequently a linear regression line was fitted to the depth as a function of t_r; the residuals were fitted to an integral Beta-one probability function. The procedure adopted generates τ and t_r from the respective Weibull distribution and d from the linear regression line supplemented by a generated residual. Urn models are then used to synthesize the storm interior. This model was applied at two locations (one in Nova Scotia and the other in Vermont) to synthesize convective storm events. This model is also discussed by Randkivi and Lawgun [1970].

Grayman and Eagleson [1969] simplified the Grace-Eagleson model which has 10 parameters. An exponential function was fitted to the times between storms and the storm durations, and a 2-parameter Gamma distribution, conditional on t_r was fitted to the storm depth.

The storm interior was represented by an isocele triangle, adjusted to preserve the storm total depth. This four parameter model gave adequate results in modeling the rainfall process at Boston, Ma., and at Ely, Nevada.

Leclerc and Schaake [1972] developed a model similar to the Grace and Eagleson model which (i) provides several first order probability functions to sample each variable from and (ii) allows seasonal non-homogeneity in the rainfall parameters.

3.2.2 Models of Spatially Distributed Rainfall Events.

Franz [1970] proposed a multivariate model to synthesize hourly precipitations at several locations where the rainfall variables (or their transforms) are normally distributed. He applied the model to a network of three stations, located 70 miles north of San Francisco, where orographic effects are important. The model can be used for flood analysis but is totally unfitted for water supply purposes because the serial correlation is not preserved over a period compatible with the correlation required for the latter case. This rainfall model is a special case of the general desaggregation model developed by Valencia and Schaake [1973].

Schaake et al [1972] proposed a rainfall model for the Island of Puerto Rico which uses the desaggregation model. The rainfall model was developed for water supply purposes and would require important updates to make it suitable for short-time interval rainfall synthesis. Rainfall depths are generated on an annual basis and

then distributed into seasonal, monthly, and daily rainfall depths.
The annual series can be simulated by any method, (i.e. Markov model,
fractional Gaussian noise, broken line, etc.) method that can pre-
serve the low frequency statistical properties of the process. The
summation of the precipitation at each lower level of desaggregation
equals the precipitation at the next higher level. At the daily level,
the monthly precipitation is preserved and the expected number of
rainy days in the month is maintained.

        The preceeding models may be called Eulerian models because
they describe at fixed locations the rainfall process. Grayman and
Eagleson [1971] developed a Lagrangian rainfall model where the
rainfall processes are represented in time and space as they move
over a region. The rainfall model involves a hierarchy of several
scales of activity (synoptic, large and small mesoscale, and cells).
At the smallest scale are cells which are 2.0 mile square and can
be "active" only if the small mesoscale where it is located is active;
the latter only if the large mesoscale where it is located is active.
The activity at each level of the hierarchy is determined by an appro-
priate probability model. The storm movement is modeled by the
travel velocity and direction of the synoptic system. This model is
versatile as it allows short time intervals and a relatively fine grid
on the basin. One of its main limitations is that the model as it
now stands is computationally too costly to use for runoff frequency
studies. Another limitation is that adequate data to estimate model
parameters are not generally available.

3.3 Rainfall Model Design

The desired rainfall model would generate rainfall events which statistically resemble the kinds of events that cause significant variations in the catchment response. This means that the volumes of rainfall that occur in different parts of different storms (as generated by the model) must resemble the volumes that occur naturally.

There are two possible quantitative measures that might be used to judge this resemblance. One of these would be the intensity-duration frequency (IDF) curves. The other would be the frequency distributions of total storm depths, durations and numbers of storms per month during each month of the year. The IDF criterion is important because it gives a statistical measure of the amounts of rain that may occur during certain limited periods of time. This is an important measure both with respect to peak runoff rates and the required detention storage for runoff control. The criterion should be applied to the model to see if the generated storms give IDF curves that agree with historical sample IDF curves for certain critical durations.

It would be desirable to generate storms directly on the basis of the information contained in the IDF curves. This information is generally available from USWB publications. Unfortunately, no way has been discovered to do this. The problem is that the IDF curves are an ensemble of marginal frequency distribution, $F(I_{t_c})$, of average rainfall intensities, I_{t_c}, given the averaging time,

t_c. To generate storms directly from IDF curves it would be necessary to know the joint distribution of I_{t_c} over a range of values of t_c and then it would be necessary to transform the generated values of I_{t_c} into a function $I(t)$ of rainfall intensity as a function of time. In addition, some means would be needed to generate spatial variations in $I(t)$. This remains an area of importance for future research.

The other important criterion is that the total depths, durations and numbers of storm events per month resemble the natural process. A model patterned after the work of Grace and Eagleson [1967] would give theoretical, explicit assurance that this criterion would be met. The historical rainfall data needed to estimate the model parameters are readily available from USWB data tapes for many locations. Accordingly, the model developed permits the user to specify the PDF for: the time between storms, τ ; either the total storm depth, d, or the average storm rainfall intensity, $\bar{i}$; and, the storm duration, t_r, given the depth or average intensity. Each month requires a different PDF for each variable. The most appropriate PDF's may vary from one climatic region to another and must be determined on the basis of local rainfall data.

It is assumed that the storm interior pattern of rainfall may be generated after the storm exterior variables are generated. The notion of a storm interior could be extended to account for both spatial and temporal distribution of the rain during an event. In this study, however, stochastic spatial variations were not included.

Orographic effects which may cause important spatial variations are accounted for by a constant orographic multiplier(which may vary from month to month) applied to each storm event.

The model sequentially generates all rainfall events during the year. Information is readily available on the antecedent precipitation conditions. By correlating this information with antecedent soil moisture variables, the rainfall model offers one way to generate antecedent soil moisture conditions as well as rainfall intensities. Storm interiors are generated only for the largest generated events to reduce the computational cost. It is important to have storm interiors only for those storms that will be processed through the catchment model to derive $F_V(v)$. The problems of selecting these storms and of deciding how many years of simulation are required are discussed in Chapter 6.

The greatest limitation of the proposed rainfall model is that the historical IDF curves do not govern any of the model parameters. Instead, the IDF curves of the generated storm events are implicit in the model and in the input data to the model. Therefore, it may require careful evaluation of the input data to achieve generated output data that meet the IDF criterion.

3.4 Storm Exterior Distributions for Baltimore, Md.

Hourly rainfall data for the Custom House Gage, Baltimore, Md., for the period May 1948 to June 1970 were analyzed. Example distributions of the parameters τ , d and t_r appear in Figure 3-1.
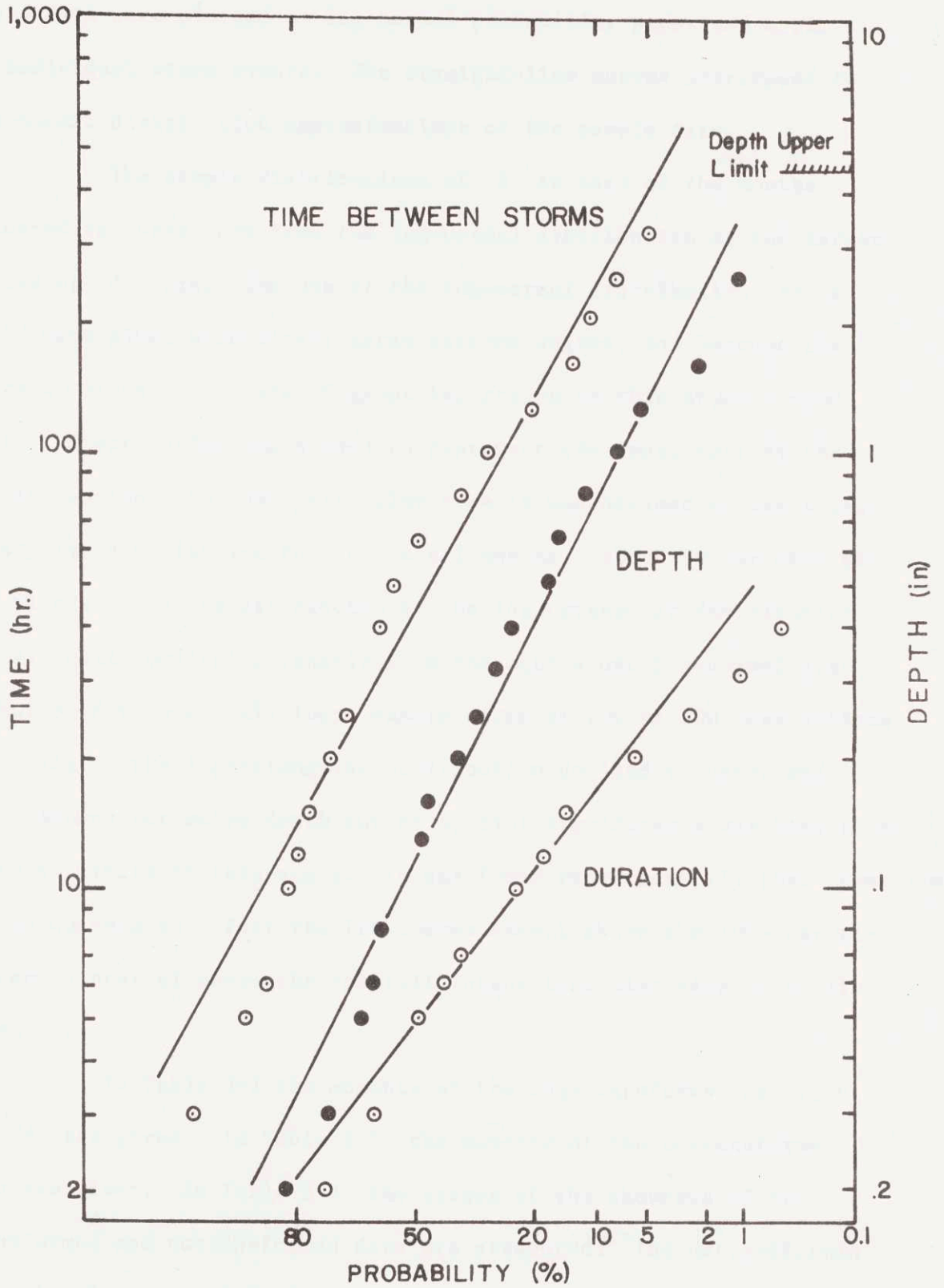
Figure 3-1: Example Distribution of the parameters τ, d and t_r

These data were plotted on log-normal probability paper and apply
to individual storm events. The straight-line curves correspond to
log-normal distribution approximations of the sample data.

The sample distributions of d in each of the months
appeared to curve away from the log-normal distribution at the larger
values of d. Since the use of the log-normal distribution for d
would have given excessively large extreme values, and because the
extreme values of d are of great importance to this study some
sort of distribution was needed to represent the upper tail of the
d-distribution. In this particular case it was decided to use a log-
triangular distribution for d in all months. About 90 per cent of
the values of d as distributed by the log-triangular distribution
are virtually undistinguishable from the equivalent log-normal dis-
tribution for moderately large sample sizes of 100 to 200 observations.
The tails of the log-triangular distribution do lead to upper and
lower bounds for storm depth but no special significance has been given
to these limits in this study. It was found experimentally that these lim-
its do not seem to affect the IDF curves except above the 100-year re-
currence interval where the rainfall intensities also seem to be li-
mited.

In Table 3-1 the moments of the log-transforms of τ, t_r
and d are given. In Table 3-2 the moments of the untransformed
data are given. In Table 3-3 the ranges of the skewness of the
transformed and untransformed data are presented. The untransformed
data clearly are positively skewed. Note that the ratio of $\bar{d}/\bar{t}_r$ is
much greater in the summer months than in winter. Most of the intense

Table 3-1

Moments of Storm Exterior Parameter Distributions for Baltimore, Md.
(Log Transformation)

Means

Month	Time Between Storms (log (hrs))	Storm Duration (log(hrs))	Storm Depth (log(in))	Number of Storms Month
Jan.	3.76	1.58	-2.17	8.32
Feb.	3.63	1.67	-1.92	7.95
Mar.	3.26	1.55	-1.89	9.38
Apr.	3.31	1.26	-2.15	11.32
May	3.53	1.19	-2.09	10.39
June	3.49	1.05	-1.89	9.09
July	3.73	.86	-1.96	8.55
Aug.	3.51	1.04	-1.80	9.14
Sep.	3.55	1.15	-2.05	7.45
Oct.	3.73	1.39	-1.98	6.19
Nov.	3.88	1.55	-1.90	7.05
Dec.	3.70	1.87	-1.58	6.86

(Continued)

(Continuation Table 3-1)

Standard Deviations

Month	Time Between Storms (log(hrs))	Storm Duration (log(hrs))	Storm Depth (log(in))	Correlation Between Log (Duration) log(Depth)
Jan.	1.368	.985	1.496	.89
Feb.	1.382	.883	1.471	.88
Mar.	1.381	.997	1.553	.84
Apr.	1.411	.911	1.410	.84
May	1.295	.885	1.476	.74
June	1.407	.870	1.517	.67
July	1.267	.771	1.521	.60
Aug.	1.321	.835	1.507	.67
Sep.	1.539	.895	1.532	.76
Oct.	1.619	.885	1.564	.82
Nov.	1.438	.874	1.421	.85
Dec.	1.526	.895	1.484	.84

Table 3-2

Moments of Storm Exterior Parameter Distributions for Baltimore, Md.
(Untransformed Data)

Means

Month	Time Between Storms (hrs)	Storm Duration (hr)	Storm Depth (in)	Storm Intensity (in/hr)
Jan.	90.7	7.54	.303	.040
Feb.	76.0	7.53	.346	.046
Mar.	77.2	7.42	.394	.053
Apr.	60.0	5.56	.286	.052
May	64.6	4.99	.322	.065
Jun.	75.1	4.28	.398	.093
Jul.	80.0	3.32	.390	.118
Aug.	69.4	4.09	.439	.107
Sep.	97.4	4.95	.409	.083
Oct.	109.9	5.83	.385	.066
Nov.	111.1	6.89	.377	.055
Dec.	95.1	9.07	.455	.051

(continued)

(Continuation Table 3-2

Standard Deviations

Month	Time Between Storms (hrs)	Storm Duration (hrs)	Storm Depth (hrs)	Correlation Between Depth and Duration
Jan.	117.6	7.20	.441	.80
Feb.	80.5	6.28	.420	.76
Mar.	89.9	6.88	.550	.76
Apr.	64.8	8.16	.497	.93
May	64.3	5.39	.498	.69
June	105.3	4.37	.567	.56
July	86.1	3.29	.611	.51
Aug.	79.5	4.24	.751	.72
Sep.	135.9	6.02	.770	.62
Oct.	128.3	5.15	.602	.73
Nov.	147.5	7.05	.616	.84
Dec.	109.7	6.67	.474	.70

Table 3-3

Comparison of Skewness of Untransformed and Transformed Data

	Skewness		Coefficient	
	Untransformed		Log-Transformation	
Parameter	Minimum	Maximum	Minimum	Maximum
τ	1.34	3.80	-.50	.11
t_r	.87	7.94	-.52	.64
d	1.13	6.41	.11	-.50

summer storms are caused by thunderstorms, although a few are also caused by hurricanes.

3.5 Storm Interior Distributions for Baltimore, Md.

Temporal variations of rainfall within a storm are important to the extent they influence $F_V(v)$. A sound theoretical basis for judging this matter remains to be developed although some of the elements have been investigated. Eagleson [1968] reported that the sampling rate necessary to define all of the harmonic constituents of the instantaneous unit hydrograph contributing at least 5% of the maximum constituent is approximately equal to one third of the time of concentration. This suggests that higher frequency components in the rainfall inputs have little influence on the runoff outputs for individual storms. Since the present interest is in the variability of V over a wide range of storms, and since the variations in the storm exterior variables are likely to have the most significant influence on the variation of V over the ensemble of storms, the critical harmonic constituents of the storm interiors are likely to be the lower frequency constituents.

The simplest approach to modeling storm interiors is to assume a fixed pattern such as a triangle. More complex approaches would involve stochastic variations of the interiors. Since the main emphasis of this research was not directed toward the modeling of storm interior distributions only some preliminary investigations were made. These revealed that IDF curves were, in fact, sensitive to the

rainfall interiors. Therefore, it would be expected that $F_V(v)$ also would be sensitive to storm interior variations. Additional research is needed on this topic.

Two storm interior models were considered in this research. One of these was a symmetrical triangular distribution, the other was a stochastic rainfall interior.

To formulate a stochastic model of storm interiors, each individual event was re-scaled to have a total depth of unity and a total duration of unity. The cumulative distribution function of rainfall for any given event would be a random function as illustrated in Figure 3-2. The interior of the storm was divided into 10 intervals. The proportions of the total storm depth in each interval form the vector

$$\Phi_j = \begin{bmatrix} \Phi_{1j} \\ \vdots \\ \Phi_{10j} \end{bmatrix} \tag{3-1}$$

where the index j refers to the j-th event. Vector Φ_j is illustrated in Figure 3-3.

The elements of Φ_j are correlated random variables. It is impossible for them to be statistically independent because their sum is equal to unity by definition. The mean of these elements is the vector μ and the covariance is the matrix Σ. Let

$$\psi_j = \Phi_j - \mu \tag{3-2}$$

The mean of ψ_j is zero and the covariance is Σ. The
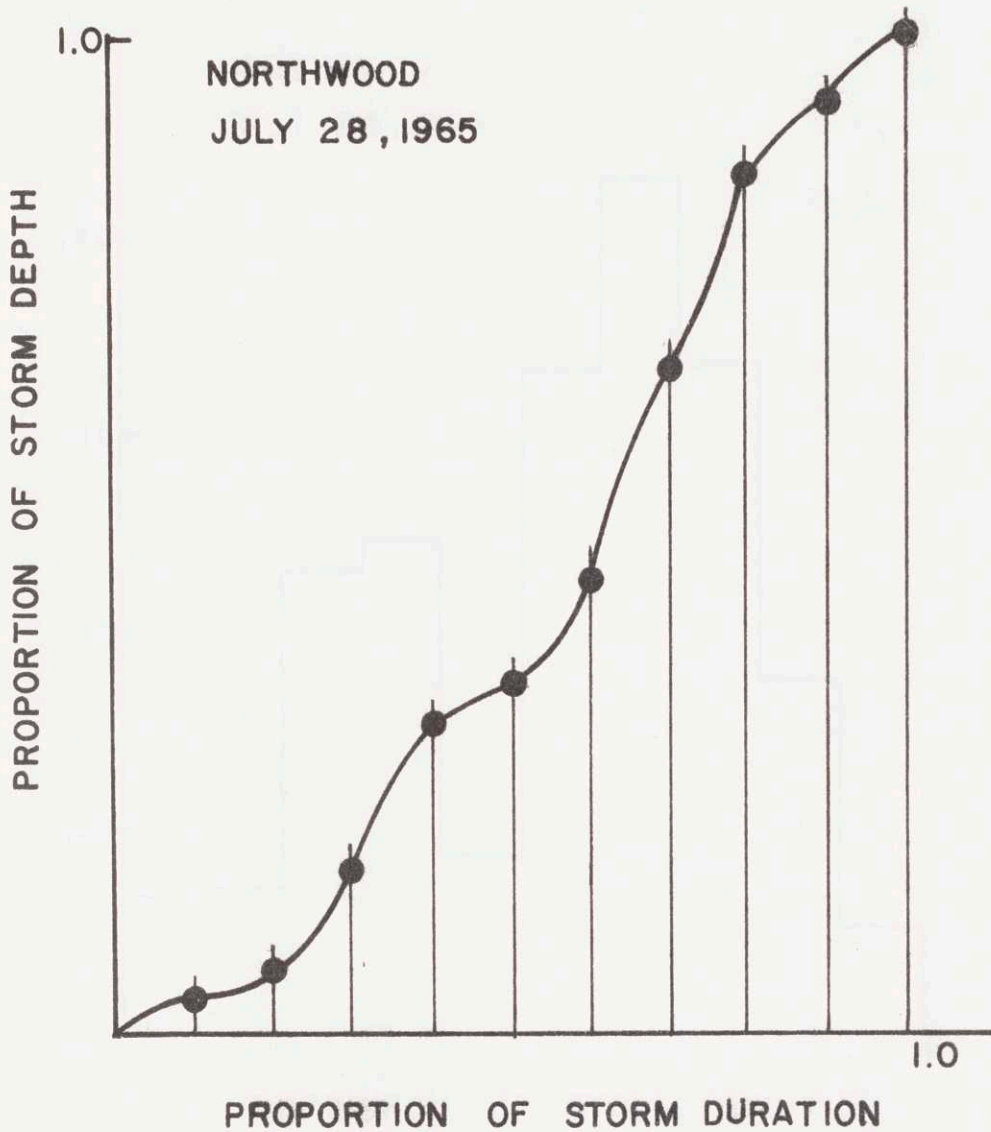
Figure 3-2: Typical Cumulative Distribution of Rainfall
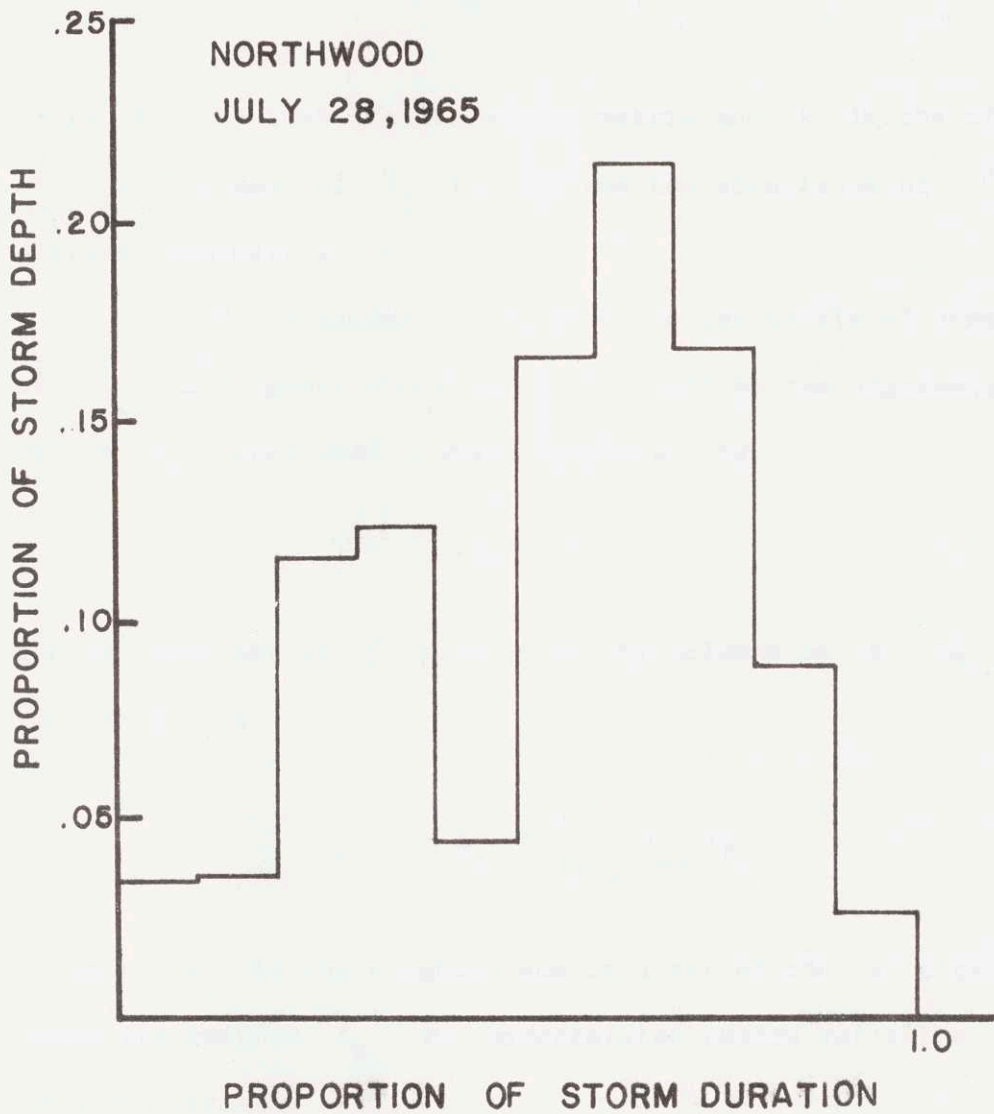
Figure 3-3: Typical Rainfall Distribution Φ_j

vector ψ_j may be expressed as a linear transformation of the vector Π_j of uncorrelated random variable

$$\psi_j = B \; \Pi_j \tag{3-3}$$

where B is a 10xk transformation matrix and k is the dimension of Π_j. The mean of Π_j is zero and the covariance of Π_j is the diagonal kxk matrix Λ^2.

If the matrix B is taken as the matrix of eigenvectors of Σ, the diagonal elements of Λ^2 will be the eigenvalues. B will be an orthonormal transformation so that

$$B^T B = I \tag{3-4}$$

The eigenvectors of Σ will be in the columns of B. Eq. 3-3 may be expanded as

$$\psi_j = \left| \sum_{\ell=1}^{k} B_{i\ell} \; \pi_{\ell j} \right| \tag{3-5}$$

to show ψ_j is the weighted sum of a set of the k eigenvectors, where the weights π_{k_j} are uncorrelated random variables with zero mean and variance λ^2_k .

The parameters in this model are μ , B, Λ and k. Values of these were estimated from a set of 25 observed storm events at the Gray Haven and Northwood catchments in Baltimore, Md. The elements of μ were found to be

$$\mu^T = [.117, \ .168, \ .140, \ .109, \ .089, \ .121, \ .097, \ .077,$$
$$.051, \ .035] \qquad\qquad (3\text{-}6)$$

The eigenvalues appear in Table 3-4 where we see that more than 90 per cent of the total variability of all of the elements of ψ is accounted for by the first 5 eigenvalues.

In the generation of storm interiors, the first step is to generate a vector η_j of k standard normal deviates then Π_j is computed as

$$\Pi_j \ = \ \Lambda\eta_j \qquad\qquad (3\text{-}7)$$

This implies that

$$\psi_j \ = \ B\Lambda\eta_j \qquad\qquad (3\text{-}8)$$

where $B\Lambda$ is a 10xk matrix. As k increases, the elements in the column of $B\Lambda$ decrease in magnitude. The first 5 columns of k for Baltimore are given in Table 3-5.

Storm interiors sampled at any arbitrary time interval, Δt, are generated by the following procedure. First d and t_r are generated for the storm. Second, a vector $\Phi_j = \mu + \psi_j$ is generated. Third, the cumulative values of Φ_j are computed. (For theoretical reasons, these values will always sum exactly to unity). Fourth, d and t_r are used to get the rainfall mass curve for the storm. Finally, the mass curve is interpolated at intervals of Δt and rainfall intensities are calculated as the ratio $\Delta d/\Delta t$.

Table 3-4

Eigenvalues of 25 Baltimore Rainfall Events

k	Eigenvalue λ^2_k	Cumulative Distribution of Variance Among Eigenvectors
1	.032533	.465
2	.012199	.639
3	.010398	.788
4	.005465	.866
5	.003886	.921
6	.002634	.959
7	.001323	.978
8	.001157	.994
9	.000387	1.000
10	.000000	1.000

Table 3-5

Matrix BΛ for 25 Baltimore Rainfall Events

k = 1	k = 2	k = 3	k = 4	k = 5
.032129	-.016716	.016886	-.050184	-.019123
.119936	.041595	-.049671	.006835	.003071
.069333	-.037178	.034548	-.010273	.020873
.008141	-.029396	.030051	.042407	.016979
-.024673	-.032993	.002564	.004940	-.023856
-.062643	-.036744	-.058366	.001862	-.006436
-.064148	.009336	-.024037	-.020385	.040319
-.057897	.061594	.038743	-.006872	.001290
-.014502	.040295	.007291	.014467	-.016087
-.005676	.000208	.001988	.017202	-.017030

3.6 Comparison of Generated and Historical IDF Curves.

An important criterion for verifying the generated rainfall data is that the IDF curves of the generated data should agree with the historical curves. In this case it is possible to make a number of comparisons.

A 200-yr. sample function of storm events was generated. Each storm was assumed to have a triangular interior distribution of rain. The IDF curves for this 200-yr sample function appear in Fig. 3-4. A second 200-yr sample function was generated to illustrate the sampling variations in these curves. The IDF curves for this second sample function appear in Fig. 3-5. There is no simple theoretical way to compare these curves. The maximum difference between any two points on these sample functions is about 10 per cent.

The largest storms in the first 200-yr sample function were selected for storm interior generation. The selection procedure was as follows:

(i) from the set of storms generated in each year, the storms that produced the largest depths during any 30 min., 1 hr, 2 hr, 3 hr, 6 hr and 12 hr, periods were selected (assuming a triangular interior) as tentative candidates. A total of 461 storms were selected from the 200 yr. sample function.

(ii) the storm exterior parameters for these 461 storms were input to the storm interior generator which ranked these storms by order of magnitude according
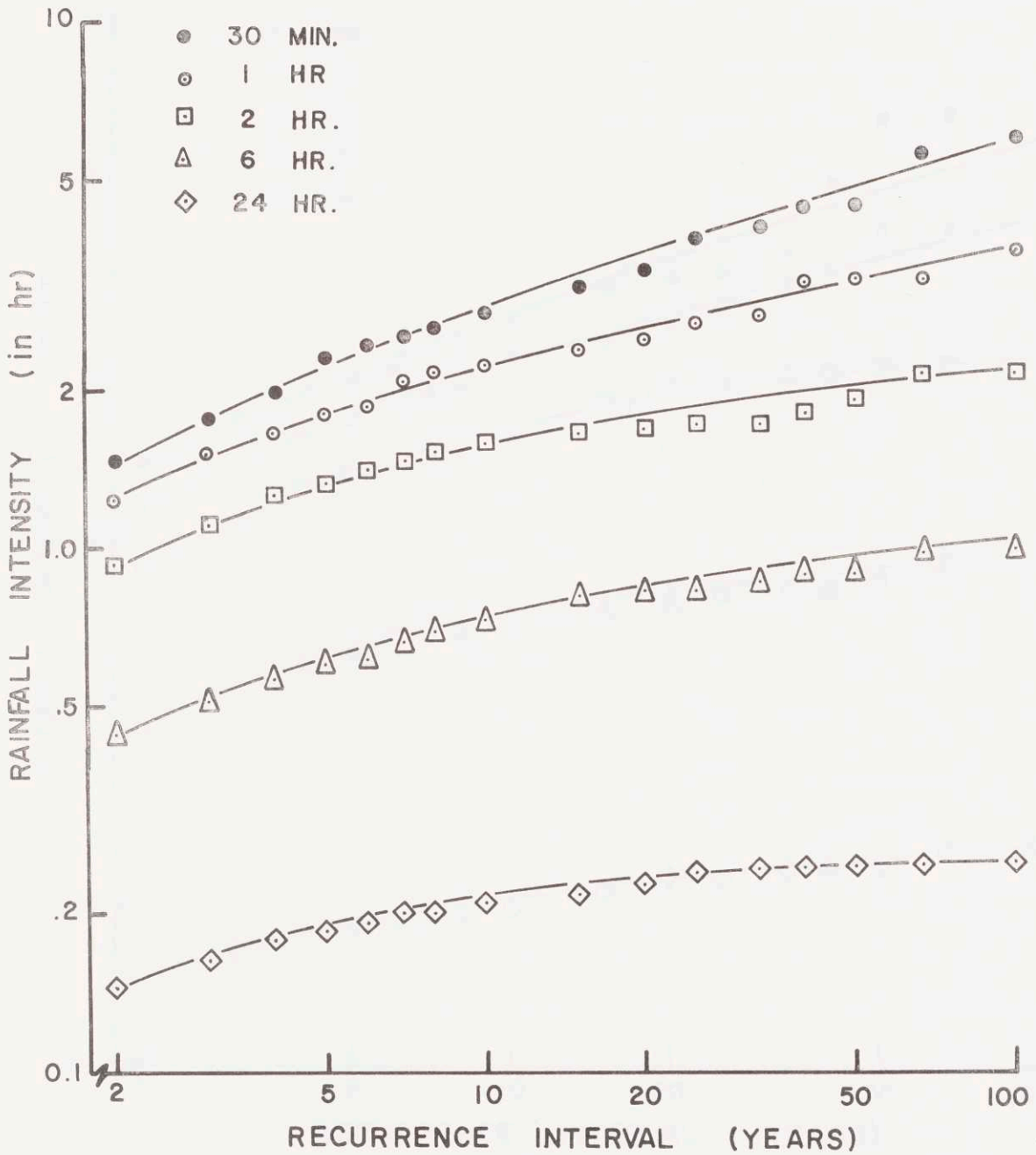
Figure 3-4: Intensity-Duration-Frequency Curves, 200 Year Generated
Sample Function (A), Triangular Interiors
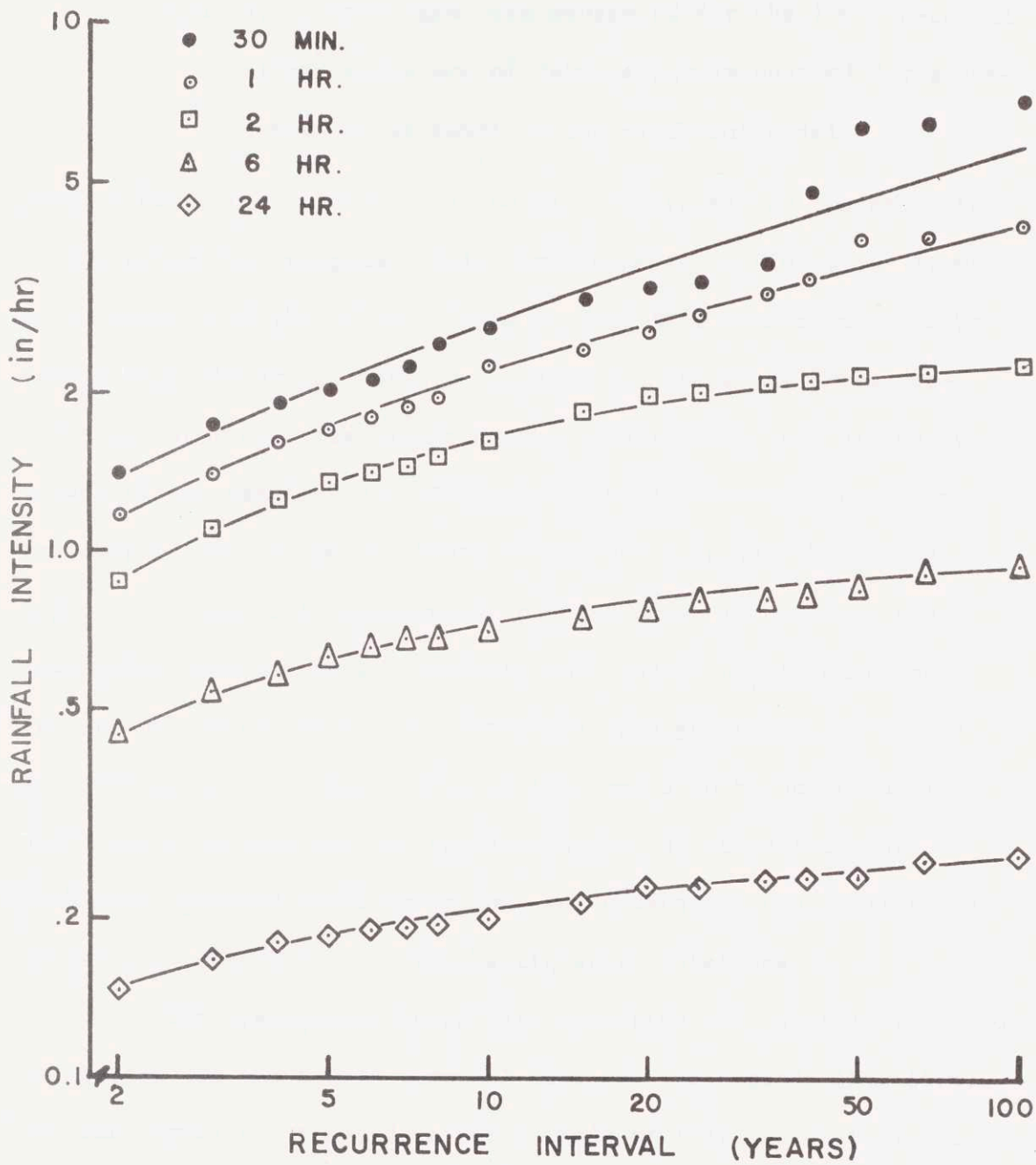
Figure 3-5: Intensity-Duration-Frequency Curves, 200 Year Generated
Sample Function (B), Triangular Interiors

to the maximum 30-min. depth, assuming a triangular interior.

(iii) storm interiors were generated for the 100 top-ranked storms and a set of data cards was punched for subsequent use as input to the catchment model.

The IDF curve for a 30-min. period was constructed by the storm interior generation program. This curve appears in Fig. 3-6. It may be compared with the 30 min. curve in Fig. 3-4. There seems to be very little difference between these curves above the 5-year recurrence interval. The differences at the 100-year end may be due to additional sampling variations introduced by the interior generation process. Below the 5-yr. recurrence interval the curves begin to separate, the generated interior curve lying below the triangular interior curve. Some of this may be due to sampling variations introduced because interiors were generated only for a selected group of storms. Some of this may also be due to basic differences between the two representations of storm interiors. Much more research needs to be done to understand the implications of using deterministic vs. stochastic storm interiors.

The historical record used to derive the rainfall generator parameters was the hourly rainfall data for the period 1948-1970. The IDF curves for these data for periods of 1 hr, 2 hr, 6 hr and 24 hr. appear in Fig. 3-7. These curves seem to agree well with the IDF curves for both sample functions of generated data. The fitted curves agree within 10% over most of their ranges. Since the
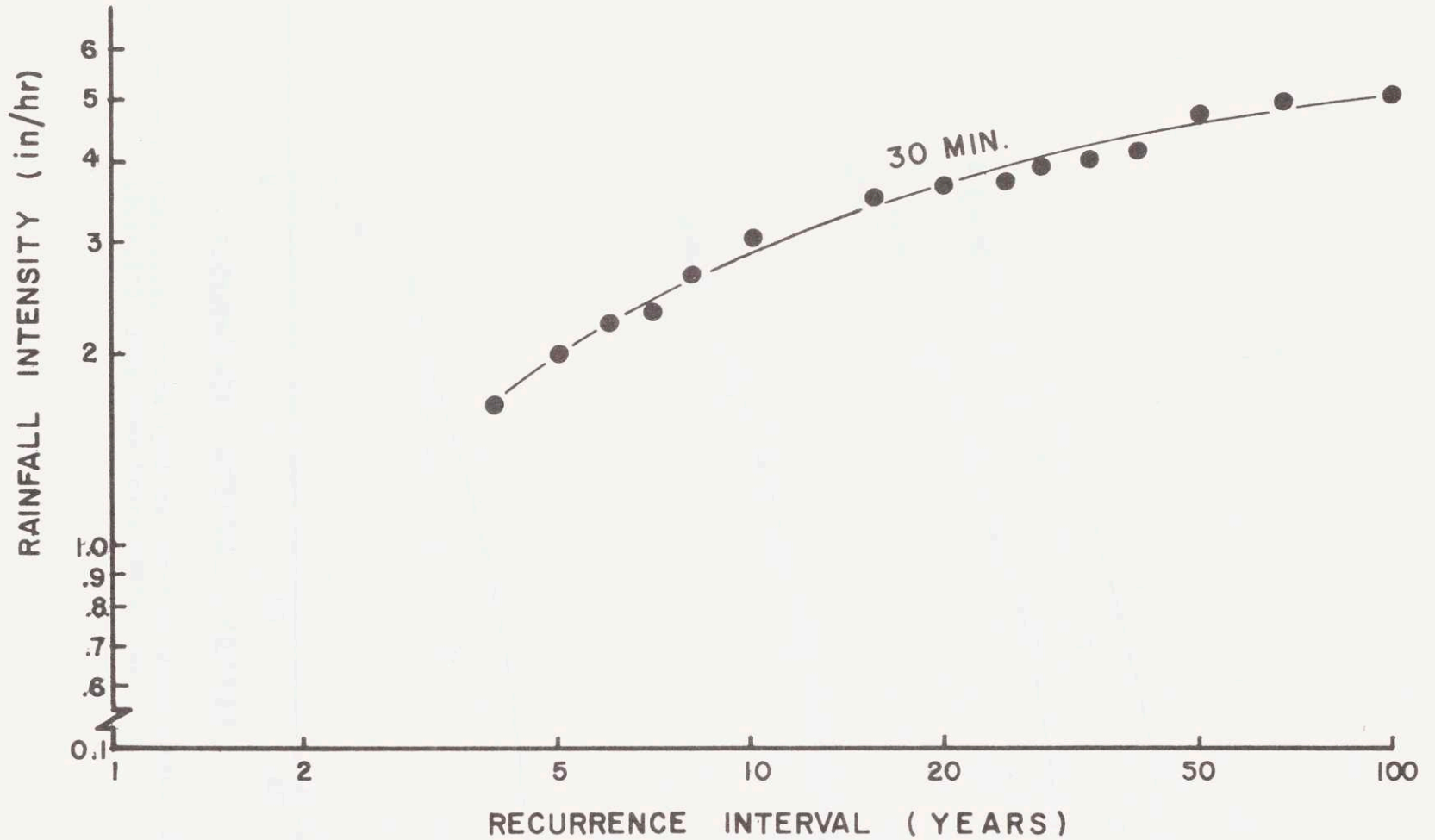
Figure 3-6: Intensity-Duration-Frequency Curves, 200 Year Generated Sample Function (A), Random Interiors
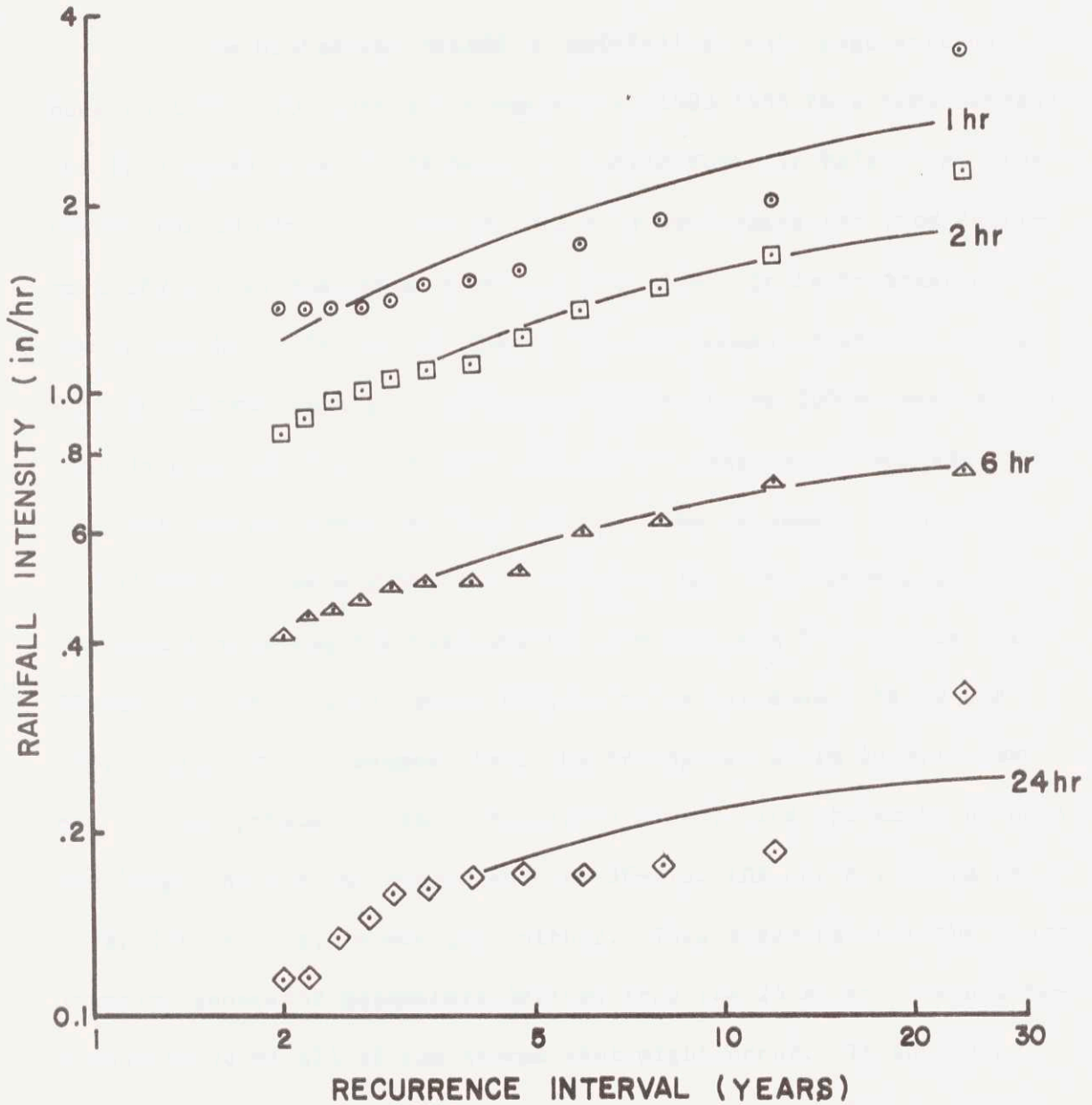
Figure 3-7: Historical Intensity-Duration-Frequency Curves, Baltimore, 1948-1970 (From USWB Hourly Data Tape)

USWB data tape did not contain data for time intervals less than one hour, there is no way to make a similar comparison with the 30 min. IDF curve for the generated interiors.

The historical record of rainfall at this gage extends back to 1903. IDF curves for the period 1903-1953 have been extracted from these data by the Dept. of Public Works in Baltimore. IDF curves for 30 min., 1 hr, 2 hr. and 6 hr were extracted from Baltimore DPW curves and these appear in Fig. 3-8. It is interesting now to see how well the IDF curves for the generated storms compare with the longer record. The agreement with first 200-yr sample function is best for the 2 hr curve and within reasonable sampling fluctuations for the 1-hr, and 6 hr curves. The agreement with the second 200-yr sample function is best for the 1 hr curve and within reasonable sampling fluctuations for the 2-hr and 6-hr curves. The 30-min. curves of both sample functions lie far enough below the historical curve to suggest that the triangular storm interior may not be appropriate for short averaging times. The agreement between the longer historical record and the 30-min. IDF curve for the generated interiors, is not good either. This suggests that the storm interior generator parameters derived from the 25 storms are not representative of all of the storms that might occur. It should be possible to use the hourly rainfall data to estimate better parameters for the storm interior generator, but this remains a topic for further research.
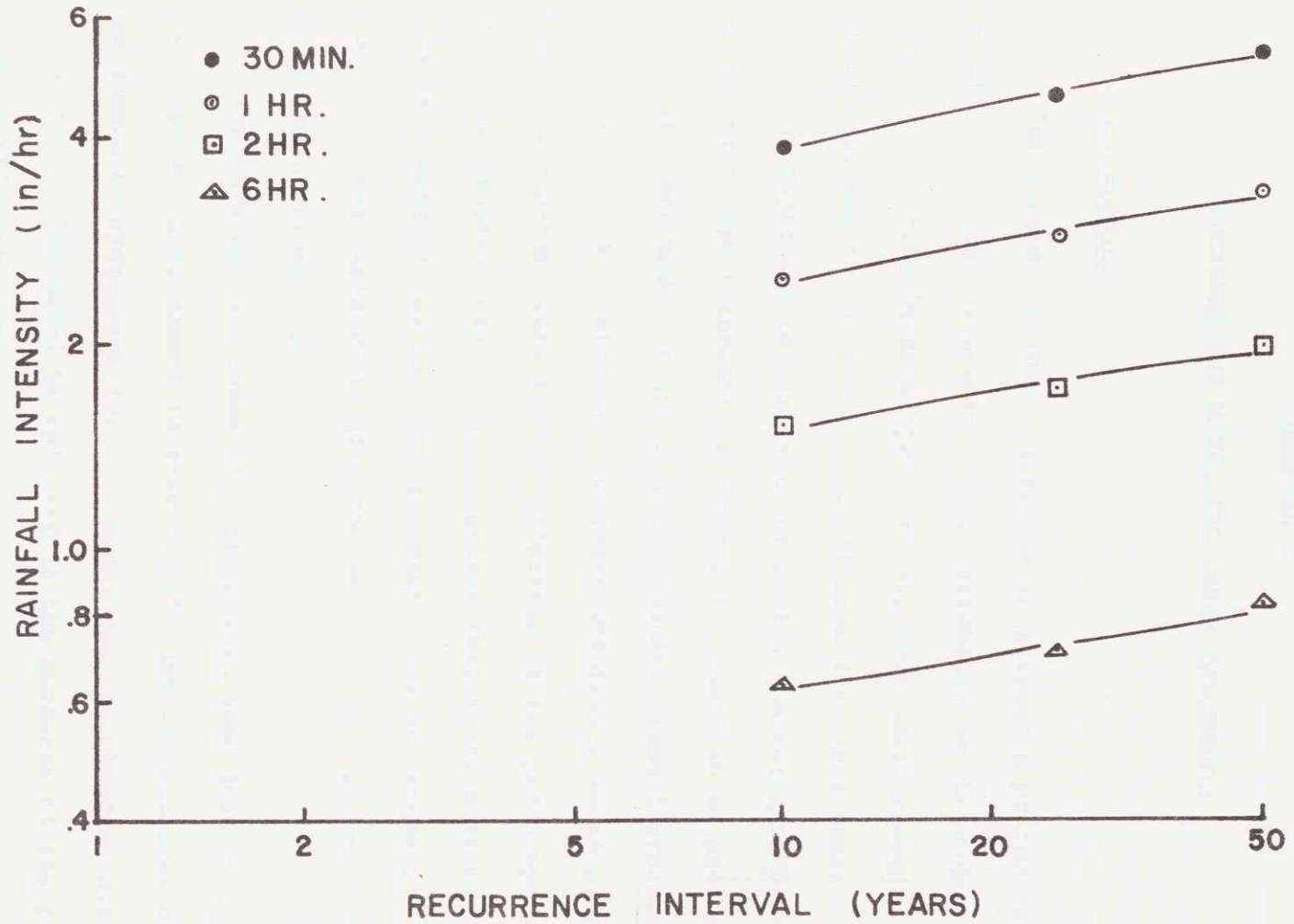
Figure 3-8: Historical Intensity-Duration-Frequency Curves, Baltimore, 1903-1953
(From Department of Public Works, Baltimore City)

CHAPTER 4

PROCEDURE FOR MODELLING URBAN CATCHMENTS

4.1 Introduction

The purpose of this chapter is to present a procedure for modelling urban catchments. Such catchments may be undeveloped partially or totally developed, or may have small reservoirs or ponds designed to control the runoff from developed areas.

The objective herein is to propose a conceptual description of the prototype catchment, a description that can be used as input to a catchment model to simulate the rainfall-runoff process. The objective of the strategy is to create physically sound as well as economical-to-use, idealized descriptions of the prototype catchment

The proposed procedure recognized that there must be a balance between computational cost and accuracy. The procedure to be proposed has been designed to give the best possible accuracy for a given computational cost.

The physical soundness of a given idealized description of the prototype model catchment is measured through the goodness of fit of the simulated hydrograph for this model and the observed hydrograph of the site. The model is rejected if the goodness of the fit is not judged sufficient. No mathematical criteria are used to accept or reject a given model of the catchment. On one hand such a criterion may be desirable to generalize the results, on the other it may be diffi-cult to develop a criteria that is practical and relevant for the analysis.

The economical quality of a given model is readily evaluated by comparison of the costs of simulating the runoff of a storm, for several models of the catchment. In general, as the description of the catchment is improved, the physical soundness of the model is increased as is the cost of simulating the rainfall-runoff process. The strategy sought recognizes explicitly the trade-off between the physical soundness and the cost of using the model.

This chapter is organized into several main parts. First the mathematical basis for modeling urban runoff is considered (including the opportunities for segmentation and the mathematics of the routing scheme). Next, a gaged urban catchment named Gray Haven near Baltimore is used to show that the theory can be applied in practice. Then, some alternative simplified configurations are considered (including an analysis of why each configuration was or was not an appropriate model of the detailed configuration presented previously.) Finally, the procedure (on the basis of this work) that seems most appropriate for modeling is presented.

4.2 Modular Representation of an urban catchment.

A catchment is an ensemble of connected flow segments which carry the water received as precipitation to the catchment outlet where the flow can be measured. In the urban catchment, several types of segment are identified, to name a few, there are the roofs, the grass areas of the backyard, the lawn in front of the house, the streets and the alleys, the gutters and small channels receiving water from those seg-

ments cited above, the pipe network etc. The land use in the urban catchment may vary from playgrounds to shopping centers--land uses that are very different relative to their response to a rainfall.

To model the non-homogeneity of these catchments,

ideal flow segments are created.

Four types of segments are identified to model the prototype catchment relative to direct surface runoff;

1- overland flow plane

(to model roofs, lawns, streets, parking lots, or other catchment surfaces)

2- stream element

(to model gutters, pipes, swales, channels and streams)

3- junctions

4- reservoir

(to model detention storage and flood control facilities)

The first type of segment is the overland flow plane which models the catchment surface which receives the precipitation and which drains to a downstream overland flow plane or to a stream element. The former receives the water as an upstream inflow whereas the latter receives it as a lateral inflow as illustrated in Figure 4-1. The stream S1, for instance, receives the discharges from catchment C2 as a lateral inflow; catchment C2 receives the discharges from catchment C1 as an upstream inflow.

The overland flow plane may be pervious or impervious. In this urban routing model the only segment that is subject to the infiltra-
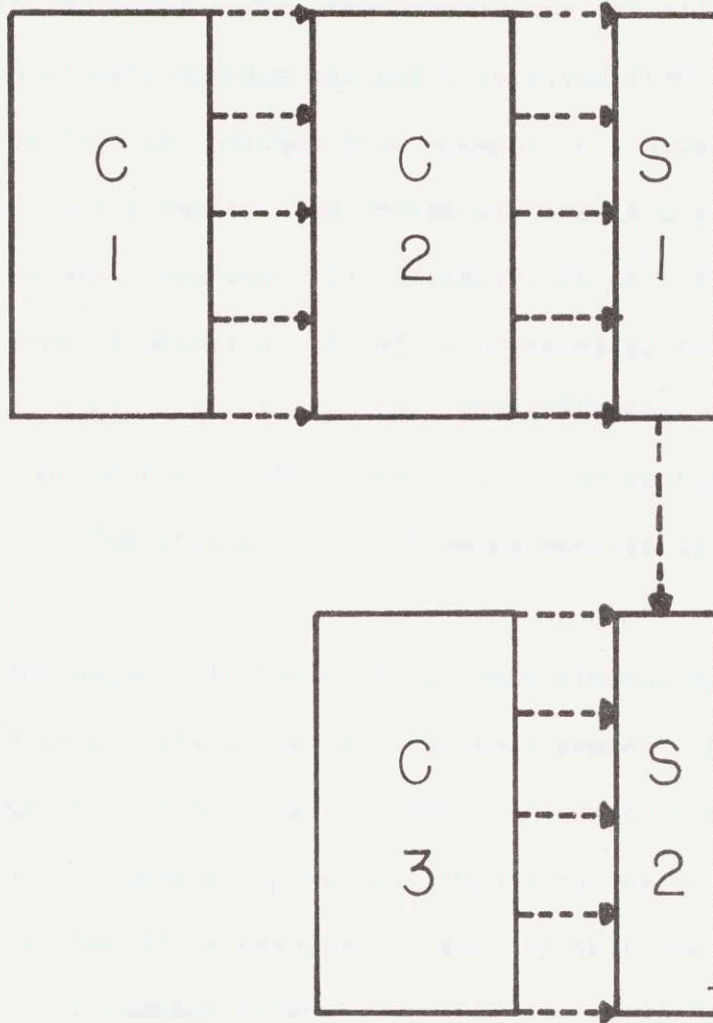
Figure 4-1: Modular Representation of a Catchment

tion process is the overland flow plane. The other elements are all considered impervious.

The areas modeled by an overland flow plane include the roofs, the backyard and the front lawns, the streets and the alleys, etc.

The stream element carries the water received from an overland flow catchment or from an upstream flow element to a downstream stream, junction or reservoir element. The stream element is a generic term that describes several segments; for instance, it describes a river, a triangular channel symmetrical or not, a trapezoidal channel, a rectangular channel, a pipe, a gutter, etc. The difference among these segments are accounted for in the parameters of the routing model adopted for the study. The estimation of these parameters is discussed in a following section.

The junction segment is basically a dummy element which receives only upstream inflows. The discharge from this segment is equal to the summation at time t, of all the upstream inflows to the junction . This element does not have any physical dimensions and is used only for modeling purposes when it is required to add the outflows of two or more branches of the segment network, as illustrated in Figure 4-2. (Dummy streams are also used to respect the dimensionality of the variables in the computer version of the routing model. In the computer model used in this study, three upstream inflows are allowed. If more than three upstream inflows need to be accounted for at a node of the network, a dummy stream is then required.)

The reservoir element is an ideal segment that receives only upstream inflows and discharges water to a stream or junction segment. For this element the outflows are computed as a function of the average

-63-
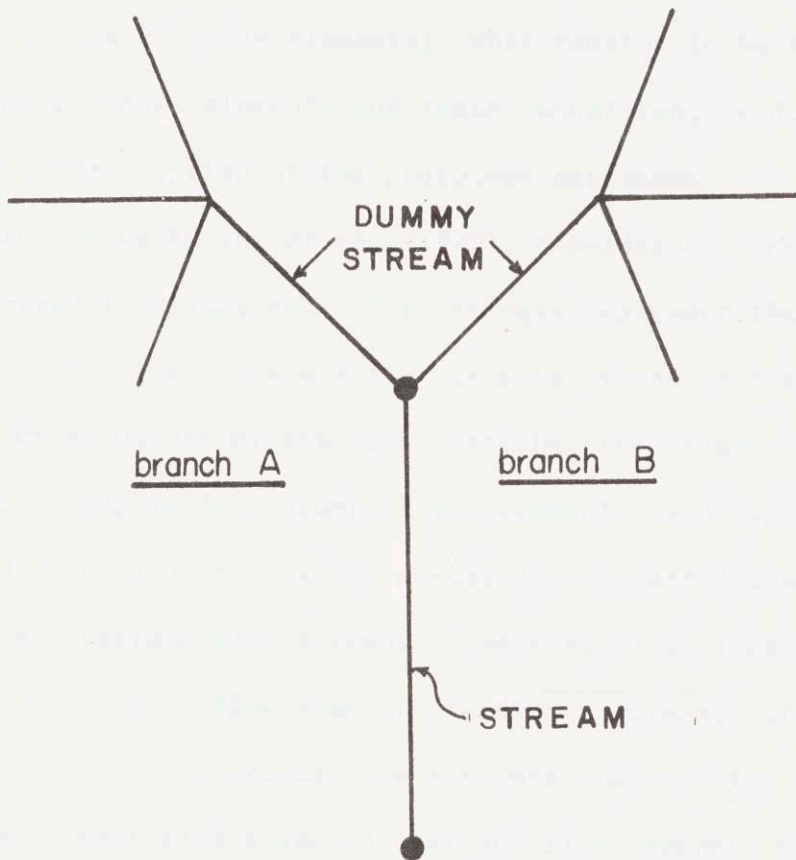
Figure 4-2:   Illustration of Utilization of
Dummy Streams

depth of water (during a given time interval in the reservoir.)

These four basic elements are sufficient to create a model of
the catchment. Each segment of the prototype catchment can be des-
cribed by one of these elements; what remains to be described are the
location of these elements and their connection, leading to a complete
idealized description of the prototype catchment.

Following Harley et al. (1970), consider the three links
illustrated in Figure 4-3. The linkages represent the connectivity
graph of the links, where a link is made of one or more ideal elements.
The inner structure of the link describes the connectivity of these
elements. Figure 4-4 illustrates commonly used link arrangements
For instance, link a) is the so-called standard catchment where two
identical overland flow segments feed a stream; link b) has two
different overland flow segments feeding a stream; link c) has a
stream fed by two overland flow segments that receive as upstream in-
flow the runoff from a second overland flow segment, where the overland
flow segments may all be different. Many other link arrangements may
be created to fulfill the needs of a given prototype. Links d) to f)
in Figure 4-4 are some examples.

A set of physical parameters describes each ideal element; the
parameters are:

    1- length

    2- slope of the segment

    3- perviousness

    4- roughness

    5- etc.
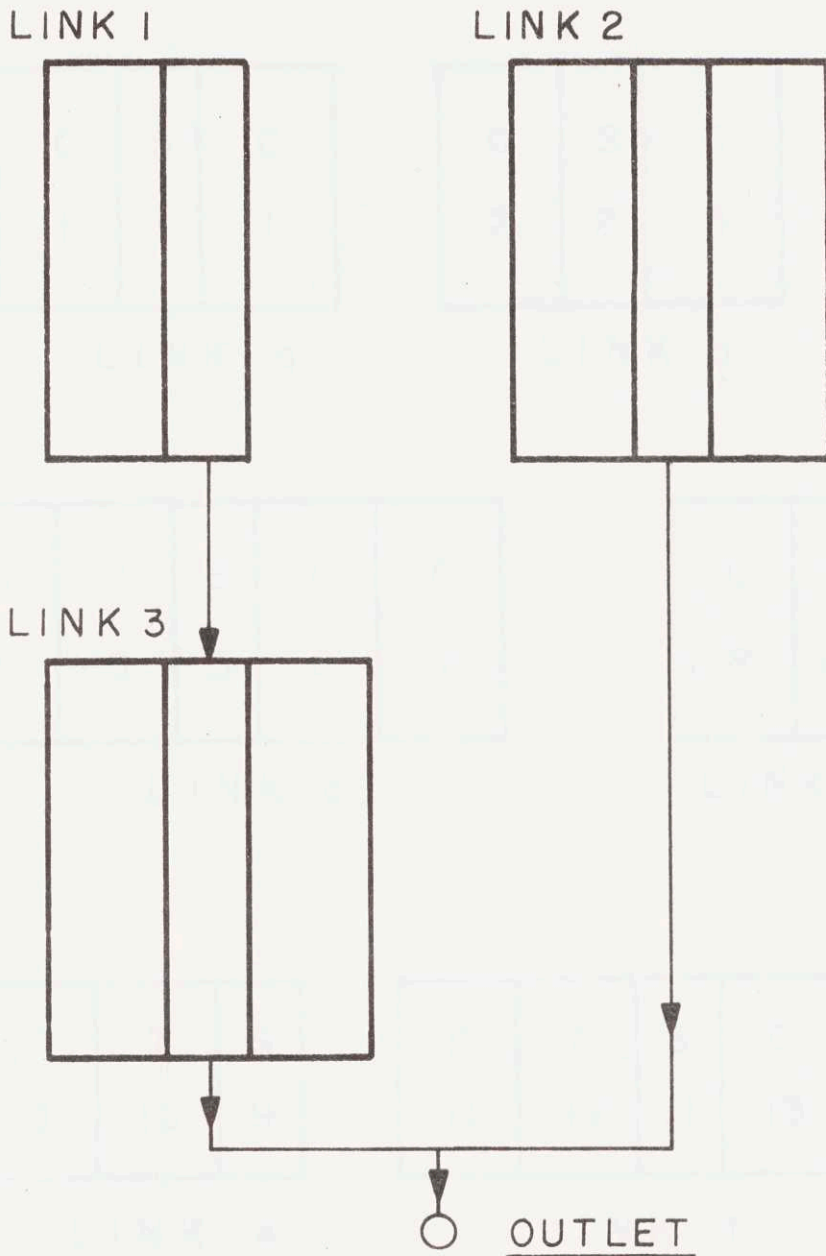
Figure 4-3:   Illustration of a Connectivity Graph
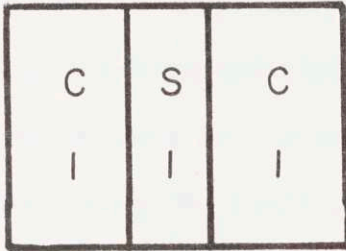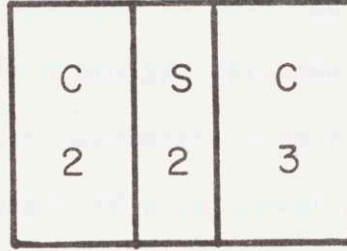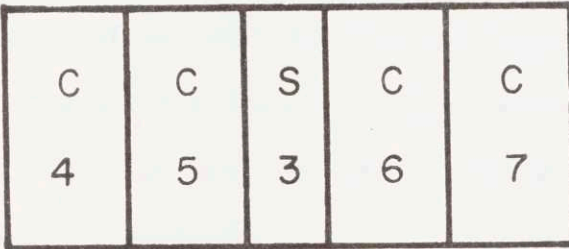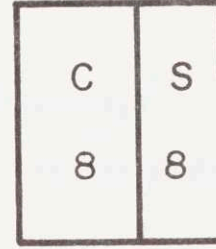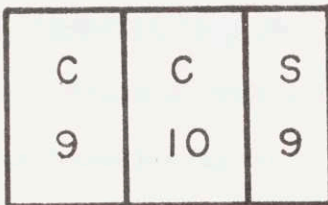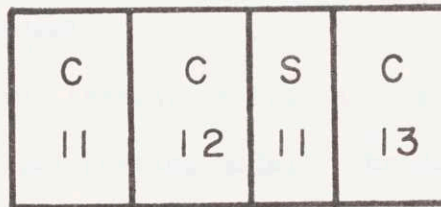
Figure 4-4: Illustration of Commonly Used Link Arrangements

They completely describe the element and are subsequently used to estimate the parameters of the routing model.

The modular representation described in this section is used to model the non-homogeneities of the prototype catchment. Many elements can be used in a model of the catchment. The computational cost of simulating the runoff hydrograph of a catchment is proportional to the number of different elements used in the model of the catchment. It is thus preferable to reduce to a minimum the number of elements needed to model the catchment while preserving the goodness of fit between simulated and observed hydrographs.

To achieve this goal it is necessary to understand

(i) how best to model a catchment with a limited number of segments,

and (ii) how the accuracy would improve if additional segments were added.

4.3 The Kinematic Wave Routing Model

The dynamic behavior of each segment of the catchment is modeled mathematically by a so-called routing model. The modular representation may indeed be used with any routing model that is judged adequate for the study at hand. In this work, the kinematic wave routing model (see Eagleson, 1970), is adopted because is fully represents the dynamics of the flow resulting from the rainfall.

This model is written as

$$\frac{\partial A}{\partial t} + \frac{\partial Q}{\partial x} = q(x,t) \qquad (4-1)$$

and

$$Q = \alpha A^m \qquad (4-2)$$

Equation 4-1 is the continuity equation and Equation 4-2 is the momentum equation; $Q(x,t)$ is the discharge, $A(x,t)$ the crossection of the flow, $q(x,t)$ the lateral inflow to the segment. The parameters of the model are α and m which depend upon the physical characteristics of the segment. Table 4-1 presents the equation used to estimate α and gives the magnitude of m.

Figure 4-5 illustrates the cross-section of the segment. In Table 4-1, S_o is the longitudinal slope of the segment, n is the Manning's roughness parameter, z is the horizontal component of the slope of the banks ($[z]$ = Feet) and D is the diameter of the pipe ($[D]$ = Feet).

The selection of Manning's n is a function of the segment type. For overland flow, n is a surrogate allowing the use of the Manning's equation to define α and m; a magnitude of 0.50 is generally used for pervious segment and a magnitude of 0.15 for an impervious segment. For a small stream the range of n varies from 0.02 to 0.10 - 0.12; where the upper limits are used when the stream is not well defined. For a pipe, n is chosen as 0.014 for Gray Haven. [Chow, (1964)] summarizes the magnitude of n for stream type elements.

A finite difference method of solution was developed to solve the kinematic wave equations. Upon substitution of Equation 4-2 in Equation 4-1, the kinematic wave model is written as

$$\frac{\partial A}{\partial t} + \alpha \frac{\partial A^m}{\partial x} = q(x,t) \qquad (4-3)$$

Table 4-1

Estimation of the Parameters α and m

Segment	α	m	
Overland flow	$\dfrac{1.49}{n} S_o^{1/2}$	1.67	(4-4)
Symmetrical triangular channel	$\dfrac{0.94 \, S_o^{1/2}}{n} \left[\dfrac{z}{1+z^2}\right]^{1/3}$	1.33	(4-5)
gutter	$\dfrac{1.182 \, S_o^{1/2}}{n} \left[\dfrac{z^{1/2}}{1+\sqrt{1+z^2}}\right]^{2/3}$	1.33	(4-6)
rectangular channel	$\dfrac{1.49 \, S_o^{1/2}}{n}$	1.67	(4-7)
pipe*	$\dfrac{0.804 \, S_o^{1/2}}{n} D^{1/6}$	1.25	(4-8)

---

* see Harley et al. [1970]

GUTTER
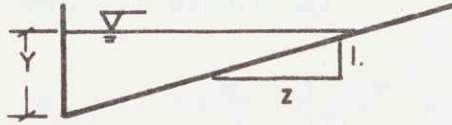
TRIANGULAR
CHANNEL
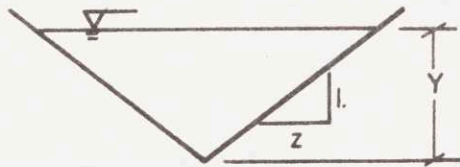
PIPE
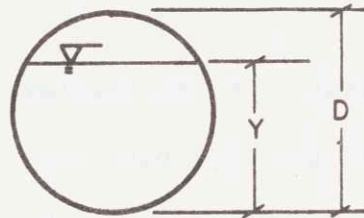
RECTANGULAR
CHANNEL
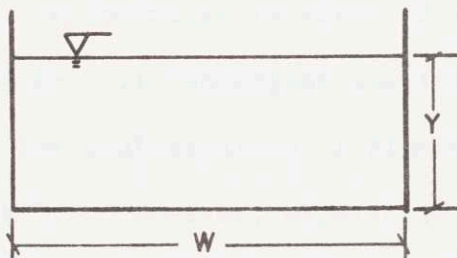
Figure 4-5: Cross Section of Commonly Used Stream Segments

Equation 4-3 , known as the conservation form of the kine-
matic wave model, can be approximated by the following finite difference
equations for the configuration shown in Figure 6a)

$$A_{i+1}^{j+1} = q(x,t) \cdot \Delta t + A_{i+1}^{j} (1 - \alpha \frac{\Delta t}{\Delta x} (A_{i+1}^{j})^{m-1}) + \frac{\alpha \Delta t}{\Delta x} \left(A_{i}^{j}\right)^{m} \quad (4-9)$$

and for the configurations of Figure 6b)

$$A_{i+1}^{j+1} = \left\{ \frac{q(x,t) \cdot \Delta x}{\alpha} + \frac{\Delta x}{\alpha \Delta t} \cdot A_{i}^{j} + A_{i}^{j+1} [(A_{i}^{j+1})^{m-1} - \frac{\Delta x}{\alpha \Delta t}] \right\}^{1/m}$$

$$(4-10)$$

where Δx and Δt are the space increment and time increment as shown
in Figure 6;   and where j is associated with the time axis and i
with the space axis. The other variables have been defined earlier in
the presentation .

Equation 4-9 is stable if the magnitude of Θ defined by
Equation 4-11 is smaller than or equal to   1.0   and Equation 2-10 is
stable if Θ is greater than or equal to 1.0.

$$\Theta = \alpha\, m\, \frac{\Delta t}{\Delta x} \left(\frac{A_{i+1}^{j} + A_{i}^{j+1}}{2} \right)^{m-1} \qquad (4-11)$$

The two configurations are complementary in terms of stability.

The configuration of Figure 6a) is convergent and its accuracy
is perfect if Θ is equal to 1.0. The configuration of Figure 6b) is
not convergent if Θ is not equal to 1.0. However, experience with the
model shows that the second configuration is very well behaved for values
of Θ_{max} up to 2.0. The finite difference solution model and its per-
formance have been presented in detail in Leclerc and Schaake, [1973], a
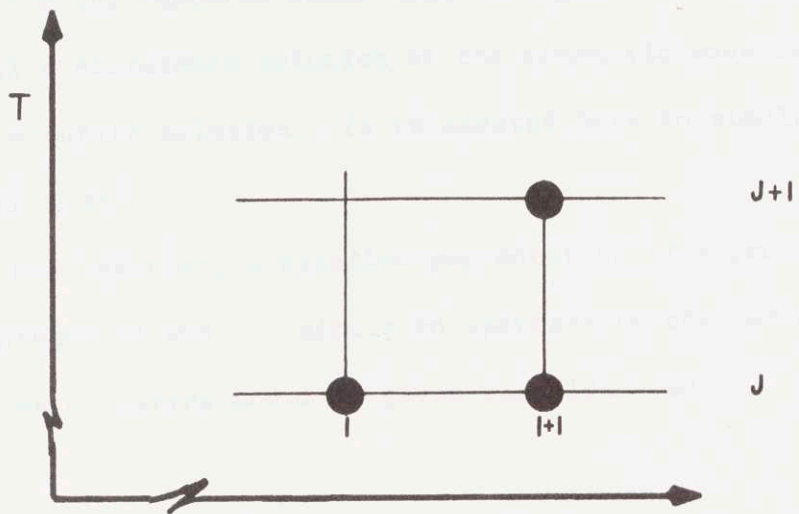
Figure 4-6 a): Finite-difference Grid #A
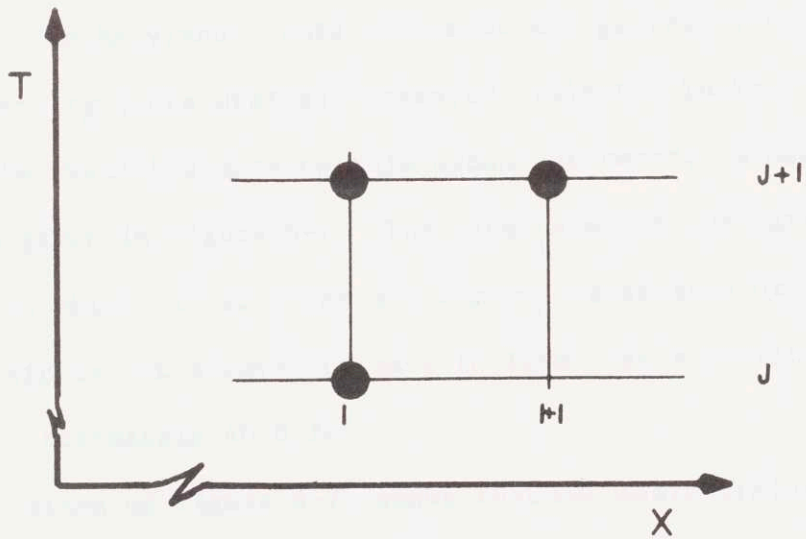
Figure 4-6 b): Finite-difference Grid #B

user's manual for the computer model used throughout the analysis.

The finite difference solution of the kinematic wave is an efficient and accurate solution. It is adopted here to simulate the rainfall-runoff model.

In the next section, a detailed segmentation of a prototype catchment is presented and   simulated hydrographs obtained with the kinematic wave routing model are given and discussed.

4.4 Detailed Segmentation of an Urban Catchment.

4.4.1- Model of the Prototype.

The modular representation is used to create a detailed segmentation of an urban catchment; this segmentation is then input to the routing model and several storms are simulated.

The urban catchment selected is Gray Haven, located near Baltimore City in Maryland; this catchment was gauged by the Johns Hopkins University Storm Drainage Research Project. Tucker [1969] summarized the available data on this urban catchment. A map of the catchment is given in Figure 4-7. The total area of the catchment is 23.29 acres of which 12.12 acres are impervious streets or roofs. The roofs drain to the alleys but have to flow over a pervious grass surface of approximately 40.0 ft.

Observation of Figure 4-7 shows that two basic drainage modules are utilized   in   the drainage pattern of Gray Haven. These basic drainage modules are illustrated in Figure 4-8.

Six overland flow segments are identified on the map of Gray Haven (Figure 4-7). The first is the street overland flow plane
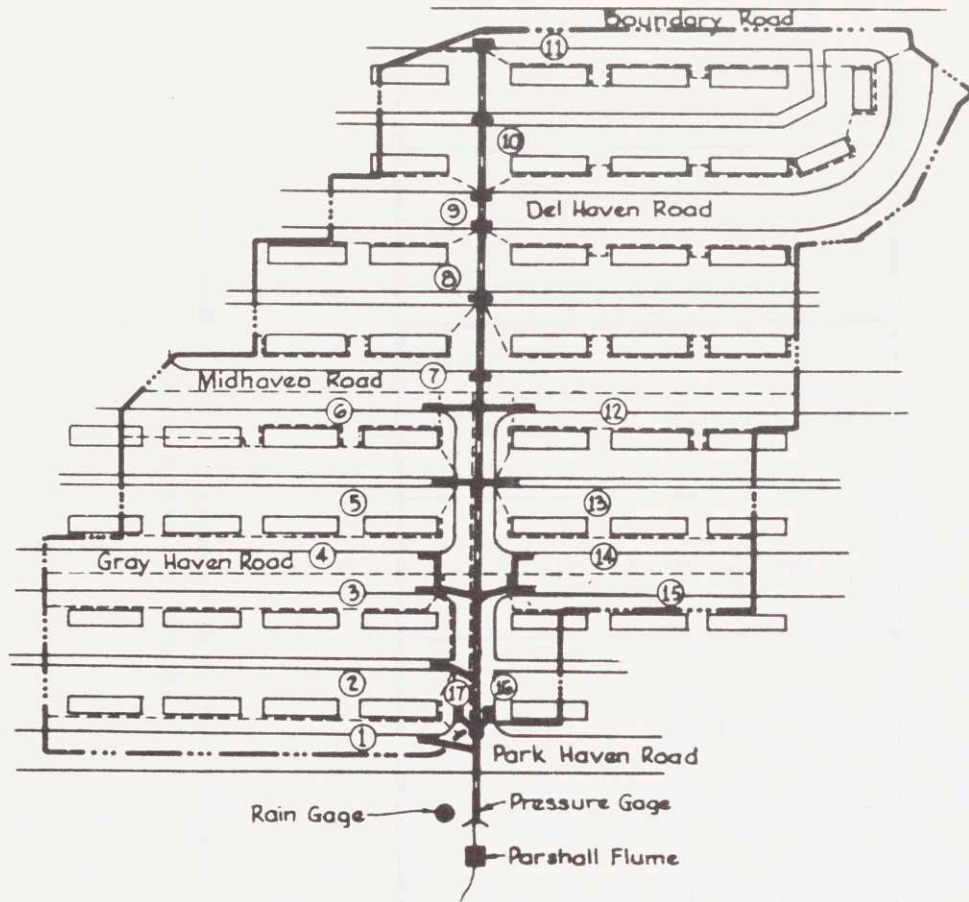
PLAN
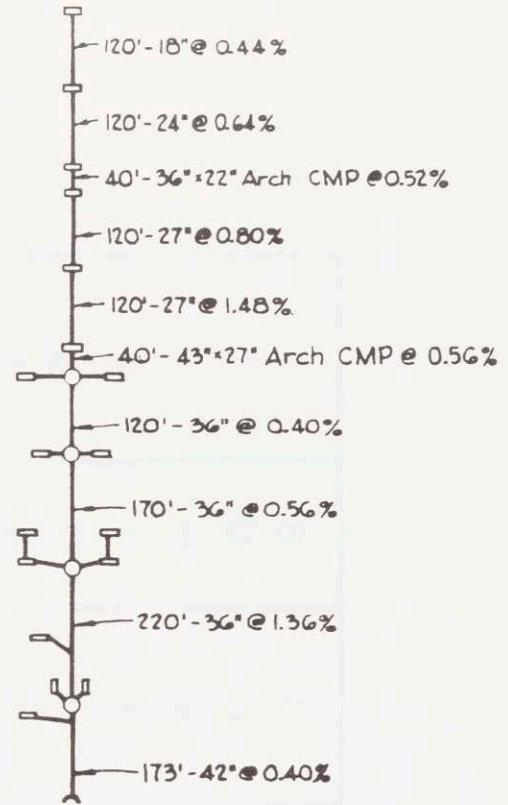
Figure 4-7: Map of the Gray Haven
Urban Catchment

```
┌─────────┬─────────┬─────────┐
│    S    │    G    │    L    │
│    T    │    U    │    A    │
│    R    │    T    │    W    │
│    E    │    T    │    N    │
│    E    │    E    │         │
│    T    │    R    │         │
└─────────┴─────────┴─────────┘
```

```
┌───────┬───────┬───────┬───────┬───────┬───────┬───────┐
│   R   │   Y   │   A   │   C   │   A   │   Y   │   R   │
│   O   │   A   │   L   │   H   │   L   │   A   │   O   │
│   O   │   R   │   L   │   A   │   L   │   R   │   O   │
│   F   │   D   │   Y   │   N   │   Y   │   D   │   F   │
│       │       │       │   N   │       │       │       │
│       │       │       │   E   │       │       │       │
│       │       │       │   L   │       │       │       │
└───────┴───────┴───────┴───────┴───────┴───────┴───────┘
```
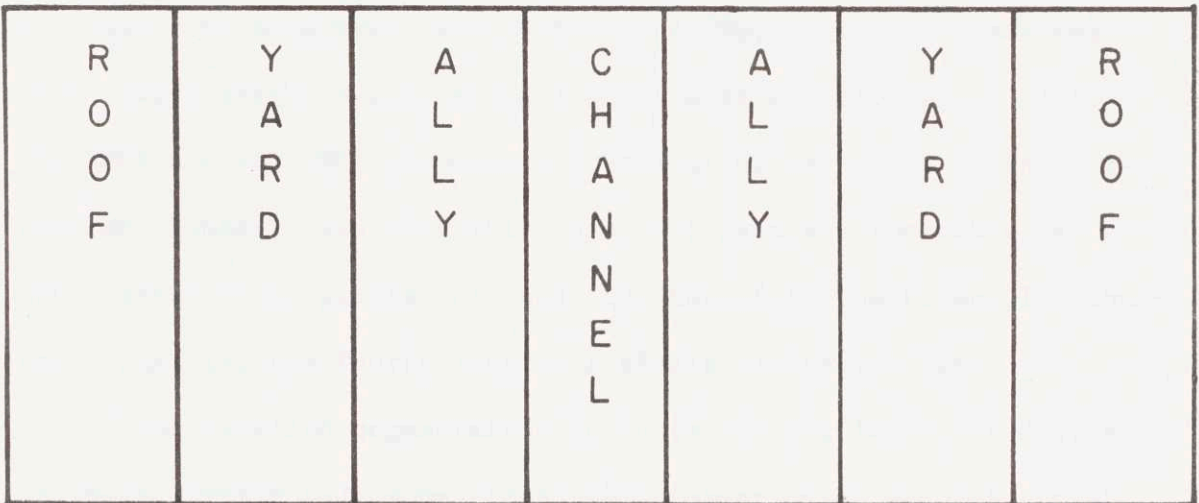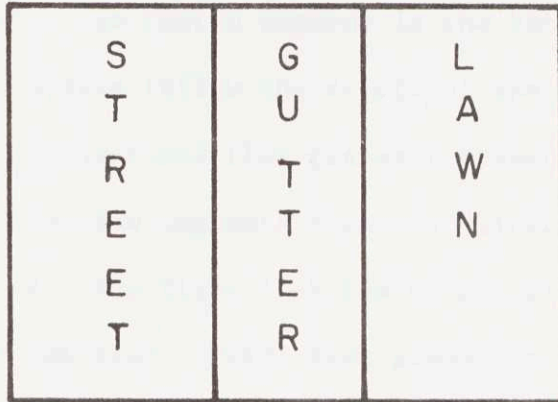
Figure 4-8: Basic Drainage Modules of the
Gray Haven Catchment

which drains one half of the street width. The second is the lawn
segment which drains the grass area in front of the houses. The third
segment is the roof; the fourth segment is the backyard grass which
also receives as upstream inflow the runoff of the roof. The fifth
and sixth segment are overland flow planes representing the alleys.

These overland flow segments form four"links" which are illus-
trated in Figure 4-9. The first link has on one side of the gutter
segment the street overland (STRT) flow plane and on the other side
the lawn (GRST) overland flow plane. The second link has a gutter
that receives water only from the street overland flow plane. The
third link has on both sides of a small triangular channel, three
overland flow segments; the roof drains (ROOF) to the grass seg-
ment (GRBY) which in turn feeds a short overland flow plane (ALLY).
The ROOF and the GRBY planes are identical on each side of the tri-
angular channel. One ALLY (L1) has 10.0 feet and the other has
20.0 feet. These planes L1 and L2 then feed the triangular chan-
nel. Finally, the fourth link is a single element, a pipe.

The detailed segmentation accounts for all important drainage
channels. Table 4-2 summarizes the information on each of the 42
segments of the segmentation, and Figure 4-10 illustrates the connec-
tivity of these 42 segments.

The total area modeled is 23.29 acres, which is distributed
as follows:

     1-   Street   :   STRT   3.433

     2-   Roof   :   ROOF   4.476
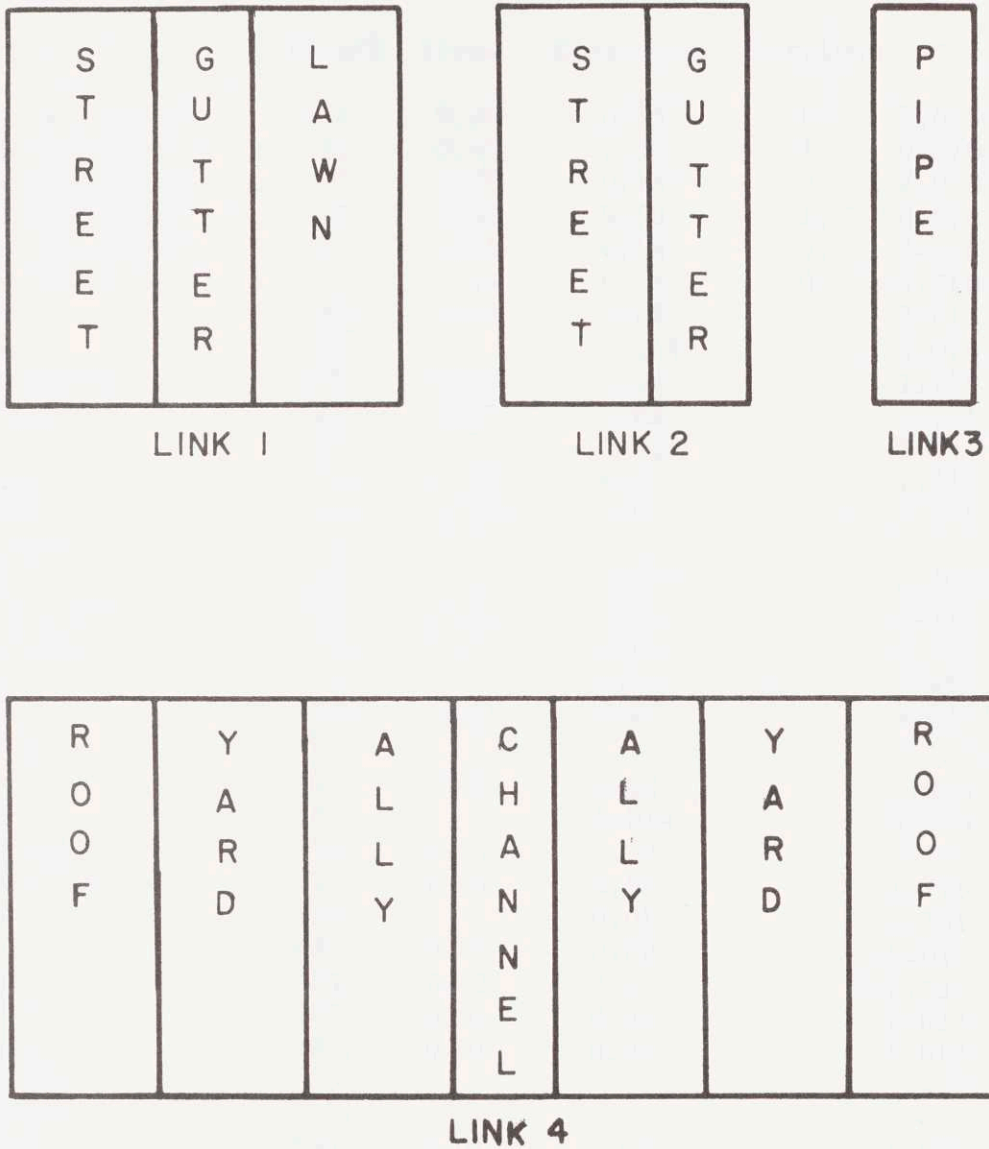
Figure 4-9: Links Adopted to Model the Gray Haven Urban Catchment

Table 4-2

PARAMETERS OF THE DETAILED SEGMENTATION[*]

	Type	Length	Slope	Roughness	Pervious	α	m
C1	overland flow	18.	0.04	0.15	0	2.000	1.67
G1	overland flow	42.	0.05	0.50	1.	0.670	1.67
C2	overland flow	30.	0.05	0.15	0.	2.000	1.67
G2	overland flow	40.	0.05	0.50	1.	0.670	1.67
L1	overland flow	10.	0.05	0.15	0.	2.340	1.67
L2	overland flow	20.	0.05	0.15	0.	2.340	1.67
11	gutter	680.	0.02	0.02	–	2.015	1.33
P11	pipe	120.		0.014		4.076	1.25
10A	triangular	600	0.01	0.02		1.725	1.33
10B	triangular	160.	0.01	0.02		1.725	1.33
P10	pipe	120		0.014		5.157	1.25
9A	gutter	810.	0.01	0.02		2.015	1.33
9B	gutter	230.	0.01	0.02		2.015	1.33
P9	junction	0					
P8	pipe	160.		0.014		6.000	1.25
8A	triangular	480.	0.01	0.02		1.725	1.33
8B	triangular	350.	0.01	0.02		1.725	1.33
P7	pipe	120.		0.02		8.269	1.25
7	gutter	480.	0.01	0.02		2.015	1.33
P6	junction	0				–	–
6	gutter	520.	0.01	0.02		2.015	1.33
P5	pipe	160.		0.014		4.400	1.25
13	triangular	400.	0.01	0.02		1.725	1.33
5	triangular	520.	0.01	0.02		1.725	1.33
P4	pipe	170.		0.014		5.161	1.25
4A	gutter	630.	0.01	0.02		2.015	1.33
4B	gutter	220.	0.01	0.02		2.15	1.33
14A	gutter	200.	0.01	0.02		2.015	1.33
14B	gutter	400.	0.01	0.02		2.015	1.33
J1	function	0.				–	–
J2	function	0.				–	–
3	gutter	630.	0.01	0.02		2.015	1.33
15	gutter	380	0.01	0.02		2.015	1.33
P3	pipe	130.		0.014		8.043	1.25
2	triangular	640.	0.01	0.02		1.725	1.33
P2	pipe	80.		0.014		8.043	1.25
17	gutter	250.	0.01	0.02		2.015	1.33

(Continuation of Table 4-2)

16A	triangular	100.	0.01	0.02	1.725	1.33
16B	gutter	200.	0.01	0.02	2.015	1.33
J3	junction	0	–	–	–	–
1	gutter	640.	0.01	0.02	2.015	1.33
P1	pipe	173.			4.475	1.25

Total area   =   23.29

Imperviousness ratio   =   0.434

* for the gutter $z = 25$
  for the triangular channel $z = 20$
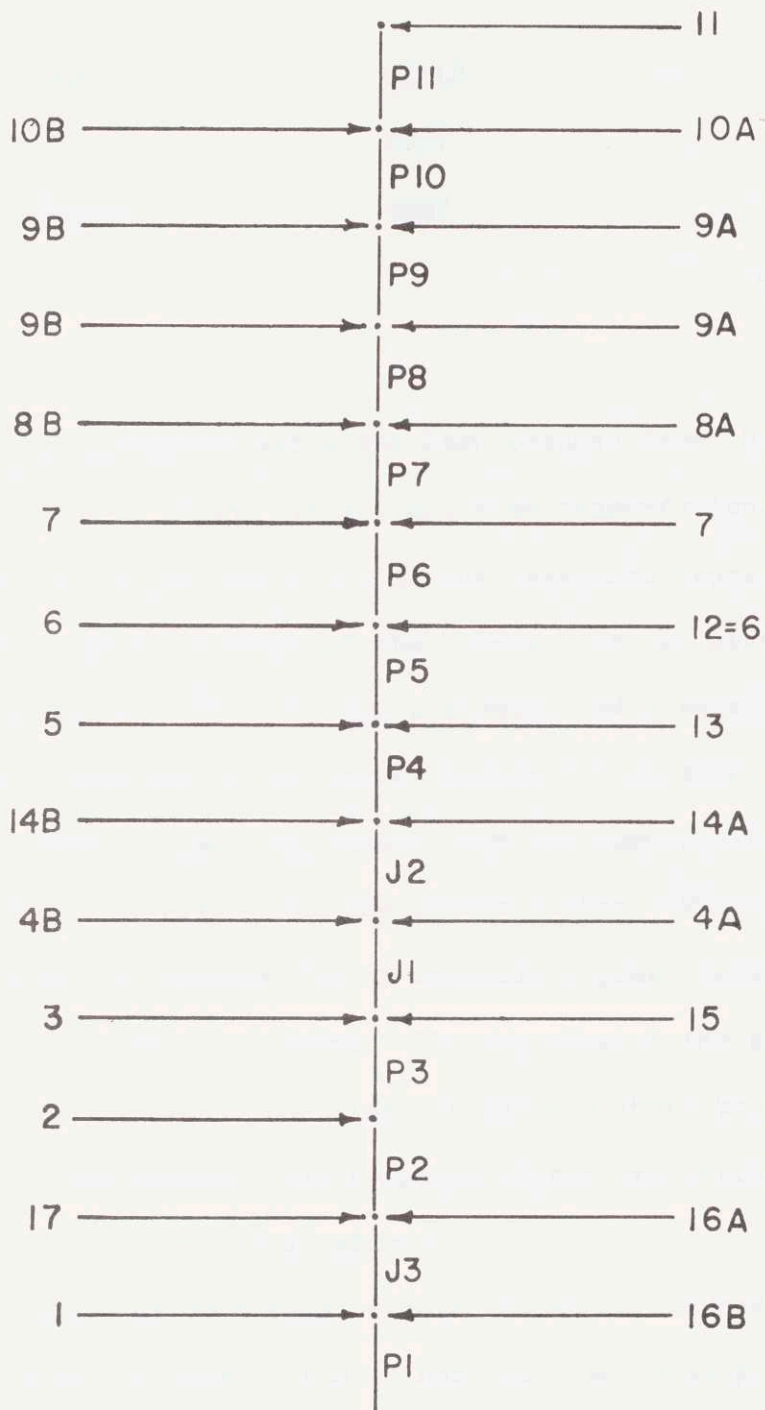
Figure 4-10: Connectivity of the Gutters, Channels and Pipes for Gray Haven

3-	Alley	:	L1+L2	2.238
4-	Lawn	:	GRST	7.173
5-	Backyard	:	GRBY	5,968

23.288 acres

The imperviousness ratio has been reduced from 0.52 in the prototype down to 0.435 in the detailed segmentation. Most of this reduction is accounted for in the idealized representation of the pervious plane in front of the houses. In the prototype, this segment is made of the lawn, the sidewalk, and a short band of grass immediately adjacent to the street gutter. This short band, in many instances, will impound the runoff from the lawn and the sidewalk instead of discharging it to the street gutter. When the sidewalk is eliminated and replaced by an equivalent grass length, the total imperviousness area is reduced. The response of the grass segment representing the grass, the sidewalk and the short band of grass should well approximate the response of the grass-sidewalk-grass component of the prototype catchment.

The slopes of each segment were chosen on the basis of qualitative observations made by the authors because no slope magnitudes were measured by the Hopkins Project. The slope of each gutter and triangular channel was also assumed constant. The magnitude of the roughness parameter, n, was selected to satisfy the range of values presented earlier.

This detailed segmentation is used in the kinematic wave routing

model to simulate the direct surface runoff of Gray Haven.

4.4.2 Simulated Runoff Hydrographs

Several storms were routed through this detailed segmentation. The selected storms cover the range of events observed at the site, (see Tucker [1969]). The precipitation sampling time interval was one minute as was the runoff sampling time interval. The rainfall series are illustrated in the figures showing the simulated hydrographs. The infiltration process was modeled by the Horton's law of infiltration, expressed mathematically by:

$$\phi(t) \; = \; f_c + (f_o - f_c) \, e^{-kt} \qquad\qquad (4\text{-}12)$$

where $\phi(t)$ is the instantaneous rate of infiltration

  f_c the rate when the soil is saturated

  f_o the initial rate

and   k   a constant.

t is the time elapsed since the beginning of the storm. All the simulated runoff hydrographs presented in this chapter are derived for a constant infiltration process, defined with

  f_c = 1.5 in/hr

  f_o = 2.0 in/hr

and   k = 0.023 minutes^{-1}

Comparison of the observed and simulated runoff hydrographs, for the selected storms, are presented in Figures 4-11 to 4-15.

-83-
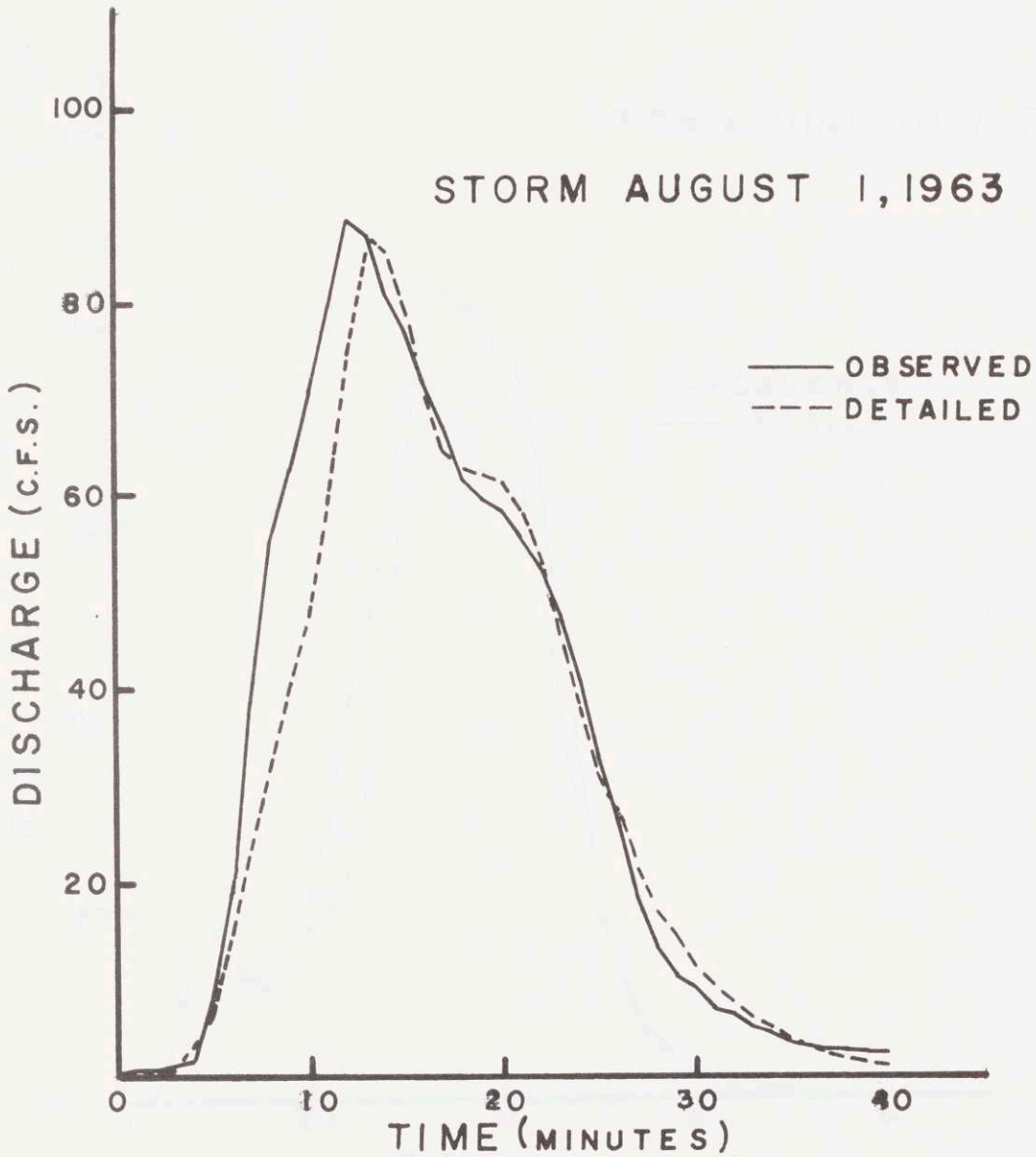
Figure 4-11: Detailed Configuration: Observed vs Simulated
Hydrographs: Storm of August 1, 1963

STORM JUNE 10, 1963

DISCHARGE (c.f.s.)

100

80

———OBSERVED
— — —DETAILED

60

40

20

0

0   20   40   60   80

TIME (MINUTES)
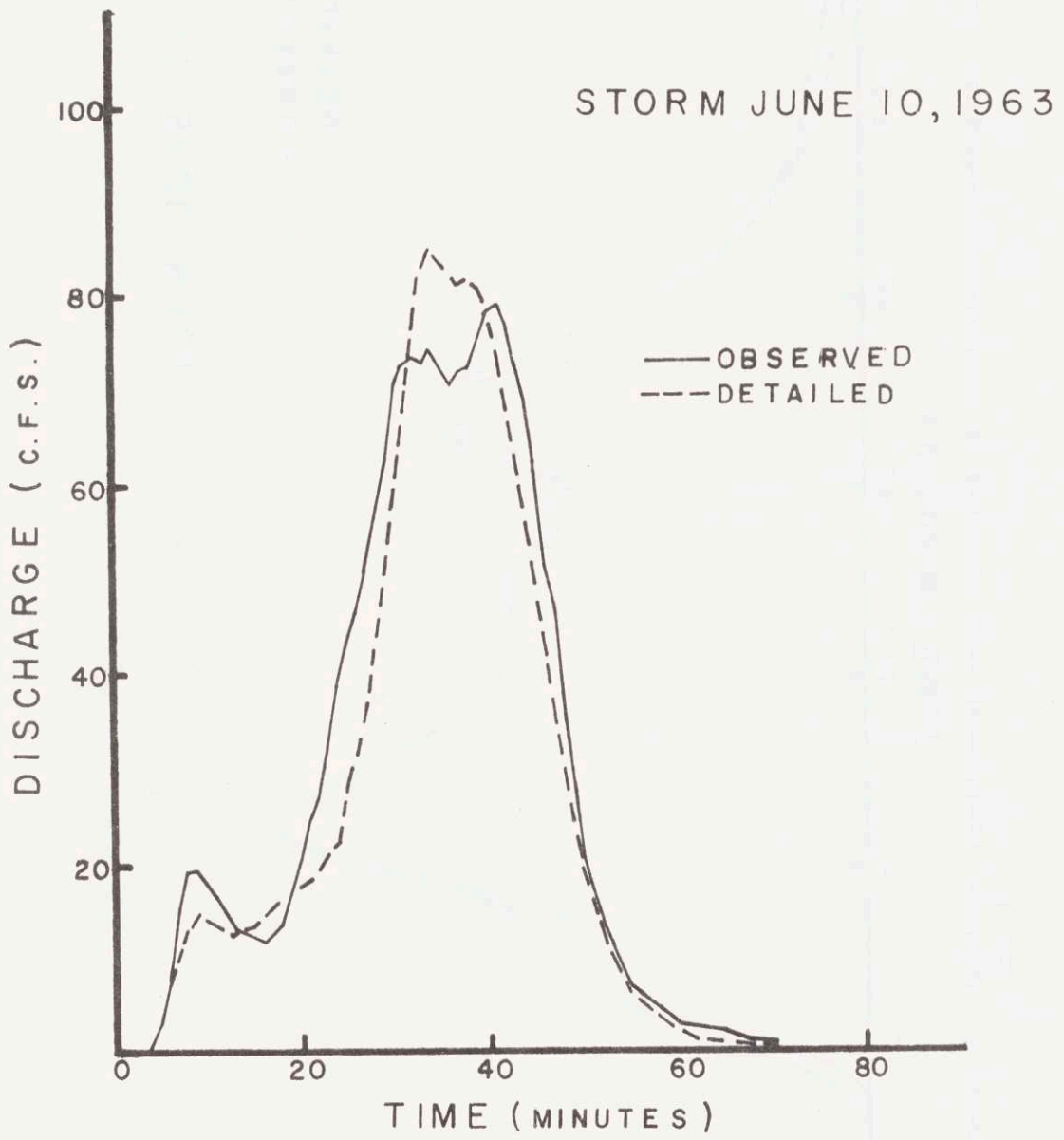
Figure 4-12:   Detailed Configurations : Observed vs
              Simulated Hydrographs: Storm of June 10, 1963
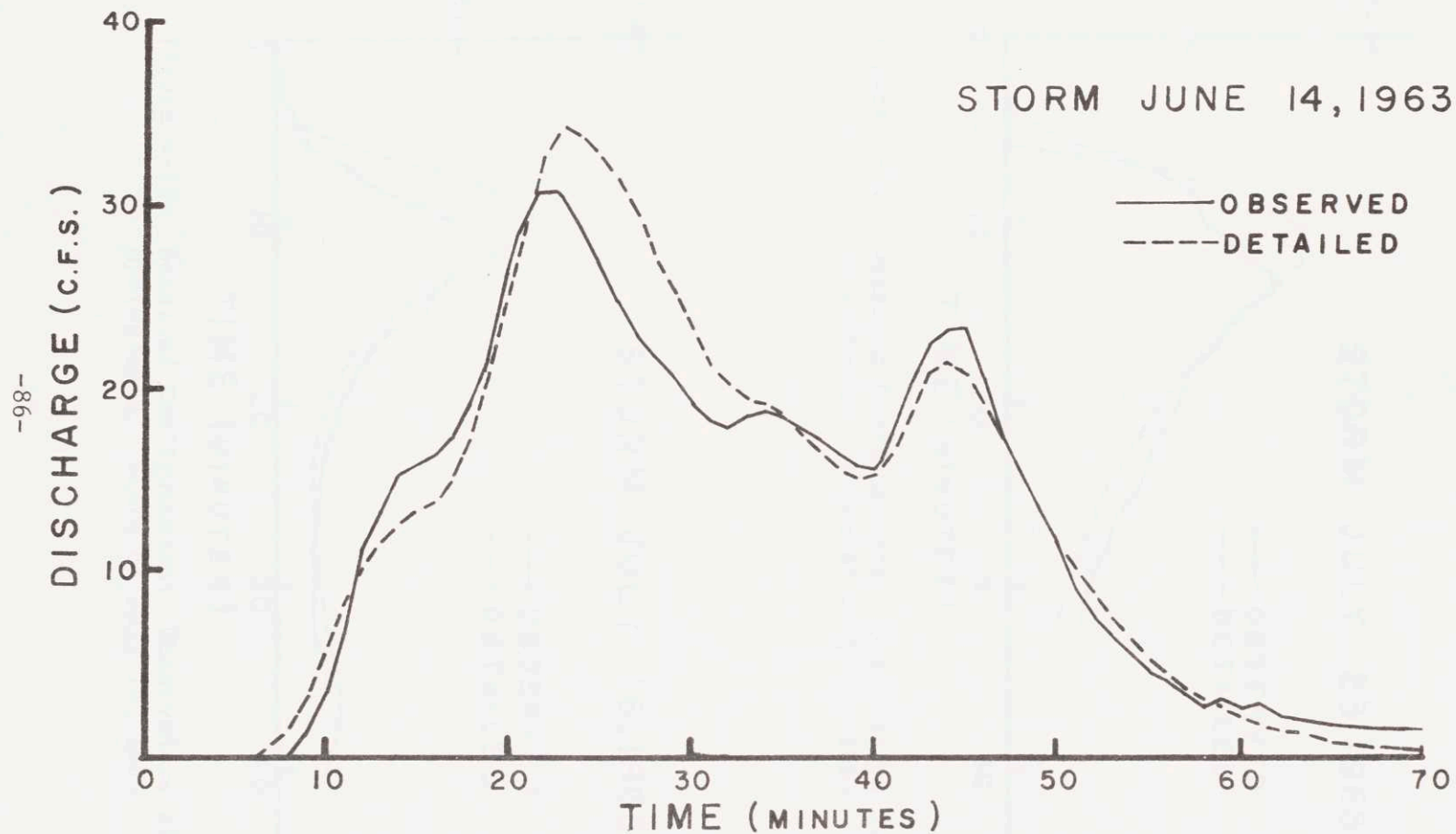
Figure 4-13: Detailed Configuration : Observed vs Simulated Hydrographs: Storm of June 14, 1963
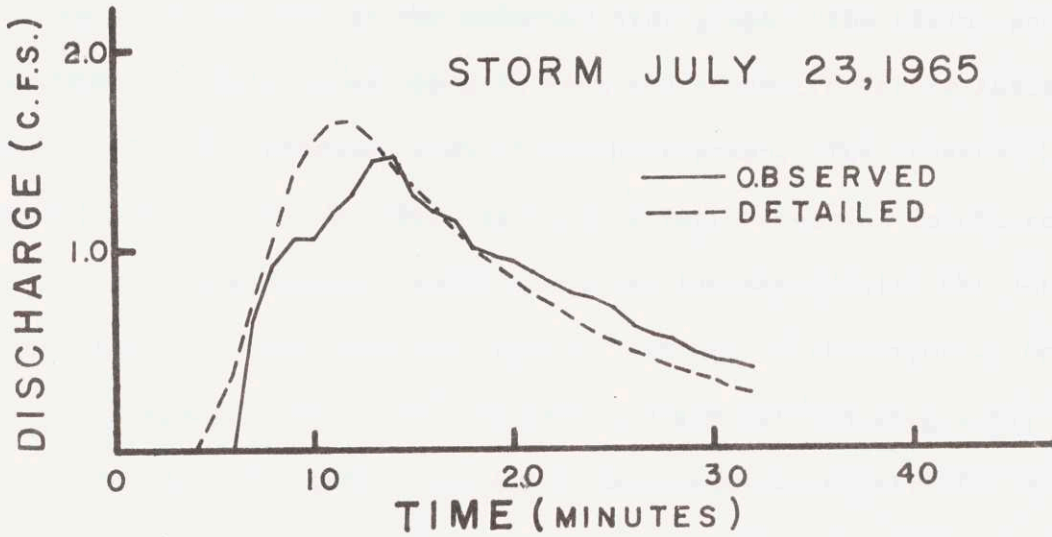
Figure 4-14:   Detailed Configuration: Observed vs Simulated
              Hydrographs: Storm of July 23, 1965
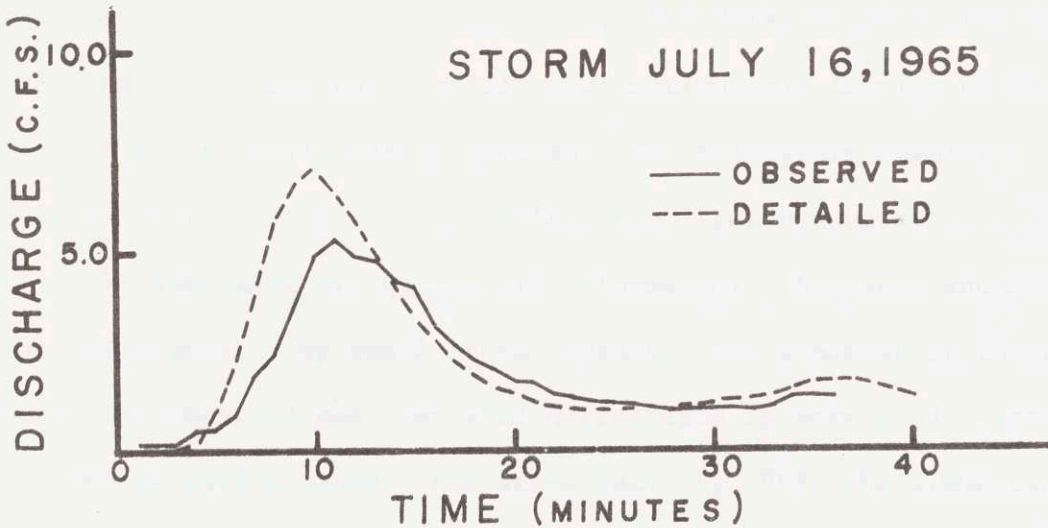
Figure 4-15:   Detailed Configuration: Observed vs Simulated
              Hydrographs: Storm of July 16, 1965

The simulated hydrographs of storms August 1, 1963, and June 10, 1963, which are large storms, reproduce well the observed hydrographs. The rising limb does not go up as quickly in the simulated hydrograph as it does in the observed hydrograph. The timing and the magnitude of the observed peak is well reproduced for storm August 1, 1963, as is the recession limb of the hydrograph. The observed hydrograph of storm June 10, 1963, exhibits erratic behavior in the region of the peak flow, behavior which cannot be reproduced with the detailed segmentation for the recorded rainfall pattern of this storm. Despite this discrepancy between the observed and simulated hydrographs, the match is still very good because the important characteristics of the observed hydrographs are well approximated in the simulated hydrograph.

The simulated runoff for storm June 14, 1963, which is an intermediate storm event, compares very well with the observed runoff. The rising and recession limbs match very well. The two peaks of the observed hydrographs are well reproduced; the differences in the magnitude of the peaks are not significant, particularly in view of the uncertainty in the infiltration process. For this storm event the detailed segmentation leads to an excellent simulated hydrograph.

The simulated hydrographs for storms July 16, 1965, and July 23, 1965, are generated by small storm events. The goodness of the fit between the observed and simulated hydrographs is very good, particularly in the recession phase. For storm July 16, 1965, the simulated raising limb is too fast and the resulting peak is also too large. However, in absolute magnitude the differences are small and the simulated solution

proves to be an adequate representation of the observed runoff hydro-graph.

The goodness of fit between the simulated and observed hydro-graphs of storm July 23, 1965, is excellent. The discrepancy observed is very small and is accounted for in the uncertainties and assumptions inherent in the modeling effort of the rainfall-runoff process.

4.4.3 Examination of the Differences between Observed and Simulated Hydrographs.

The hydrographs simulated with the detailed segmentation give an excellent representation of the observed hydrographs. The representation is not perfect because several unknowns are present in the solution and several assumptions are made in the modeling effort. These unknowns and/or assumptions are presented below.

1. Spatially homogeneous rainfall: the rainfall, observed at the raingage, is assumed spatially homogeneous over the entire catchment. This assumption was made for Gray Haven because only one raingage was used to measure rainfall. In engineering practice it would always be assumed that the rainfall intensities were spatially uniform over a 23 acre area. Nevertheless some of the observed variations may be due to spatial variations in the rainfall.

2. Magnitude of α : The magnitude of α is computed from the Manning's formula; α is also kept constant throughout the storm and from storm to storm. The results of the simu-

lated hydrographs show that this characteristic may be the source of some error in the solution. Recall that for the large storms, the simulated hydrographs were not going up as fast as the observed hydrographs and that for the small storms, (especially storm July 16, 1965), the hydrograph is raising up too fast. Since α is related to the velocity of the wave, its magnitude may be a function of the mean depth of water in the segment, and consequently of the intensity of the storm.

A correction on α as a function of the storm intensity may lead to improved simulated hydrographs but it is not the principal source of error between simulated and observed hydrographs.

α is a function of the catchment slope. Some of these slopes were not measured, but assumed on the basis of a visual inspection of the catchment. Some parts of the catchment may have different slopes than were estimated.

3. Idealized Behavior of the Prototype Catchment: Each segment of the prototype catchment is modeled by a conceptualized process which behaves in a much simpler fashion than the natural process. Each individual drainage path could never be modeled in detail. Only the aggregate behavior of many complex processes can be represented. The model results suggest that the model has successfully aggregated these processes although some of the deviations may occur because

of the simplifications inherent in the model.

Certain kinds of physical phenomena cannot be modeled with a deterministic model. For example, trash and debris may accumulate in the drainage system and retard runoff from small storms. The behavior of storm September 3, 1965, may be explained by an obstruction of this type. The volumes of runoff expected for this storm and the volume simulated with the detailed segmentation are equal, but the runoff rates are very very different, as shown in Figure 4-16, with an obstruction near the outlet of the site, the simulated hydrograph is expected to look like the observed hydrograph.

Even though one cannot prove that such an obstruction was present during this storm, the possibility that it was present (and it explains then the observed hydrograph), is sufficient to reject the storm on one hand and to accept the simulated hydrograph as the correct response of the catchment on the other hand.

4. Infiltration and Detention : The total volume of runoff is generally smaller than the input volume of rain because of some initial detention effect and of infiltration occur- ring over the pervious segment. Modeling the losses of wa- ter is important to the simulation of a good hydrograph. Many unknowns on these water losses still persist and avail- able models are very simplified representations of complex processes.
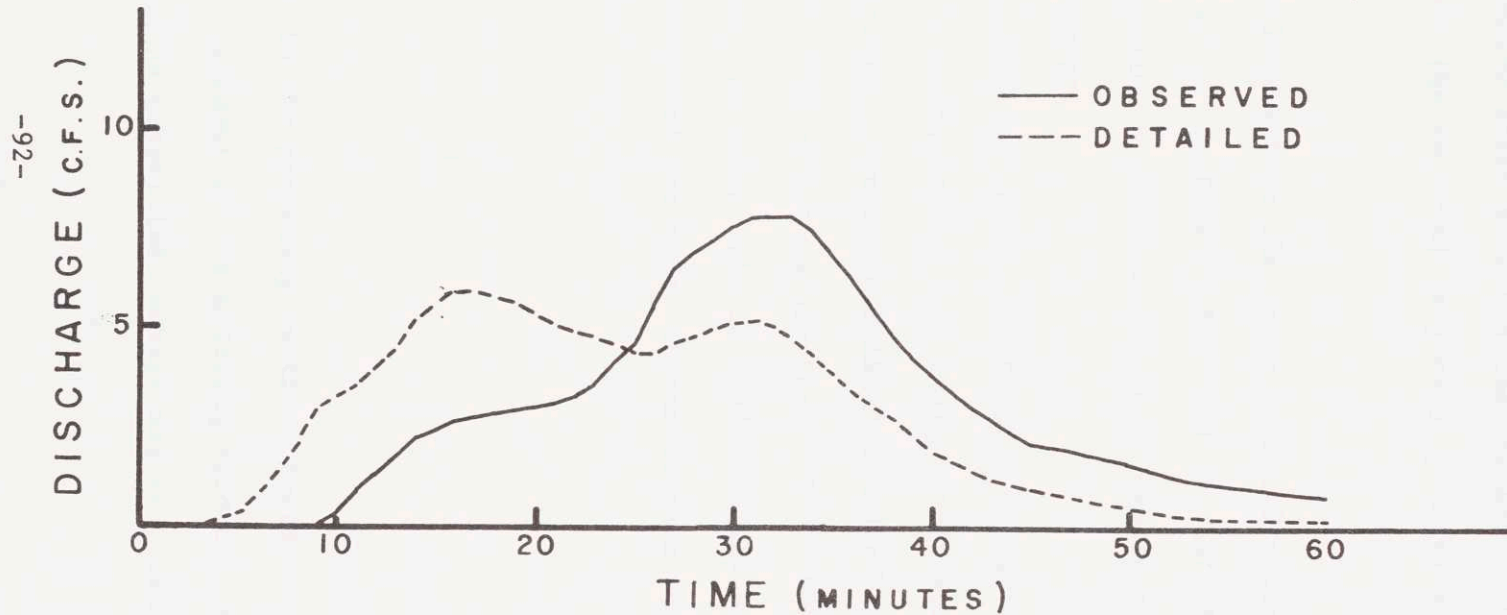
Figure 4-16: Detailed Configuration: Observed vs Simulated Hydrographs: Storm of September 3, 1965

The infiltration process for instance is modeled by the Horton's law of infiltration which is a very simplified model. Its three parameters also are not well known and are estimated after some run test to approximate the losses between the observed samples of precipitation and runoff.

It is most unlikely that the rates of infiltration experienced during a storm are those defined by the infiltration law adopted, thus causing some systematic but unknown errors in the simulated hydrograph.

The initial detention causes a retention of water which will be lost later by evaporation. The small storms are mostly sensitive to this process. In the simulated hydrographs presented so far, no initial detention is provided. If it were the simulated hydrograph for storm July 16, 1965, would be improved; the simulated hydrograph of the other storms however would not be improved.

4.4.4 Conclusion

As discussed in the preceding section, there are many uncertainties   present in the modeling effort. Some of the uncertainties cannot be quantified, others may and when they are,

-93-

the accuracy of the simulated hydrograph is expected to be
increased.

The simulated hydrographs, computed with the detailed
segmentation, are based on numerous assumptions which are appar-
ently reasonable in this case. The simulated hydrographs do re-
produce the essential features of the observed hydrographs; the
accuracy of the simulated hydrographs is high enough for the pur-
pose of this study and the detailed segmentation is adopted as
representation of the prototype catchment.

It is important to note that the only parameters which
were established on the basis of the observed runoff data were the
infiltration parameters. Even these could have been estimated a
priori on the basis of soil type. The model seems to offer a
sound physically-based explanation of the dynamic behavior of this
catchment.

4.5 Simplified Segmentation of the Catchment

4.5.1 Introduction

The detailed segmentation yields excellent simulated hydro-
graphs but is expensive to use frequently. Consequently a simpli-
fied segmentation, where the prototype catchment is modeled with as
few segments as required to preserve the principal characteristics
of the detailed simulated hydrographs, is sought. Finding a suitable
simplified model of the catchment is essential to the derivation
of runoff frequency curves which are inexpensive to simulate.

In this section, four simplified segmentations are presented
and discussed in detail for the conditions of storm June 14, 1963.
Before beginning this discussion, it is worth emphasizing the nature
of the response of the simplified segmentation with respect to the
response of the detailed segmentation.

4.5.2 Interpretation of the Simplified Segmentation.

The simplified segmentation contains fewer segments than the
detailed segmentation, and is thus less expensive to use in the routing
model. The reduction in the number of segments, however, reduces the
resolution of the hydrographs derived with the simplified segmentation.
An adequate simplified model is a trade-off between the resolution ob-
tained in the simulated hydrographs and the cost of computations.

A linear catchment is analyzed briefly to point out the ex-
pected changes that will occur when a detailed segmentation is replaced
by a simplified segmentation.

Consider the catchment and its impulse response functions illus-
trated in Figure 4-17, and consider one possible simplified segmenta-
tion of this catchment, illustrated in Figure 4-18. The time of concen-
tration of the overland flow segment, t_c, is preserved in the simpli-
fied segmentation. The impulse response function of this segmentation,
also illustrated in Figure 4-18, preserves the volume of the detailed
impulse function but starts to rise at time t=0 rather than time $t=t_p$.
It reaches the same peak magnitude and enters its recession at time
$t=t_c$ rather than time $t=t_p+t_c$ in the case of the detailed segmenta-
tion. The deformations observed in the simplified hydrograph are
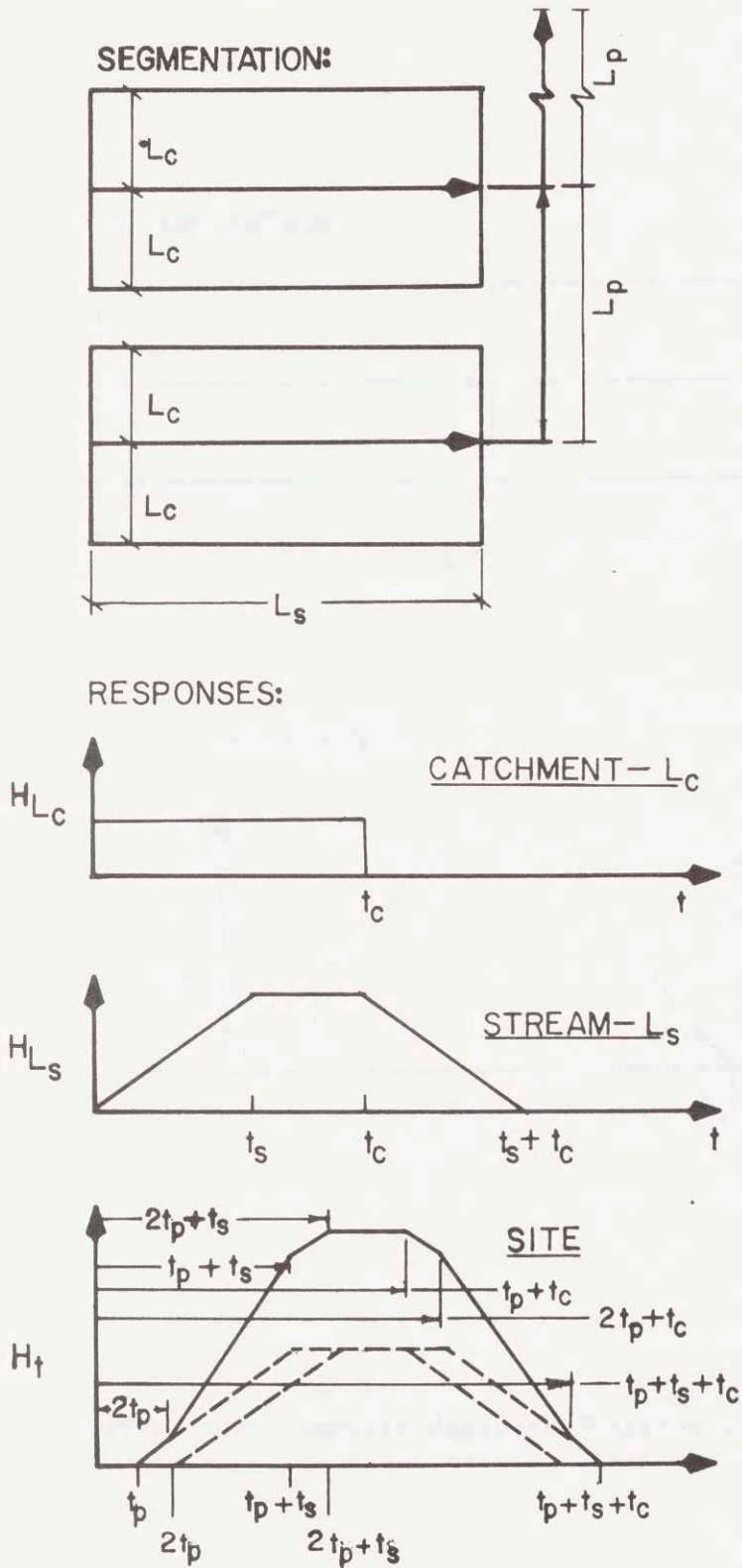
Figure 4-17: Impulse Response Function of the Detailed Configuration of a Linear Catchment

SEGMENTATION:
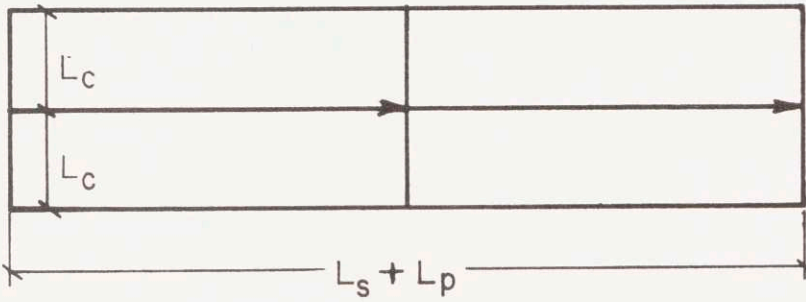
RESPONSES:
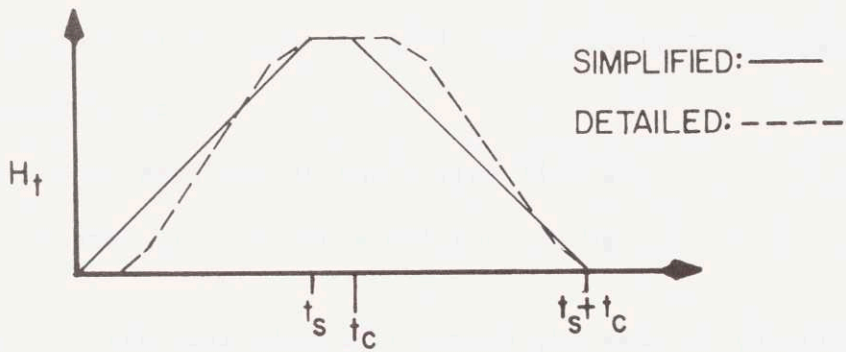
Figure 4-18: Impulse Response Function of the Simplified
Configuration of a Linear Catchment

typical   of the simplified approach.

The total duration of the impulse functions is

detailed   simplified

$$2 t_p + t_c + t_s \qquad\qquad t_c + t_{L1}$$

so that $\qquad t_{L1} = 2 t_p + t_s \qquad\qquad\qquad\qquad$ (4-13)

Since $t = \alpha L \qquad\qquad\qquad\qquad\qquad\qquad$ (4-14)

Equation 4-13 becomes

$$\alpha_{L1} = \frac{2\alpha_p L_p + L_s}{L1} \qquad\qquad\qquad (4\text{-}15)$$

which is used to estimate the α for the stream in the simplified seg-
mentation.

When the detailed segmentation is simplified, the changes most
likely to be observed are

1- a faster response of the rising limb and

2- recession limb of the simulated hydrograph

For a linear model, the peak flow will remain the same if the time t_c
is larger than the time t_s, which is usually the case.

In the following sections, the effects of the simplifications
of the model, when used in a non-linear routing model, are investigated
and four simplified configurations are developed.

4.5.3 Simplified Configuration # I

This segmentation illustrated in Figure 4-19 has a single node
where a stream is fed by two overland flow segments. One of them repre-
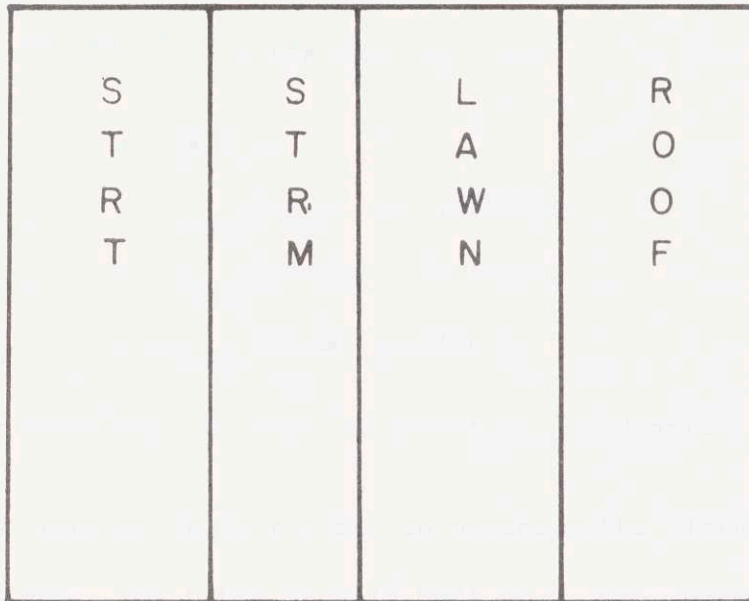
Figure 4-19: Simplified Configuration I of the Gray
Haven Detailed Configuration

sents the street; the second one represents the roof, and the per-
vious area that receives the runoff from the roof. The stream is a dis-
torted stream whose length is adjusted to preserve the overland flow
length of the street segment, and the total area. The other overland
flow segments (roof and grass) also have distorted lengths, which are
determined to preserve the total area of the roof and the grass.

The length of each segment are

$$I_{STRT} = 18.0 \text{ ft}$$

$$L_{STRM} = A_{STRT}/18.0 = 13280.0 \text{ ft}$$

$$L_{LAWN} = A_{LAWN}/13280 = 44.0 \text{ ft}$$

$$L_{ROOF} = A_{ROOF}/13280 = 15.0 \text{ ft}$$

The total area of this catchment is 23.3 acres.

A correction is introduced to preserve the timing of the simu-
lated hydrograph. The correction is made on α the parameter related
to the velocity of the flood waves; the correction is [Perkins and
Harley,1971]

$$\alpha^* = \frac{\alpha L^*}{L} \qquad (4-17)$$

where α and L are the magnitude of the undistorted element and α^*
and L^* the effective magnitude of α and L, used in the simplified
segmentation. When L* is greater than L, the flood wave is accelerated
and vice versa. The correction does not account for all of the distor-
tion introduced since the routing model is non-linear but it accounts
for its first-order effect.

Table 4-3 summarizes the data for this configuration.

Table 4-3

Parameters of the Simplified Segmentation # I

Name	L	Slope	α	L^*	α^*	m
STRT	18	0.035	2.00	18	2.000	1.67
LAWN	42	0.05	0.67	44	0.705	1.67
ROOF	30	0.035	2.00	15	1.000	1.67
STRM 1)	1700	–	5.00	13280.	39.0	1.25

1) The stream length is taken as the total length of the pipe plus the average length of a gutter.

In Figure 4-20, the simulated hydrograph for the June 14, 1963 storm, calculated for this simplified segmentation, is compared with the simulated hydrograph calculated for the detailed segmentation and with the observed hydrograph. The infiltration process is of Horton's type with f_o = 2.0 in/hr, f_c = 1.5 in/hr, and k = 0.023 minutes^{-1} . The 'simplified' hydrograph rises faster than the 'detailed' hydrograph, which is expected; the 'simplified' hydrograph has magnitudes which remain smaller than those of the 'detailed' hydrographs after time t equal to 22 minutes. Finally, the timing of the simulated hydrograph is very good, suggesting that the correction on the α is effective in reducing the distortion introduced in the segmentation.

Although the two simulated hydrographs reproduce the observed hydrograph, the location of the simulated hydrograph, after time t equal to 22.0 minutes, with respect to the detailed hydrograph raises some questions about the ability of the simplified segmentation to replace the detailed segmentation. The total outflow of water, the runoff from the site plus the volume remaining on the surface, is not equal. In the simplified segmentation, the total volume of outflow is 49,900 ft^3 , and in the detailed segmentation, the total volume is 52,600 ft.

There is therefore a loss of 2700 ft^3 in the total runoff of the site when the detailed segmentation reduces to the simplified #1 segmentation. This loss is accounted for by a larger infiltration volume in the simplified segmentation than in the detailed one; in the latter, only a fraction of the grass (LAWN) receives upstream inflow from the roof whereas in the former all of the pervious segment receives upstream inflow, causing an increase in the water infiltrated.
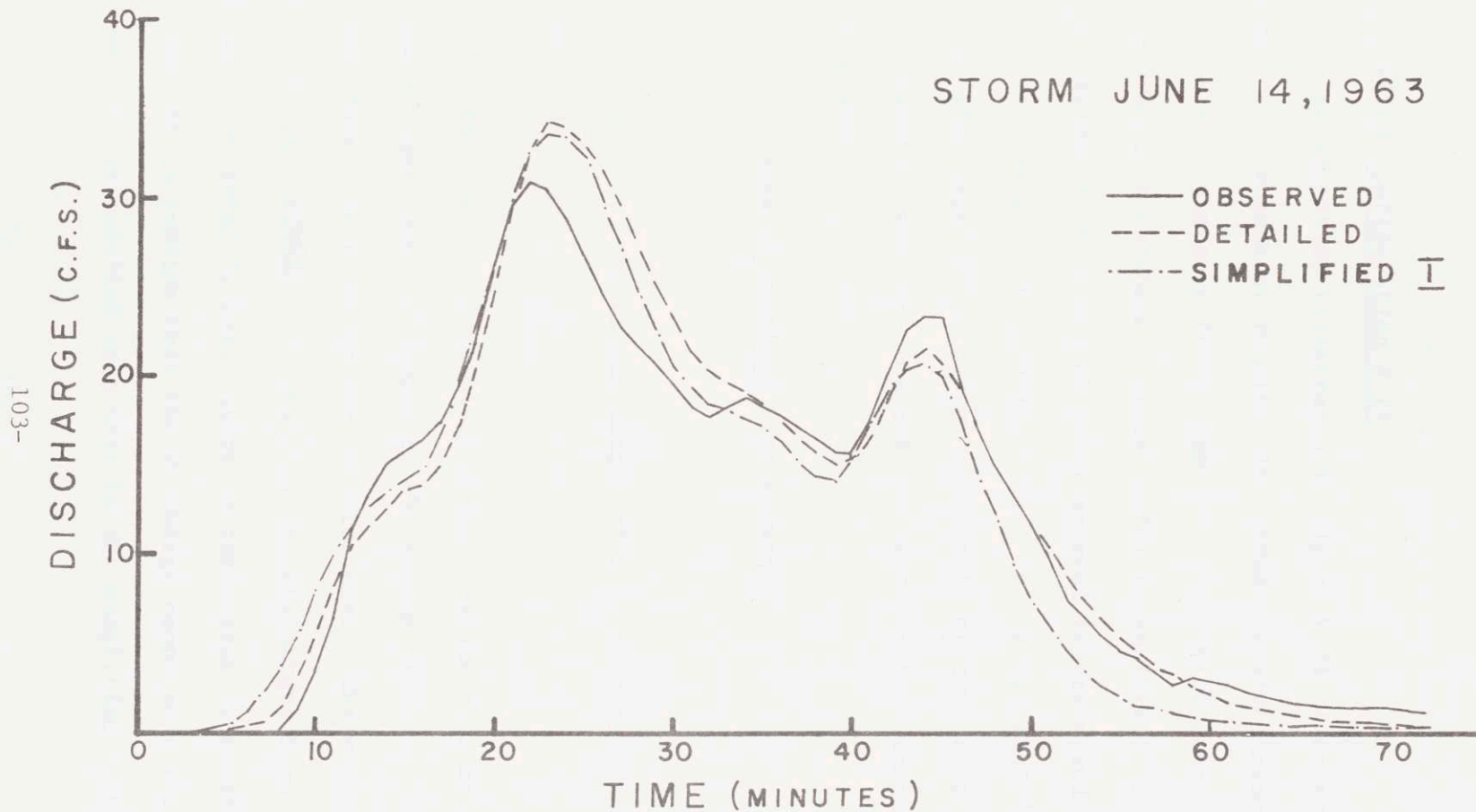
Figure 4-20: Observed Detailed and Simplified I Hydrographs: Storm of June 14, 1963

This segmentation was thus abandoned because it did not pre-serve the volume of runoff of the 'detailed' hydrograph.

4.5.4   Simplified Configuration # II

This segmentation illustrated in Figure 4-21 is created to preserve the total volume of runoff. The stream receives runoff from three overland flow segments (this segment connectivity cannot be ob-served in a prototype catchment but is useful to analyze.) In this model, the overland flow length of every segment is preserved, which preserves the volume of runoff/unit of foot of the overland flow surface.

When this approach is taken, the length of the stream that is computed to preserve both the area and the overland flow length of an overland flow segment is given by

$$L_s = \frac{\text{Area of overland flow segment}}{L_c} \qquad (4\text{-}18)$$

In Table 4-4, the stream length of each overland flow seg-ment is computed.

The lengths L_s are not equal among them and also are not equal to the average observed length of the stream taken as 1700.00 feet.

The concept of a multiplier is introduced; the multiplier of the lateral inflow, WIDTH1 ($\cdot$), modifies the discharges from each seg-ment such that the total lateral inflow to the stream is preserved. WIDTH1($\cdot$) in effect implies that the discharge computed for a unit width of one foot is modified such that in the simplified model, the
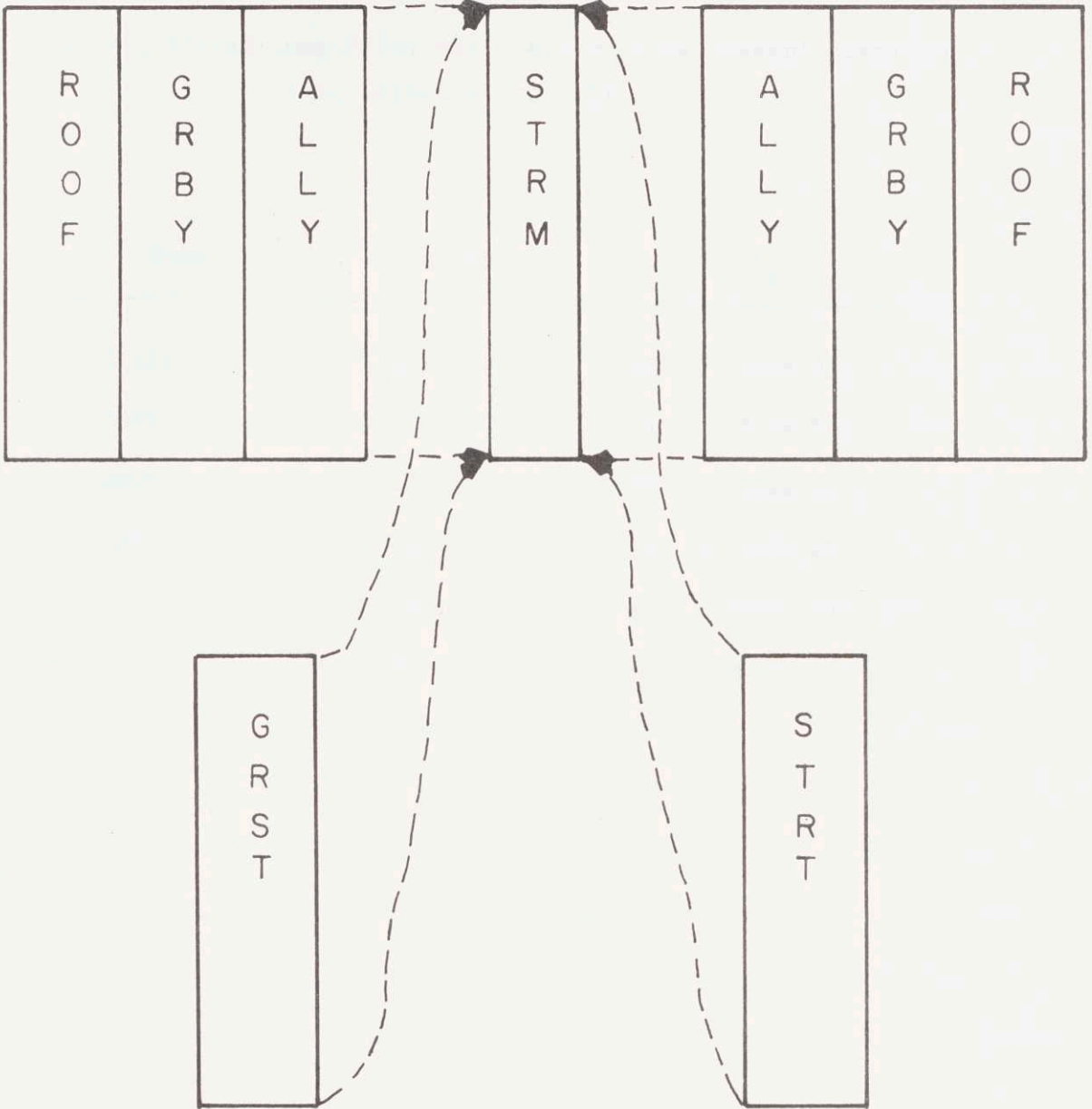
Figure 4-21: Simplified Configuration II of the Gray Haven Detailed Configuration.

Table 4-4

Initial Stream Length for the Overland Flow Segment Simpli-
fied Segmentation # II

Name	A (acres)	L_c	L_s
STREET	3.43385	18	8309.917
GRST	7.17354	42	7439.986
ROOF	4.47658	30	3249.997
GRBY	5.96877	40	3249.997
ALLY	2.23829	15	3249.997

discharge from one foot of an overland segment is equal to the discharge of WIDTH1($\cdot$) feet of the detailed segmentation. Figure 4-22 illustrates graphically the effect of the multiplier.

The total length of the initial stream is reduced by WIDTH1($\cdot$), but the discharge is increased by the same magnitude. The total volume of lateral inflow is thus preserved. Table 4-5 gives the magnitude of WIDTH1(1) for each segment.

Comparative plot of the observed, detailed and simplified # II hydrographs is shown in Figure 4-23. The simplified hydrograph, although it does not match the observed hydrograph as well as the detailed hydrograph, still reproduces the essentials of the observed hydrograph. The response of the simplified model is faster than the response of the detailed model. This is due to the non-linearity of the routing model: when the unit discharge from an overland flow segment is adjusted using WIDTH1($\cdot$), (for this model the discharge is increased), the cross-section, A, is increased. Since the flood wave celerity is a function of A, the wave moves faster in the stream channel of the simplified model than in the gutters or triangular channels of the detailed model.

The peakflow in the simplified model reaches a magnitude larger than the peakflow in the detailed model because water at the outlet of the site is piling up faster in the simplified than in the detailed model since the flood wave in the former is faster than in the latter model. Consequently, to satisfy continuity, the hydrograph recedes also faster in the simplified than in the detailed model.

-107-

2.0 FT.

DETAILED
(WIDTH(·)=1)

1 FT.
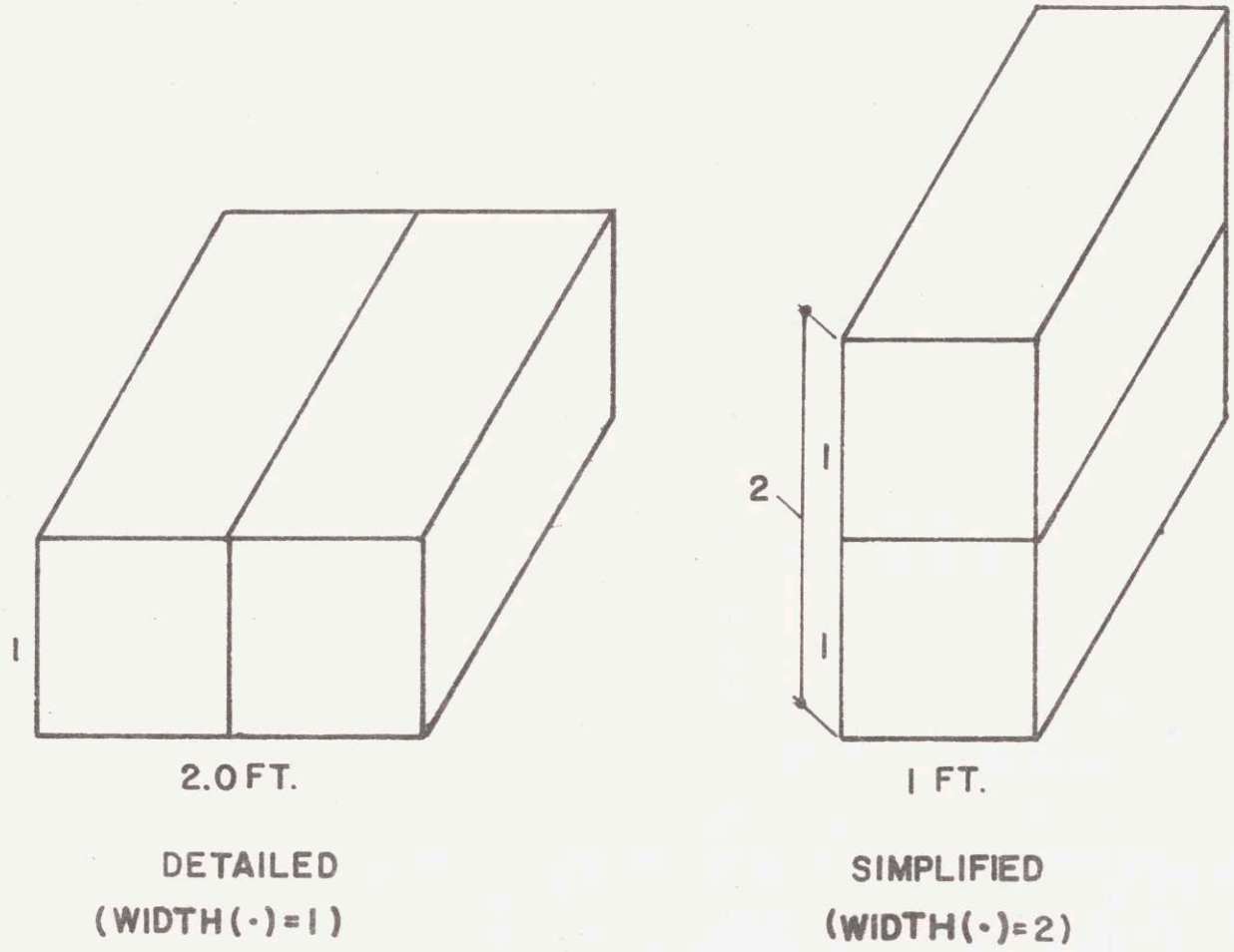
SIMPLIFIED
(WIDTH(·)=2)

Figure 4-22: Illustration of the Effect of the Multiplier

Table 4-5

Multiplier WIDTH1($\cdot$) and Parameters of the Simplified
Configuration # II

NAME	L	α	m	WIDTH1($\cdot$)
STREET	18	2.00	1.67	4.888
GRBY	42	0.67	1.67	4.376
ROOF	30	2.00	1.67	1.000
GRBY	45	0.67	1.67	1.000
ALLY	15	2.34	1.67	1.9117
STRM	1700	5.00	1.25	--
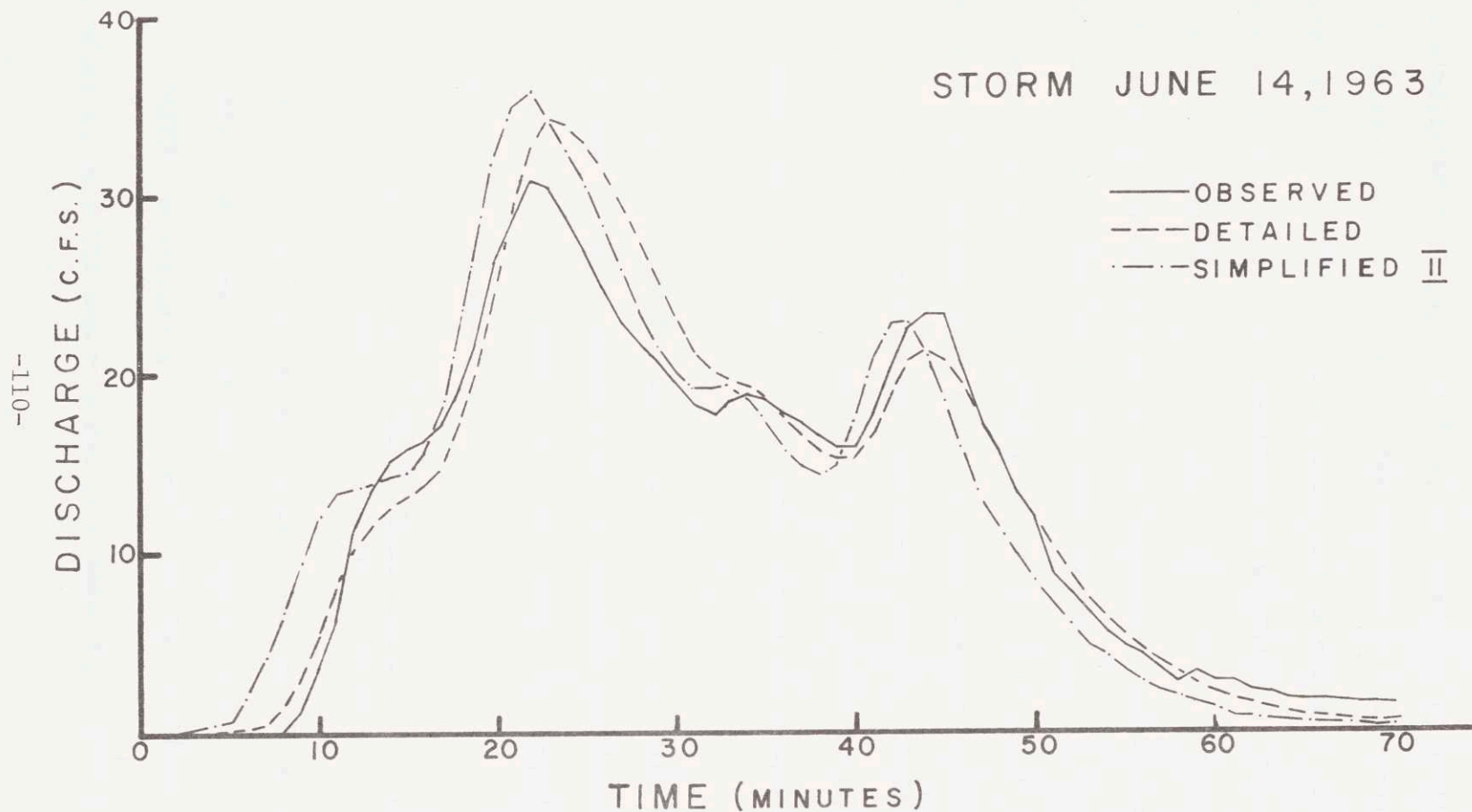
Figure 4-23: Observed, Detailed and Simplified II Hydrographs:
Storm of June 14, 1963

4.5.5 Simplified Configuration # III

The simplified configuration # III is developed to preserve the flood wave celerity in the channel. The concept of a multiplier on the lateral inflow WIDTH1($\cdot$) is retained and extended to the upstream inflow where the multiplier is identified by WIDTH2($\cdot$). Figure 4-24 illustrates the simplified configuration # III created for Gray Haven. Table 4-6 presents the magnitudes of the length, L, and of the multiplier, WIDTH1($\cdot$) and WIDTH2($\cdot$) for each segment.

In the configuration, WIDTH1($\cdot$) is retained to slightly correct the unit width of a segment such that its total area is preserved and that it fits to the stream element. The grass segment, STGR, which feeds the gutter, requires a WIDTH($\cdot$) different from 1.00 but the correction is small and will not significantly modify the response of the gutter segment.

The lengths of the gutter and of the lane are averages of the respective lengths of these segments in the detailed configuration. Once these lengths are determined, the multipliers are computed. For instance WIDTH2(GUTR) is equal to

$$\text{WIDTH2(GUTR)} = \frac{A_{STRT} \ 43560}{L(STRT) \ \ WIDTH1(STRT) \ \ L(GUTR)} \qquad (4-19)$$

where A_{STRT} is the total area of street overland flow (acres)

L(STRT) the street overland flow length   (ft)

L (GUTR) the average gutter length in the prototype

Configuration # III neglects the pipe network, implying that

-111-
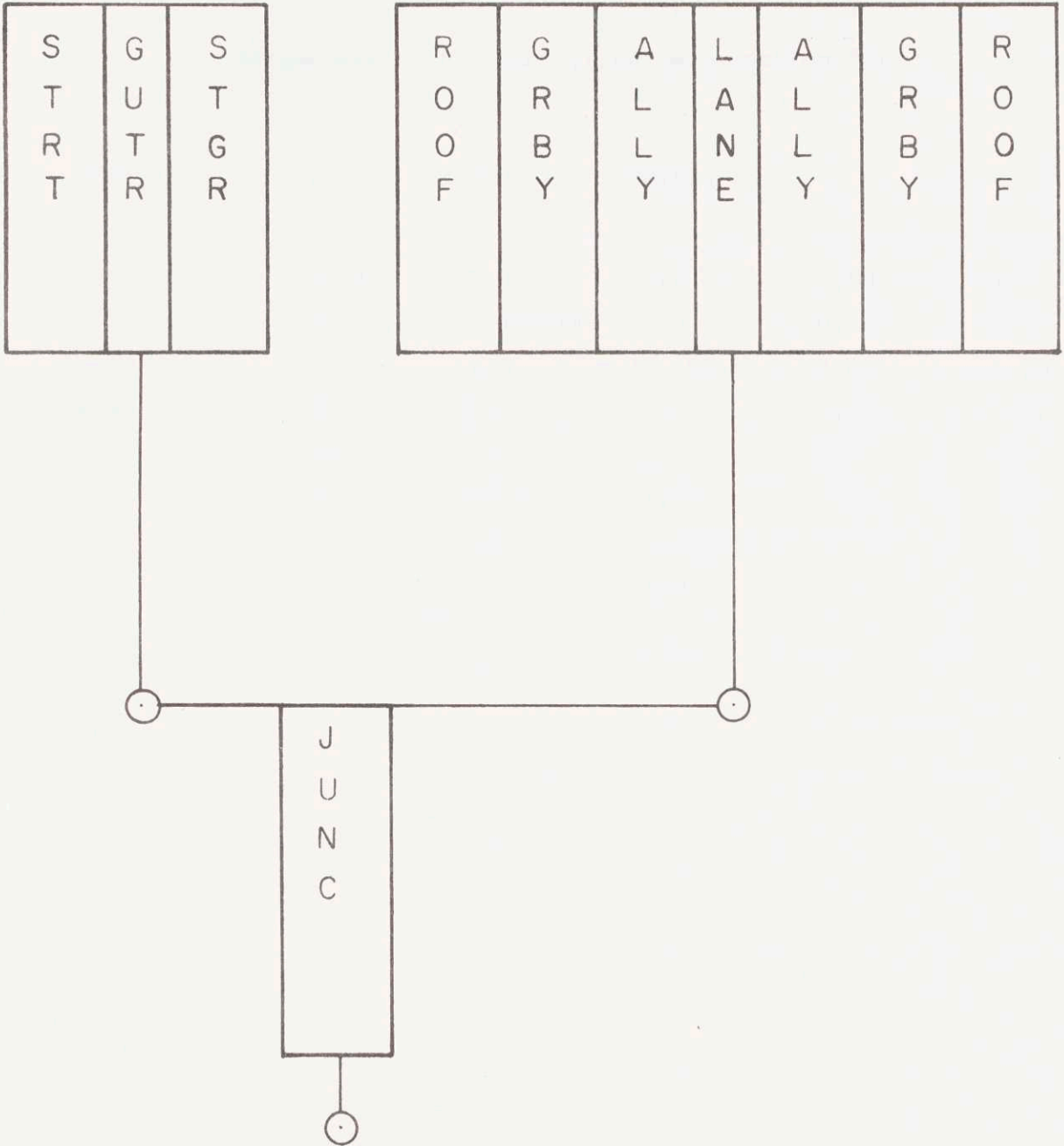
Figure 4-24: Simplified Configuration III - IV of the
Gray Haven Detailed Configuration

Table 4-6

Parameters of the Simplified Segmentation #III

NAME	L	WIDTH1($\cdot$)	WIDTH2($\cdot$)	α	m
STRT	18.0	1.0	1.0	2.00	1.67
STGR	42.0	0.895314	1.0	0.67	1.67
GUTR	450.0	1.0	18.46648	2.015	1.33
ROOF	30.	1.0	1.0	2.00	1.67
GRBY	40.	1.0	1.0	0.67	1.67
ALLY	15.	1.0	1.0	2.34	1.67
LANE	410.	1.0	7.926822	1.725	1.33
JUNC	–	1.0	1.0	–	–

its response is quick enough such that it may be taken as instantaneous which causes the WIDTH2(GUTR) and WIDTH2(LANE) to be large. This configuration implies that 18.446 nodes 1 and 7.927 nodes 2 are juxtaposed and that they are all directly connected to the outlet of the site.

For the June 14, 1963 storm, the 'simplified' runoff hydrograph is compared, in Figure 4-25, to the observed and detailed hydrographs. The response of the simplified catchment is still too fast, although it is slightly slower than the response of simplified model # II. The simplified model # III can be altered to give simplified model # IV which is a combination of the previous two simplified models.

4.5.6 Simplified Configuration # IV

This configuration retains the multipliers WIDTH1(·) and WIDTH2(·) and accounts for an average length of 'gutter-pipe' flow as does the simplified model # II. The schematic representation of this model is identical to the one shown in Figure 4-24, representation used for simplified model # III. The differences between the two models are observed in the lengths of the 'stream' segments. Table 4-7 summarizes the data for this simplified configuration.

Figure 4-26 illustrates the goodness of the fit between the observed, detailed and simplified hydrographs for storm June 14, 1963. The simplified matches very well the detailed hydrograph, which is the most that can be asked from it.

This simplified configuration is adopted to model the prototype

STORM JUNE 14,1963

——— OBSERVED
– – – DETAILED
–·–·– SIMPLIFIED $\underline{\mathrm{III}}$
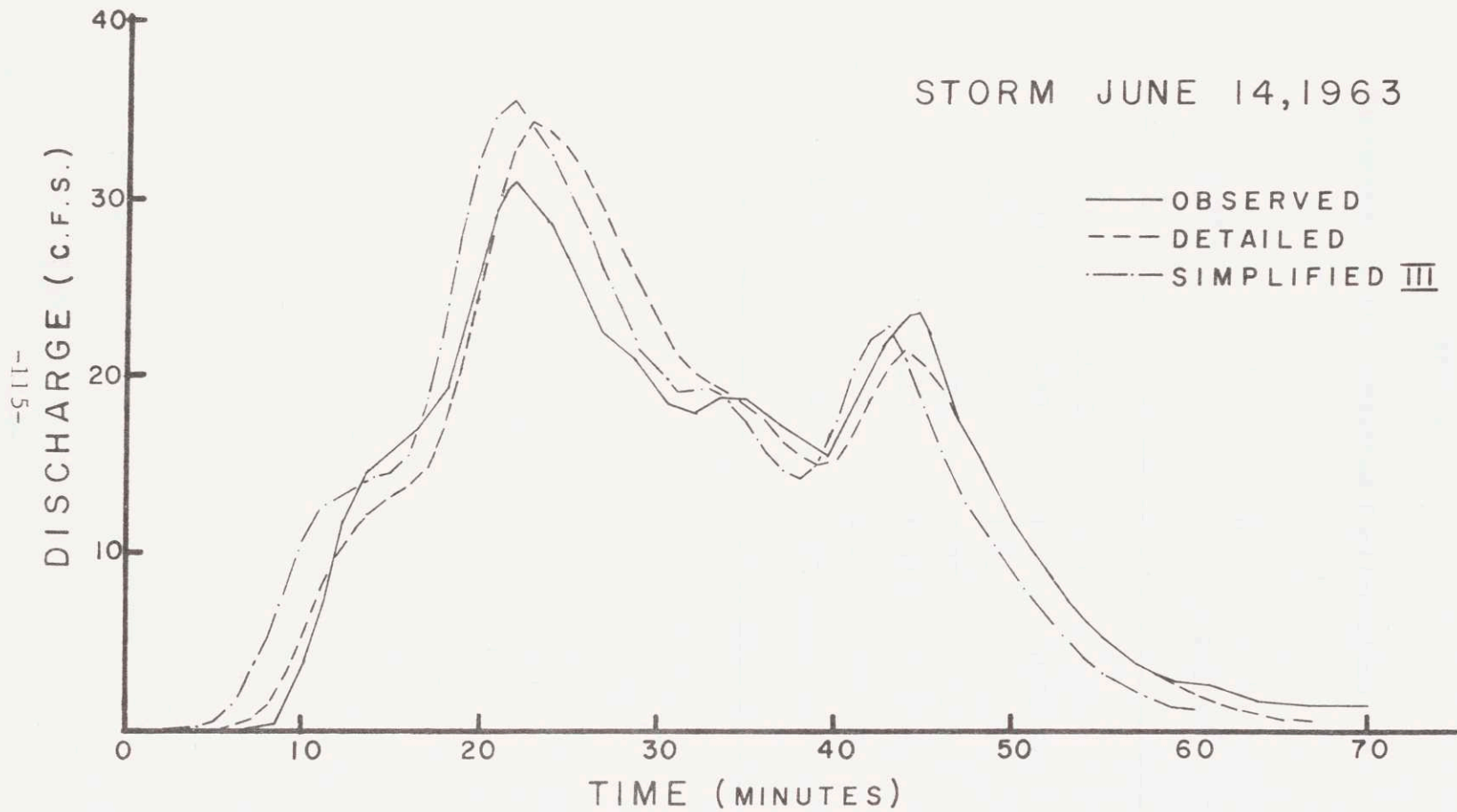
Figure 4-25: Observed, Detailed and Simplified III Hydrographs: Storm of June 14, 1963

Table 4-7

Parameters of the Simplified Configuration #IV

NAME	L (feet)	α	m	Multipliers WIDTH1(·)	WIDTH2(·)
STRT	18	2.00	1.67	1.0	1.0
GRST	42	0.67	1.67	0.92179	1.0
GUTR	1700	5.00	1.25	1.0	4.88188
ROOF	30	2.00	1.67	1.0	1.0
GRBY	40	0.67	1.67	1.0	1.0
ALLY	15	2.34	1.67	1.0	1.0
LANE	1700	4.00	1.25	1.0	1.91176
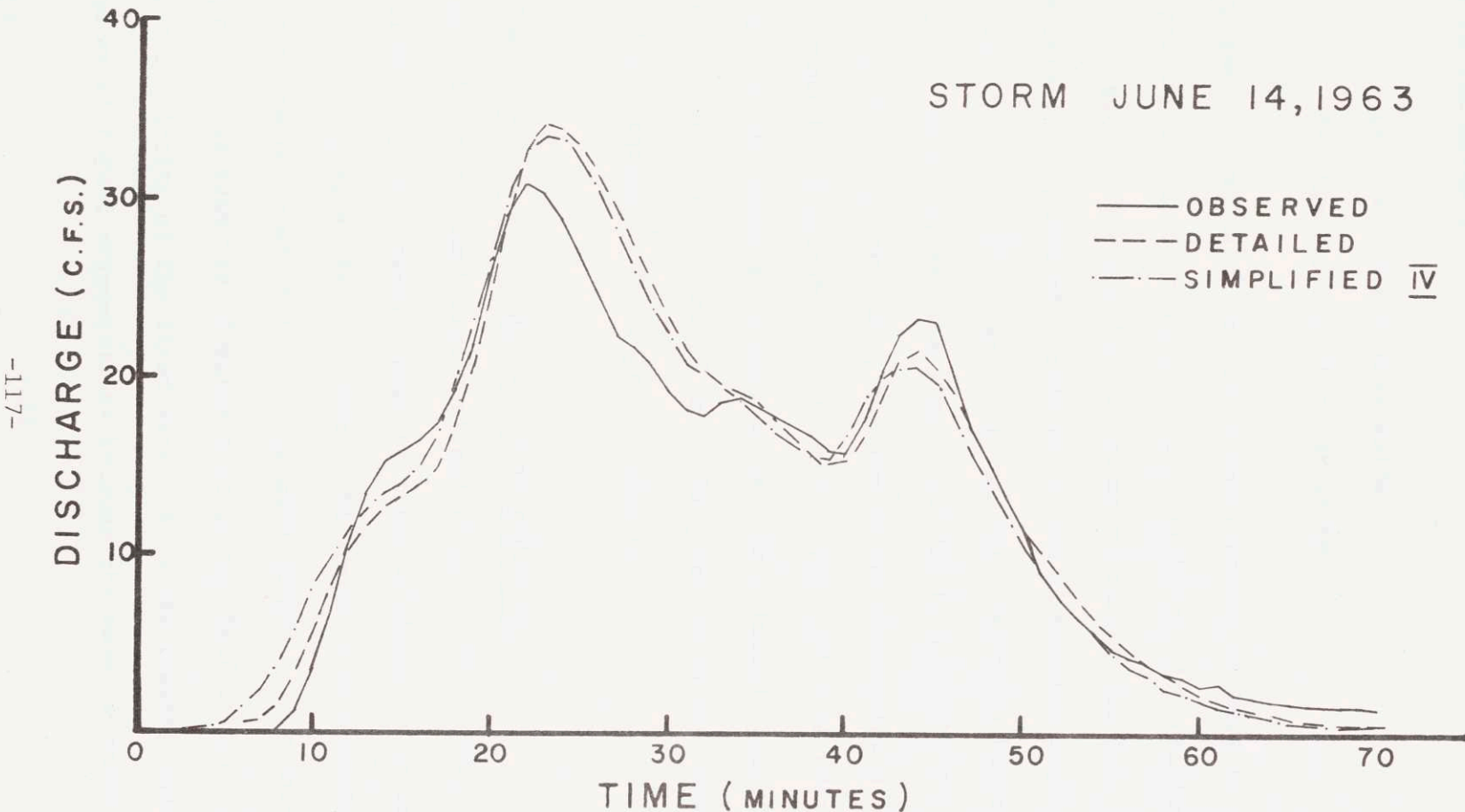
Figure 4-26: Observed, Detailed and Simplified IV Hydrographs: Storm of June 14, 1963

catchment not only on the basis of the June 14, 1963 storm simulation but also on the basis of:

1- its theoretical value

2- the results of other storms.

Its theoretical value is highly satisfactory because it accounts for the principal characteristics of the catchment, for the length of the pipe and gutter flow and for the volume of runoff which is preserved when the detailed segmentation reduces to the simplified segmentation.

Figures 4-27 to 4-30 present a graphical comparison between the observed, the detailed, and the simplified #IV hydrographs for the other selected storms. In every case, the simplified segmentation leads to simulated runoff hydrographs that reproduce very well the hydrographs simulated with the detailed segmentation. This indeed validates the simplified model of the detailed model for Gray Haven and shows that the modeling strategy is feasible and practical.

4.5.7 Some Notes on the Simplified Configurations

The different simplified configurations analyzed lead to different simulated hydrographs. Some of these differences occurred because the routing model is non-linear. Different configurations lead to different patterns of inflow to the main stream. In a non-linear routing model the quantity of water that is received by the main stream governs the velocity of the flood wave. A linear routing model is not affected by different segmentations because the wave velocity is a
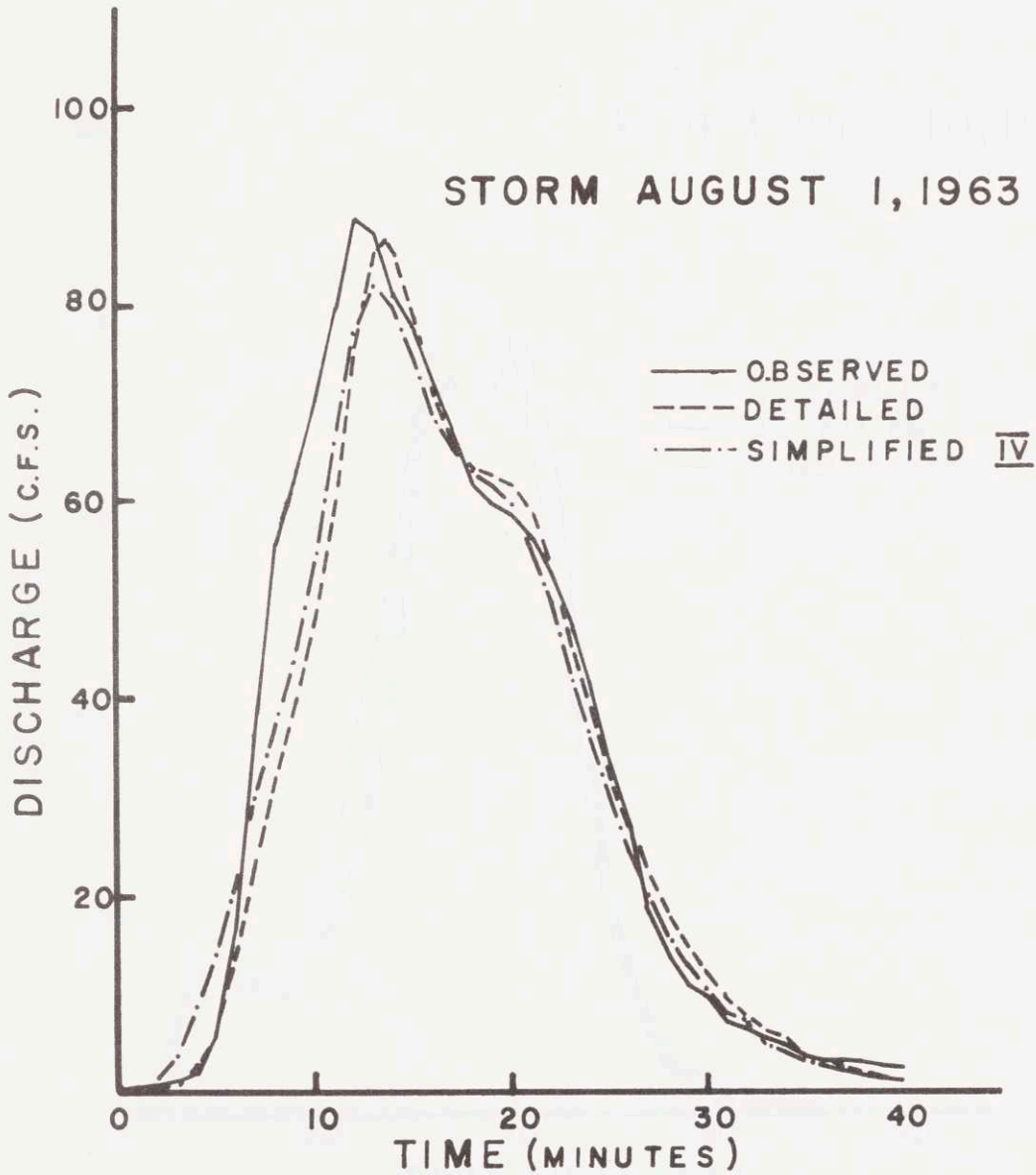
Figure 4-27: Observed, Detailed and Simplified IV Hydrographs:
Storm of August 1, 1963
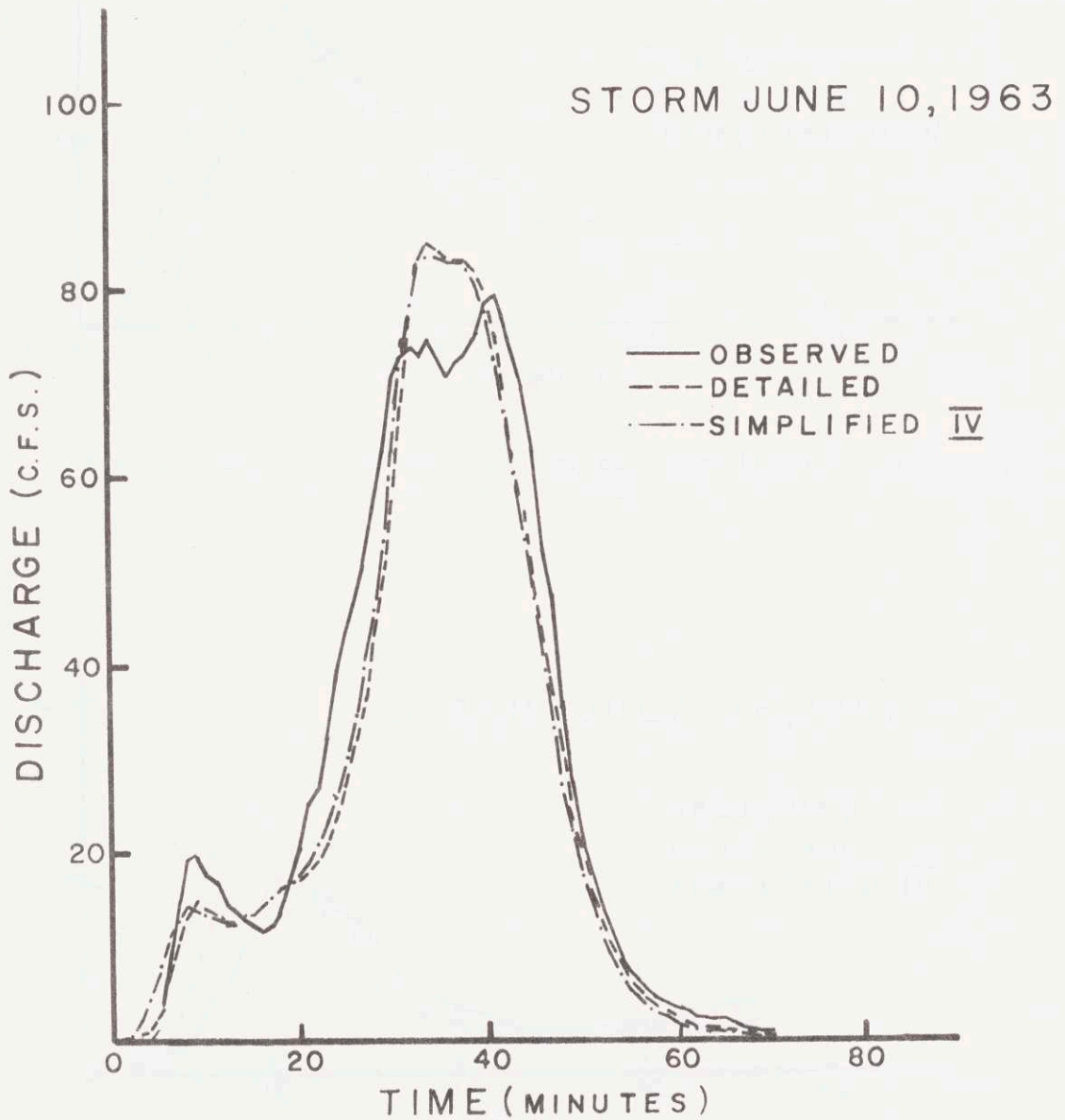
Figure 4-28: Observed, Detailed and Simplified IV Hydrographs: Storm of June 10, 1963
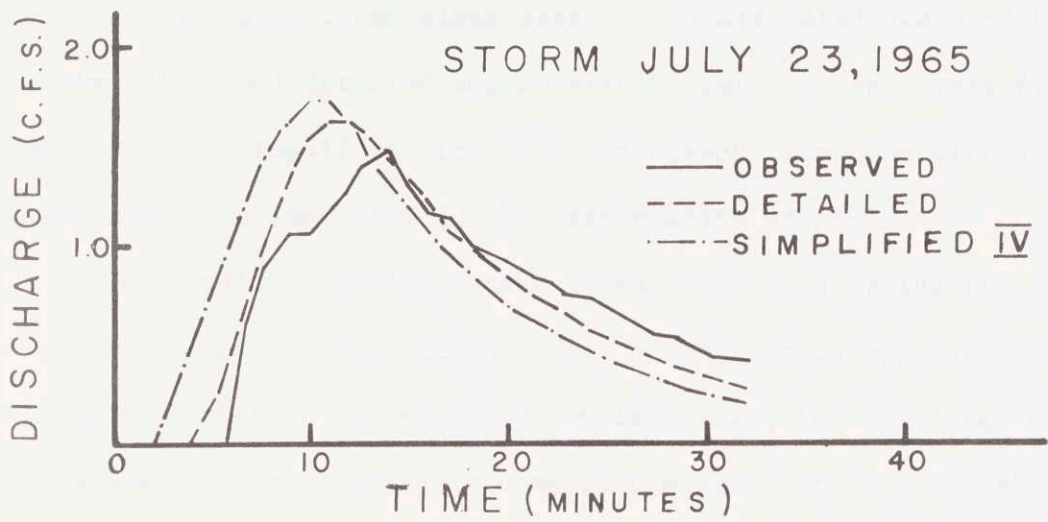
Figure 4-29:   Observed, Detailed and Simplified IV Hydrographs:
Storm of July 23, 1965
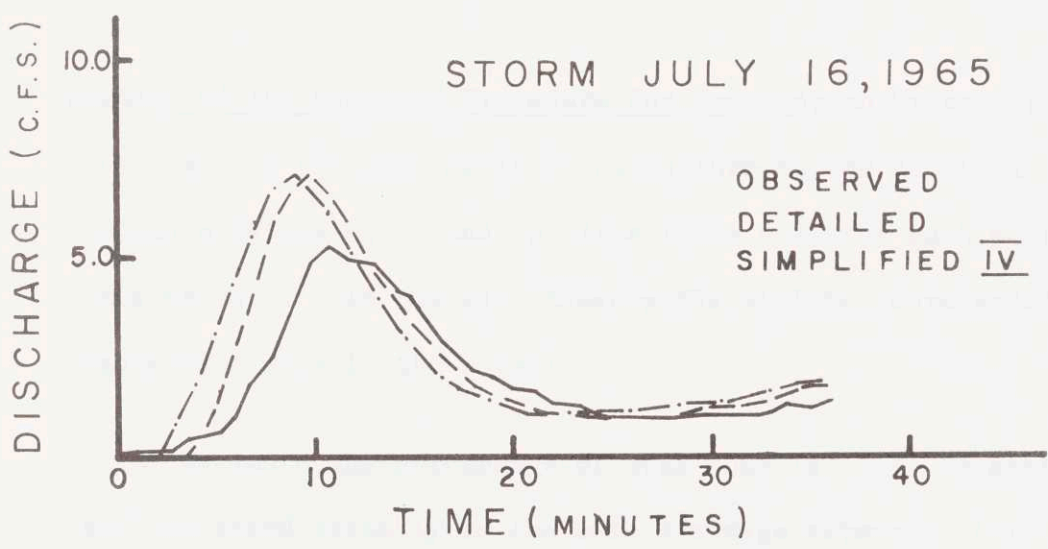
Figure 4-30:   Observed, Detailed and Simplified IV Hydrographs:
Storm of July 16, 1965

constant, not a function of the depth of flow in the segment.

Figure 4-31 illustrates the evolution of the simulated simpli-
fied hydrographs. As the segmentation is modified to reduce the ve-
locity of the 'simplified flood wave', the simulated hydrographs of
the simplified and detailed segmentations get closer. This figure
shows that the simplified simulated hydrograph, computed with a non-
linear model, is sensitive to the segmentation adopted.

The simplified configuration IV is adopted to derive the runoff
frequency curves for Gray Haven. This configuration reproduces very
well the behavior of the detailed configuration, for the large and
intermediate storms. As the storms become less intense, the effect
of the simplifications become more pronounced, but the simulated hydro-
graphs reproduce well the 'observed' ones because the absolute error are
small.

4.6 Summary of the Proposed Procedure for Modeling an Urban Catchment

(i) Lay-out the main drainage paths through the catchment and
estimate values of α and m (see Table 4-2) for each part of
this network. (In the end, these paths will be represented in
aggregated ways in the model).

(ii) Estimate the percentage of area that is (i) impervious
and connected directly to the main drainage network, (ii) per-
vious and (iii) impervious but flows over pervious areas before
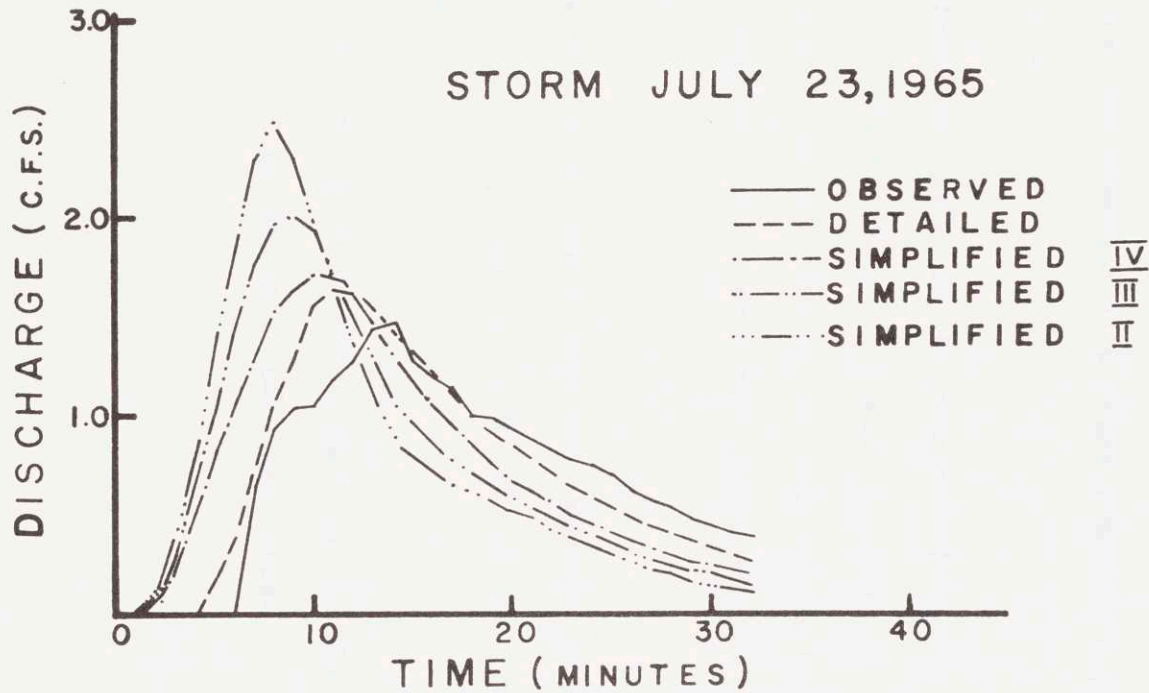
Figure 4-31: Observed, Detailed and Simplified II, III, IV Hydrographs: Storm of July 23, 1965

reaching the drainage network.

(iii) For each category of surface in (ii) above, determine
typical overland flow lengths and values of α and m.
(See Table 4-5). If the overland flow lengths or the values
of α vary widely from place-to-place (for any one type
of surface) more than one overland flow segment may be required
for that surface type.

(iv) Prepare a simplified model of the catchment based on
the ideas presented in Section 4.5 This will involve (i) a
simplified stream network of only one or two main stream bran-
ches (ii) and a simplified catchment-stream configuration simi-
lar to Figure 4-24.

(v) Overland flow multipliers (see Table 4-7) must be computed
to preserve the runoff volumes derived from each of the over-
land flow segments.

(vi) Check to see that total surface area implicit in the
simplified model is equal to the total catchment area.

4.7 Summary and Conclusion

In this chapter, the concepts of a modular description of a catchment have been presented; a routing model has been chosen and the equations to estimate its parameters developed. A detailed segmentation was used to simulate the runoff of the site segmentation that has been simplified. It was shown that the detailed and simplified segmentations lead to simulated hydrographs which adequately reproduce the observed hydrographs. Finally, a simplified segmentation was adopted to simulate the runoff of this site in the derivation of the runoff frequency curves.

The simplified configuration # IV is physically sound and economical to use. A reduction of 75% in the computational cost of simulating the rainfall-runoff of the site is obtained when the detailed segmentation reduces to the simplified segmentation # IV, and no significant loss of accuracy in the results is observed.

The objective of the modeling procedure is met with the segmentation adopted.

CHAPTER 5

ESTIMATION OF INFILTRATION RATES

One of the important problems in modeling urban runoff
is to estimate the rate of infiltration during different storm events.
These rates vary from storm to storm as the result of changes in the
soil moisture conditions and as the result of variations in the amounts
of water available for infiltration during each storm. The actual
rate of infiltration at any time and location in the catchment may be
represented by the function $\psi(x,y,t)$. There is no way to measure
$\psi(x,y,t)$ directly. At best, it is possible to make inferences about
certain special properties of $\psi(x,y,t)$ on the basis of rainfall and
runoff measurements. (For example, the total volume of infiltration,
$\iiint \psi(x,y,t)\, dx\, dy\, dt$, may be estimated as the difference between the
total volumes of measured rainfall and runoff).

The function of an infiltration model is to represent
certain variations of $\psi(x,y,t)$. Examples of infiltration models are
Horton's Equation [1940] and a model suggested by Holtan [1961]
which was revised by others [Huggins, L.F., and E.J. Monke, 1966].
Each of these infiltration models contains certain parameters, some
of which may vary from storm to storm. One way to characterize in-
filtration rates is in terms of the numerical values of the parameters
of these models.

Parameter estimation theory offers a number of techniques

-126-

for estimating numerical values of hydrologic model parameters. Certain of these techniques such as the methods of least squares and multiple regression have been widely used in hydrology. Other techniques such as filter theory [Jazwinski, 1970] have not been applied to hydrologic problems. In any case no estimation technique seems to have been applied in a systematic way to the estimation of infiltration rates during observed storms on gaged catchments.

This chapter considers the possibility of applying filter theory techniques to the estimation of infiltration parameters for individual storm events. First, a filter theory model is presented. Then two hypothetical examples serve to illustrate the application of the technique; and finally, the technique is applied to the estimation of infiltration parameters for some observed storm events at Gray Haven, near Baltimore, Md.

The application presented in this chapter was made as simple as possible to illustrate certain issues. Among these simplifications is the use here of linear hydrologic models and the derivation of the parameter estimation equations in terms that take advantage of certain special properties of the linear models. No attempt is made, therefore, to show that filter theory also applies to non-linear models. Since filter theory does indeed apply to non-linear as well as linear models, it is potentially a very valuable tool for a broad range of hydrologic estimation problems. One good exposition on the general topic of filter theory may be found in Jazwinski [1970].

5.1 The Estimation Problem.

The actual rate of infiltration $\psi(x,y,t)$ varies spatially and temporally during a storm. Since there is no way to measure $\psi(x,y,t)$ it only is possible to make inferences about $\psi(x,y,t)$ on the basis of measurements of rainfall, runoff and assumptions about the physical processes of infiltration and direct surface runoff. It will be shown in this chapter that filter theory offers not only a quantitative basis for estimating certain properties of $\psi(x,y,t)$, but also for estimating the covariance of the estimation errors as well.

The specific problem now to be addressed is to estimate $\psi(t)$, the spatial average of $\psi(x,y,t)$ over the pervious area of the catchment. Let $\hat{\psi}(t)$ denote the estimate of $\psi(t)$.

The place of a filter theory model (FTM) in computing $\hat{\psi}(t)$ is illustrated in Figure 5-1. Information required by a FTM includes measurements of rainfall, $\tilde{P}(t)$, and surface runoff, $\tilde{Q},(t)$ and mathematical models of the direct surface runoff, DSRM, and infiltration, IM, processes. There are numerous ways to create a FTM on the basis of the same DSRM and information inputs, IM $\tilde{P}(t)$ and $\tilde{Q}(t)$. According to Figure 5.1, $\hat{\psi}(t)$ depends on such information inputs as well as on the FTM. From this the important conclusion follows that different infiltration estimates could be made for the same storm event, depending on the selection of the DSRM, IM, and FTM. Whether the differences between the different values of $\hat{\psi}(t)$ are of practical significance remains to be seen.

NATURAL UNIVERSE

$P(x,y,t)$

REAL
CATCHMENT

$\downarrow(x,y,t)$

$Q_{ground}(t)$

$Q_{direct}(t) +$ $Q\ stream(t)$

SYMBOLIC

RAINGAGE
NETWORK

STREAM
GAGE

REPRESENTATION

$\tilde{P}_1(t)$ $\tilde{P}_n(t)$

$Q_{meas}(t)$

AVERAGE
RAINFALL
COMPUTATION

HYDROGRAPH
SEPARATION

$\tilde{\hat{Q}}_{ground}(t)$

$\tilde{P}(t)$

$\tilde{Q}(t)$

Direct Surface
Runoff Model
(D.S.R.M.)

FILTER THEORY

MODEL

(F.T.M)

$\hat{\downarrow}(t) =$
Estimated Spatial
Average of $\downarrow(x,y,t)$
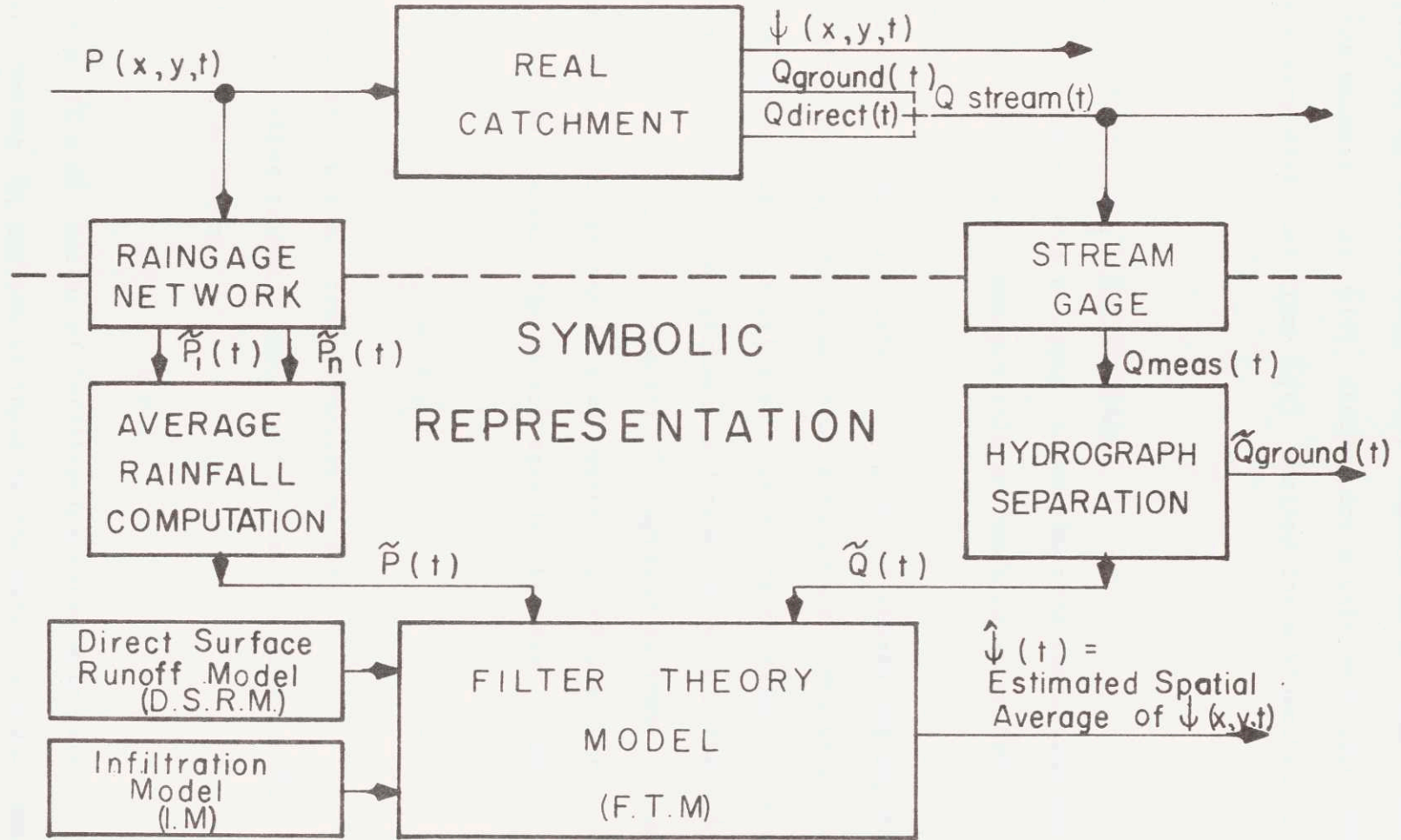
Infiltration
Model
(I.M)

Figure 5-1: The General Infiltration Estimation Problem

Nevertheless, it is notable that $\hat{\psi}(t)$ depends on the DSRM which implies, for example, that $\hat{\psi}(t)$ derived for a unit hydrograph DSRM is possibly very different from $\hat{\psi}(t)$ derived for a kinematic wave DSRM.

5.1.1 A Linear Hydrologic System Model.

There are many ways to apply filter theory in the estimation of hydrologic parameters. One possible approach is suggested in this section.

The linear DSRM illustrated in Figure 5-2 represents separately the pervious and impervious areas of a catchment. Measured rainfall is represented by P, a $(1 \times n)$ row vector of rainfall values averaged spatially over the catchment and temporally over the sampling time interval $t, t+\Delta t$. Vector P, applied as input to the impervious area, leads to the $(1 \times m)$ vector Q_1 of direct runoff from the impervious area. The linear relation between P and Q_1 is

$$Q_1 = P\, H_1 \qquad\qquad (5\text{-}1)$$

where H_1 is an $(n \times m)$ transformation matrix.

The effective rainfall input to the pervious area is the $(1 \times n)$ vector R. where

$$P = \psi + R \qquad\qquad (5\text{-}2)$$

and ψ is a $(1 \times n)$ vector of infiltration rates which are to be estimated. Vector R, applied as input to the pervious area, leads
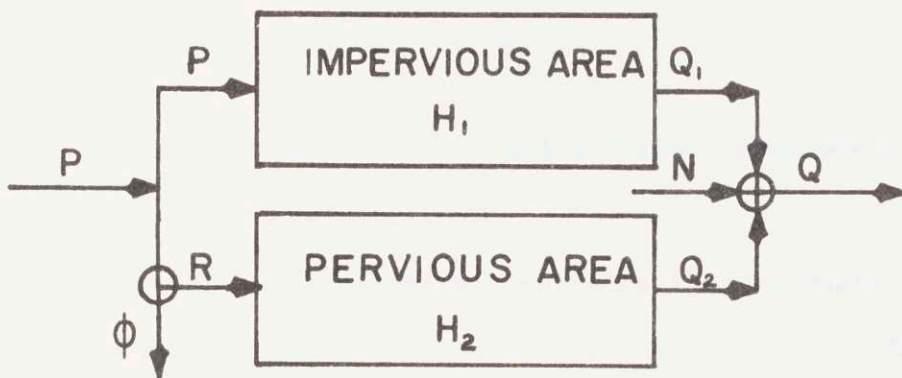
Figure 5-2:   Linear Direct Surface Runoff Model

to the (1 x m) vector Q_2 of direct runoff from the pervious area. The linear relation between R and Q_2 is

$$Q_2 = RH_2 \qquad\qquad (5-3)$$

where H_2 is an (n x m) transformation matrix.

The observed runoff from the catchment is represented by Q which is related to Q_1 and Q_2 as

$$Q = Q_1 + Q_2 + N \qquad\qquad (5-4)$$

where N is a (1 x m) vector of random "noise" components. The covariance of N is the matrix $\hat{N}$.

Vector N is a composite error term that accounts for many factors that cause Q to differ from the sum $Q_1 + Q_2$. Among these are:

    (i)   the linear DSRM is only an approximation to the actual catchment;

    (ii)   the input $P(x,y,t)$ to the actual catchment is an un-known, complex, spatially and temporally varying pattern of rainfall intensity whereas the input to the DSRM is derived by a measurement process from $P(x,y,t)$.

    (iii)   Vector Q differs from actual runoff values owing to errors of streamflow measurement.

These and other possible errors may have been modeled separately, but they are lumped together into the single error vector N.

Vector ψ may further be expressed in terms of certain basis

vectors as

$$\psi \;=\; \psi_* B \tag{5-5}$$

where B is an (r x m) matrix of basis vectors. There are r basis vectors in B and ψ_* is a (1 x r) vector of infiltration parameters. An example application of Eq. 5-5 is presented in Section 5.1.2 to the case where infiltration rates are assumed to follow Horton's equation.

Given P, Q, H_1, H_2, B and N , the problem to be solved by the FTM is to calculate $\hat{\psi}_*$ and E , the error covariance of $\hat{\psi}_*$. Before applying filtering theory, however, it first is necessary to rearrange the DSRM equations. Let

$$F \;=\; P(H_1 + H_2) - Q \tag{5-6}$$

$$G \;=\; BH_2 \tag{5-7}$$

and

$$\tilde{N} \;=\; -N \tag{5-8}$$

Then, (5-1) to (5-8) imply that

$$F \;=\; \psi_* \, G + \tilde{N} \tag{5-9}$$

The approach now is to estimate ψ_* by operating on F with a filter, L, to form the estimate

$$\hat{\psi}_* \;=\; FL \tag{5-10}$$

The filter L is an m x r matrix.   There exist several methods to determine L.   Three different methods are presented in Section 5.2.   Then, the method in Section 5.2.2 will be applied (i) to two

hypothetical examples in Section 5.3 and (ii) to the estimation of infiltration parameters for some observed storm events at Gray Haven, near Baltimore, Md.

5.1.2 An Example Model of Infiltration

One of the models that might be used to represent the variation with time of the average infiltration rate over the pervious areas of a catchment is Horton's Equation.

$$ f = f_c + (f_o - f_c) e^{-kt} \tag{5-11} $$

At discrete instants of time, $t_i = i\Delta t$, the infiltration rate is

$$ f_i = f_c b_{1i} + (f_o - f_c) b_{2i} \tag{5-12} $$

where

$$ b_{1i} = 1 \tag{5-13a} $$

and

$$ b_{2i} = e^{-kt_i} \tag{5-13b} $$

Let

$$ \psi = [f_1, \ldots, f_i, \ldots, f_n] \tag{5-14a} $$

$$ B = \begin{bmatrix} b_{1i}, \ldots, b_{1i}, \ldots, b_{1n} \\ b_{21}, \ldots, b_{2i}, \ldots, b_{2n} \end{bmatrix} \tag{5-14b} $$

$$ \psi_* = [f_c, f_o - f_c] \tag{5-14c} $$

If Eq. (5-14) were substituted into Eq.(5-5), Eq.(5-12) would be satisfied at each instant, t_i.

The numerical examples which appear in Sections 5.4 utilize the above infiltration model. Note that the value of k must be given but that the parameters f_c and $f_o - f_c$ are to be estimated from the rainfall runoff data. If k were also to be estimated, the problem would become non-linear and the linear theory presented in this chapter would not apply. In a practical application different values of k might be assumed in Eq. (5-13b). Then, the value of k which gives the smallest trace of $\mathbb{E}$ might be taken as the best estimate of k.

5.2 Estimation of ψ_*.

In this section three different procedures for finding L in Eq.(5-10) will be presented The second of these will be used in the numerical examples which follow in Sections 5.3 and 5.4.

5.2.1 Regression Approach

The traditional regression approach for estimating ψ_* is to select ψ_* so that the variance of

$$\tilde{n}_i = \hat{f}_i - f_i \qquad (5-15)$$

is minimized where f_i and $\hat{f}_i$ are the ith elements of vectors F and $\hat{F}$ respectively. Vector $\hat{F}$ is the (1 x m) vector

$$\hat{F} = \hat{\psi}_* G \qquad (5\text{-}16)$$

In this case, it can be shown that

$$L = G^T (GG^T)^{-1} \qquad (5\text{-}17)$$

Combining Eq. (5-10) and (5-17) gives the estimates

$$\hat{\psi}_* = FG^T (GG^T)^{-1} \qquad (5\text{-}18)$$

The covariance of $\hat{\psi}_*$ may be found by observing that in Eq. (5-18) the elements of $\hat{\psi}_*$ are a linear function of the random vector F (which was defined in Eq. (5-9)). Substituting Eq. (5-9) into (5-18) gives

$$\hat{\psi}_* = (\psi_* G + \tilde{N}) G^T (GG^T)^{-1} \qquad (5\text{-}19)$$

which reduces to

$$\hat{\psi}_* = \psi_* + \tilde{N}L \qquad (5\text{-}20)$$

The estimation error is

$$E = \hat{\psi}_* - \psi_* = \tilde{N}L \qquad (5\text{-}21)$$

If the expected value of $\tilde{N}$ is zero (which can be shown without additional assumption), Eq. (5-18) leads to unbiased estimates of ψ_*. The covariance of E depends on the covariance of $\tilde{N}$ according to

$$\mathbb{E} = L^T \mathbb{N} L \qquad (5\text{-}22)$$

In regression theory, it usually is assumed that $\mathbb{N} = \sigma^2 I$.

In that case Eq. (5-22) reduces to

$$\mathbb{E} = \sigma^2 L^T L \tag{5-23}$$

which further reduces to

$$\mathbb{E} = \sigma^2 (GG^T)^{-1} \tag{5-24}$$

The diagonal elements of Eq. (5-24) are given in most standard texts as the variances of the corresponding regression coefficients. Note that $\mathbb{E}$ in Eq. (5-24) depends on the true error variance σ^2 of the regression equation and that this must be estimated in practice. Usually, σ^2 is estimated from

$$\hat{\sigma}^2 = \frac{1}{n-r} (FF^T - \hat{\psi}_* GF^T) \tag{5-25}$$

Eq. (5-25) assumes that the elements of $\tilde{N}$ are uncorrelated. In cases where $\mathbb{N} \neq \sigma^2 I$ the proper expression for $\mathbb{E}$ is Eq. (5-22), not (5-24).

A word of caution is offered to the use computer library multiple regression programs to solve for $\hat{\psi}_*$. It is that the standard errors of the elements of $\hat{\psi}_*$ given by these programs are based on Eqs. (5-24) and (5-25).

5.2.2 Filter Theory Approach

Multiple regression estimate of ψ_* are based on the criterion to minimize the errors of the individual estimates of F. Eq. (5-22) shows that the error covariance $\mathbb{E}$, of the resulting parameter

estimates, ψ_*, depends on both N and L. Since the present estimation problem is to estimate ψ_*, not F, an estimation criterion to minimize some function of E might be more appropriate than that used in regression theory. Therefore, the filter problem is to find the best L that satisfies a given estimation criterion. The criterion employed is the minimization of the trace of E (i.e. the minimization of the total mean square error in the estimation of the elements of ψ_*). The approach to be presented in Case I is taken from an unpublished paper by Ross [1961].

Case I: Statistics of ψ_* Unknown.

It is assumed that the mean and covariance of ψ_* are unknown. But the mean and covariance of $\tilde{N}$ are assumed known. It is sufficient to assume $\varepsilon\{\tilde{N}\} = 0$, since if it is not the effect may be removed.

From Eq. (5-21)

$$E = \hat{\psi}_* - \psi_* = \psi_* (GL-I) + \tilde{N}L \tag{5-26}$$

The expected value of E is

$$\varepsilon\{E\} = \psi_* (GL-I) + \varepsilon\{\tilde{N}\} L \tag{5-27}$$

Since $\varepsilon\{\tilde{N}\}$ is assumed equal to zero

$$\varepsilon\{E\} = \psi_* (GL-I) \tag{5-28}$$

To minimize the trace of $\varepsilon\{E = E^T E\}$ it will be necessary to have $\varepsilon\{E\} = 0$. This requires that

$$GL = I \tag{5-29}$$

Substituting Eq.(5-29) into (5-26) gives

$$E = \tilde{N}L \tag{5-30}$$

Therefore

$$\mathbb{E} = \varepsilon\{E^T E\} = L^T \tilde{N} L \tag{5-31}$$

(which happens to be the same as Eq.(5-22)).

We now wish to find L that minimizes the trace of $\mathbb{E}$ and that satisfies GL = I (Note that G is (rxn) and L is (nxr)). The case where r = n is trivial. The case where r < n involves pseudo-inverse matrices   Both cases are covered by matrices of the form

$$L = ZG^T (G\ ZG^T)^{-1} \tag{5-32}$$

where Z is any nxn Hermitian matrix such that GZG^T is invertible (i.e., Z is of rank r).

Substituting Eq.(5-32) into (5-31) gives

$$\mathbb{E} = [(GZG^T)^{-1}\ GZ\ \tilde{N}\ ZG^T\ (GZG^T)^{-1}\ ] \tag{5-33}$$

which is simplified considerably if Z is taken as $\tilde{N}^{-1}$.

$$\mathbb{E} = (G\tilde{N}^{-1}G^T)^{-1} \tag{5-34}$$

It now remains to show that Eq.(5-32) gives the optimum filter L that minimizes the trace of $\mathbb{E}$ as given by Eq.(5-34). The proof appears in Appendix A.

Eq. (5-32) was used together with Eq.(5-10) to produce the

numerical results which are presented in Sections 5.3 and 5.4.

<u>Case II: Statistics of ψ_* Known.</u>

On the basis of prior information (perhaps derived from knowledge relating soil types and ψ_* or perhaps derived from knowledge of ψ values of ψ_* during previous storms) it is assumed that the mean $\mu_{\psi*}$ and covariance Ψ, of the a-priori distribution of ψ_* are known. Also the mean and covariance of $\tilde{N}$ are known, as in the previous case. Again, we have

$$E = \psi_* (GL-I) + \tilde{N}L \tag{5-35}$$

Taking expectations gives

$$\varepsilon\{E\} = \varepsilon\{\psi_*\}(GL-I) + \varepsilon\{\tilde{N}\} L \tag{5-36}$$

or

$$\mu_E = \mu_{\psi_*} (GL-I) + \mu_N L \tag{5-37}$$

Remove the effects of the means by introducing

$$\psi_*' = \psi_* - \mu_{\psi_*} \tag{5-38a}$$

$$F' = F - \mu_{\psi_*} G - \mu_N \tag{5-38b}$$

$$\tilde{N}' = \tilde{N} - \mu_N \tag{5-38c}$$

$$E' = E - \mu_E \tag{5-38d}$$

The optimum filter, L, will be used in the relations

-140-

$$\hat{\psi}_*' = F' L \qquad (5-39)$$

and

$$\hat{\psi}_* = \mu_{\psi_*} + \hat{\psi}_*' \qquad (5-40)$$

to estimate $\hat{\psi}_*$.

Eq.(5-35) becomes after substituting Eqs.(5-36) and (5-38)

$$E' = \psi_*' (GL - I) + \tilde{N}' L \qquad (5-41)$$

Taking expectations gives $\mu_E' = 0$ (since $\mu_{\psi_*'} = 0$ and $\mu_{\tilde{N}'} = 0$) without restriction on GL. Therefore there is a wider domain from which to select L. It should be possible to use the statistics of ψ_* and wider domain of L to produce improved estimates over the preceeding case.

Vectors ψ_*' and F' are jointly distributed according to a multivariate distribution. Form the column vector

$$W = \left| \begin{array}{c} \psi_*'^T \\ --- \\ F'^T \end{array} \right| = \left| \begin{array}{c} W_1 \\ --- \\ W_2 \end{array} \right| \qquad (5-42a)$$

where

$$W_1 = \psi_*'^T \qquad (5-42b)$$

and

$$W_2 = F'^T \qquad (5-42c)$$

The mean of W is zero and the covariance is

$$\Sigma = \begin{vmatrix} \Sigma_{11} & | & \Sigma_{12} \\ --- & | & --- \\ \Sigma_{21} & | & \Sigma_{22} \end{vmatrix} \qquad (5\text{-}43)$$

If W is multivariate normal, the conditional mean of W_1, given W_2 is

$$\mu_{W_1|W_2} = \Sigma_{12}\, \Sigma_{22}^{-1}\, W_2 \qquad (5\text{-}44)$$

and the conditional covariance is

$$\Sigma_{W_1|W_2} = \Sigma_{11} - \Sigma_{12}\, \Sigma_{22}^{-1} \Sigma_{21} \qquad (5\text{-}45)$$

If we let $\hat{\psi}_*{}' = \mu_{W_1|W_2}$, then $\mathbb{E} = \Sigma_{W_1|W_2}$. It can be shown that the trace of $\Sigma_{W_1|W_2}$ is less than the trace of the error covariance matrix $\mathbb{E}'$ for any other estimate of ψ_*

Therefore,

$$L^T = \Sigma_{12}\, \Sigma_{22}^{-1} \qquad (5\text{-}46)$$

where

$$\Sigma_{12} = \varepsilon\{\psi_*{}'^T\, F'\} \qquad (5\text{-}47)$$

Since $F' = \psi_*{}'\, G + \tilde{N}'$ and since $\tilde{N}'$ and $\psi_*{}'$ are uncorrelated,

$$\Sigma_{12} = \Psi G \qquad (5\text{-}48)$$

Also,

$$\Sigma_{22} = \varepsilon\{F'^T\, F'\} = G^T \Psi G + \mathbb{N} \qquad (5\text{-}49)$$

Thus

$$L^T = \Psi G (G^T \Psi G + N)^{-1} \qquad (5-50)$$

From Eq. (5-45) we have

$$E = \Psi - \Psi G (G^T \Psi G + N)^{-1} G^T \Psi \qquad (5-51)$$

(Note: Eq. 5-50) gives the Kalman filter for this problem).

5.2.3 Comparison of the Estimators.

Two sets of comparisons are of interest.

Comparison of Regression Approach and Filter Theory, Case I.

Eq. (5-22) gives the covariance of the regression estimator as

$$E = L^T N L \qquad (5-22)$$

and Eq. (5-31) gives the covariance of the filter theory estimator
as

$$E = L^T N L \qquad (5-31)$$

On the surface it would seem that the covariance of both estimators
would be the same. Nevertheless, L in Eq. (5-22) is not the same
as L in Eq. (5-31), unless N happens to be given by $N = \sigma_n^2 I$.
It follows that the trace of E by the regression approach is greater
than the trace of E except where $N = \sigma_n^2 I$. In that case, the
regression approach and the filter theory (Case I) model are equivalent.
Therefore, we can conclude (i) regression model is a special case of
the filter theory model, and (ii) the regression model gives inferior
parameter estimates than the filter theory model.

-143-

It has been shown above that both models give unbiased estimates.

Comparison of Filter Theory Cases I and II.

Eq. (5-34) gives the covariance of the filter theory (Case I) estimator as

$$\mathbb{E}_1 = (G N^{-1} G^T)^{-1} \tag{5-34}$$

and Eq. (5-51) gives the covariance of the filter theory (Case II) estimator as

$$\mathbb{E}_2 = \Psi - \Psi G (G^T \Psi G + N)^{-1} G^T \Psi \tag{5-51}$$

To compare these two estimators, consider the special case where

$$N = \sigma_n^2 I_n \tag{5-52a}$$

$$\Psi = \sigma_\psi^2 I_r \tag{5-52b}$$

and

$$G G^T = I \tag{5-52c}$$

In that case

$$\mathbb{E}_1 = \sigma_n^2 I_r \tag{5-53}$$

and

$$\mathbb{E}_2 = \sigma_\psi^2 \left| \frac{\sigma_n^2}{\sigma_\psi^2 + \sigma_n^2} \right| I_r \tag{5-54}$$

The ratio of the coefficients of $\mathbb{E}_1$ and $\mathbb{E}_2$ is

$$\frac{\sigma_{E_1}^2}{\sigma_{E_2}^2} = \frac{\sigma_\psi^2 + \sigma_n^2}{\sigma_\psi^2} = 1 + \frac{\sigma_n^2}{\sigma_\psi^2} \tag{5-55}$$

The interpretation of Eq. (5-55) is that Case II always gives a better estimate than Case I. In the case where $\sigma^2_\psi \gg \sigma_n^2$ the two estimators become equivalent. In cases where $\sigma_n^2 > \sigma_\psi^2$, Case I is substantially inferior to Case II.

5.3 Hypothetical Examples

Two hypothetical examples are presented in this section. In the first example, the response of a hypothetical urban catchment is fully linear; in the second example, the response is non-linear and is governed by the kinematic wave equations.

5.3.1 Linear Hypothetical Catchment

Consider an idealized urban catchment, illustrated in Figure 5-3, with impervious and pervious response functions as given in Table 5-1. These functions are also illustrated in Figure 5-3. A given precipitation, P, lasts for 20 time units and has a constant intensity of 2.0 in/hr. The true infiltration rates, ψ, are equal to 1.0 in/hr during the storm and are equal to zero thereafter. The observed runoff, Q, is the summation of the true runoff $Q_1 + Q_2$ and of a noise component, N, generated without serial correlation from a normal distribution, $N(0, \sigma^2 = 4)$.

Table 5-2 gives the true and measured runoff rates.

Now consider an infiltration model, IM, in which the total length of the storm is divided into three periods of equal duration (i.e. 10 time units). Within the i-th period the infiltration rate is assumed constant and equal to ψ_{*i}, i-th element of the (1x3) vector ψ_*.
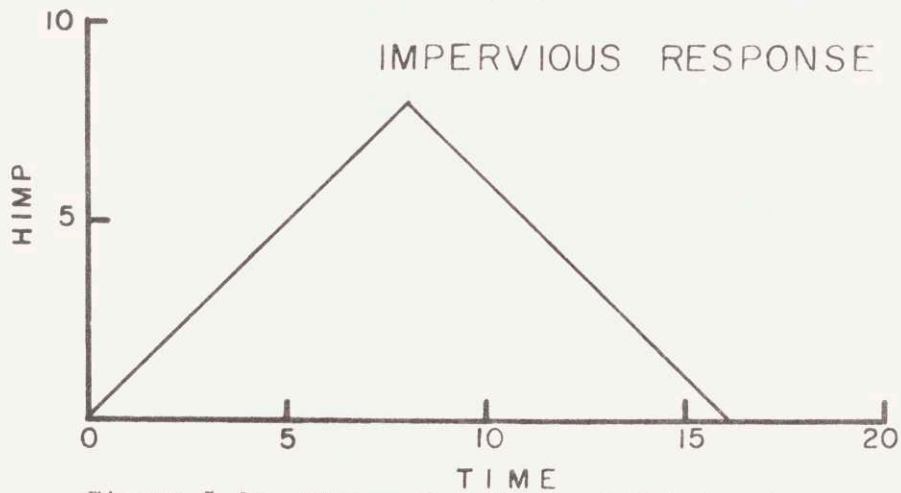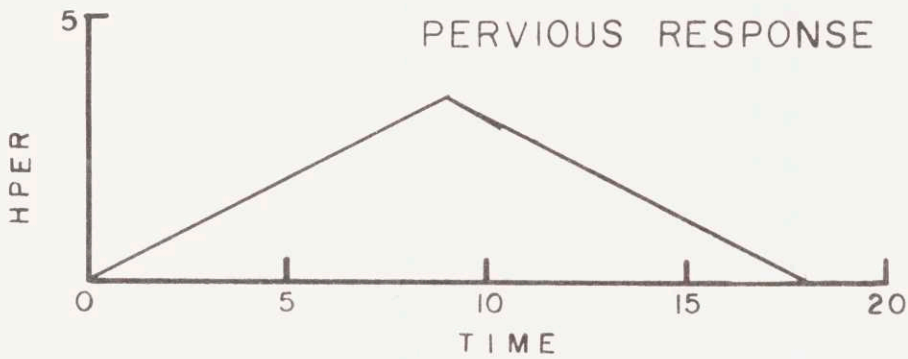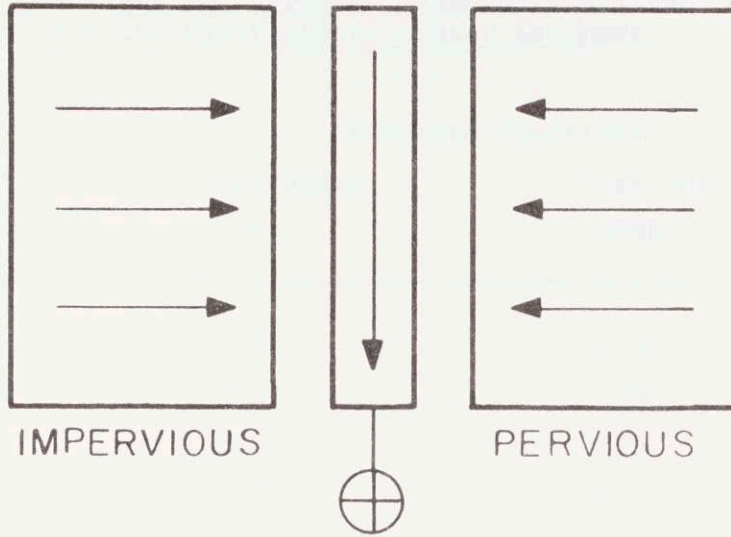
Figure 5-3:   Linear Hypothetical Catchment :
              Impervious and Pervious Response Functions

Table 5-1

Impervious and Pervious Response Functions
for the Hypothetical Linear Catchment

| Time | Response Functions | |
	Impervious HIMP	Pervious HPER
1	1.0	0.5
2	2.0	1.0
3	3.0	1.5
4	4.0	2.0
5	5.0	2.5
6	6.0	3.0
7	7.0	3.5
8	8.0	4.0
9	7.0	4.5
10	6.0	4.0
11	5.0	3.5
12	4.0	3.0
13	3.0	2.5
14	2.0	2.0
15	1.0	1.5
16	0.0	1.0
17		0.5
18		0.0

Table 5-2

True and Measured Rates of Runoff (Linear Hypothetical Catchment)

Infiltration = 1.0 in/hr

Precipitation = 2.0 in/hr for 20 time units

t	True Runoff $Q_1 + Q_2$	Measured Runoff Q	N
1	2.5	4.40	1.9
2	7.5	9.55	2.50
3	15.0	11.90	−3.10
4	25.0	26.80	+1.80
5	37.5	36.05	−1.45
6	52.5	50.80	−1.70
7	70	68.74	−1.26
8	90	89.74	−0.26
9	108.5	109.78	1.28
10	124.5	124.35	−0.15
11	138	135.13	−2.87
12	149	150.12	1.12
13	157.5	157.12	−0.38
14	163.5	163.57	0.07
15	167	168.76	1.76
16	168	172.48	4.48
17	168.5	165.94	−2.56
18	168.5	169.17	0.67
19	168.5	167.21	−1.29
20	168.5	169.23	0.73

Table 5-2 (cont'd)

t	$Q_1 + Q_2$	Q	N
21	166	165	-1.0
22	161	158.76	-2.24
23	153.5	155.92	2.42
24	143.5	142.66	-0.84
25	131	131.95	.95
26	116	119.83	3.83
27	98.5	102.22	3.72
28	78.5	77.95	-0.55
29	60	62.28	2.28
30	44	37.72	-6.28

$$\bar{N} \ = \ \frac{3.58}{30} \ = \ 0.1193$$

The (3x30) matrix B relates ψ and ψ_* by

$$\psi = \psi_* B \qquad (5-5)$$

The elements of B are

$$B = \begin{vmatrix} 111111111100000000000000000000 \\ 000000000011111111110000000000 \\ 000000000000000000001111111111 \end{vmatrix} \qquad (5-56)$$

The *a-priori* noise covariance matrix N is given as

$$N = 4\ I \qquad (5-57$$

where I is a 30x30 identity matrix.

The estimated infiltration parameters, $\hat{\psi}_*$, obtained from the estimator are given in Table 5-3.

Table 5-3

Infiltration Parameters (Linear Hypothetical Catchment)- Example 1

Time Period	Estimated $\hat{\psi}_*$ (in/hr)	True ψ_* (in/hr)	σ_{ψ_*} (in/hr)
1	1.008	1.000	0.0141
2	0.966	1.000	0.0200
3	0.056	0.000	0.0400

These estimates of the infiltration rates are very close to the true values but are not exactly equal to the given rates because Q contains noise. The standard error of estimate of $\hat{\psi}_*$ is small compared to ψ_* and compared to the variance of the noise component

A second a-priori noise covariance function was used to analyze the sensitivity of the solution to N. Consider a 30x30 tri-diagonal matrix with diagonal elements equal to 4 and elements adjacent to the diagonal equal to .5.

This covariance matrix implies that the error term $N(t)$ is serially correlated. The estimates of the infiltration parameters are given in Table 5-4.

Table 5-4

Infiltration Parameters (Linear Hypothetical
Catchment) – Example 2

Time Period	Rates		
	Estimated $\hat{\psi}_*$ (in/hr)	True ψ_* (in/hr)	σ_{ψ_*} (in/hr)
1	1.011	1.000	0.0200
2	0.959	1.000	0.0224
3	0.088	0.000	0.0469

The magnitude of $\hat{\psi}_*$ (t) was not significantly modified when the noise function contained a small amount of serial correlation. The reliability of the estimates in the second case is not as large as it is in the first case since the standard errors of estimate are increased; this shows that less information is present in Q when the noise is serially correlated than when it is not.

This first hypothetical example shows that when all the assumptions made in the simplified estimation problem are strictly valid, the solutions are well behaved.

5.3.2 Non-Linear Hypothetical Catchment

Consider a catchment that responds to rainfall according to the kinematic wave theory. This catchment, illustrated in Fig. 5-4, responds as a non-linear system since the underlying differential equations
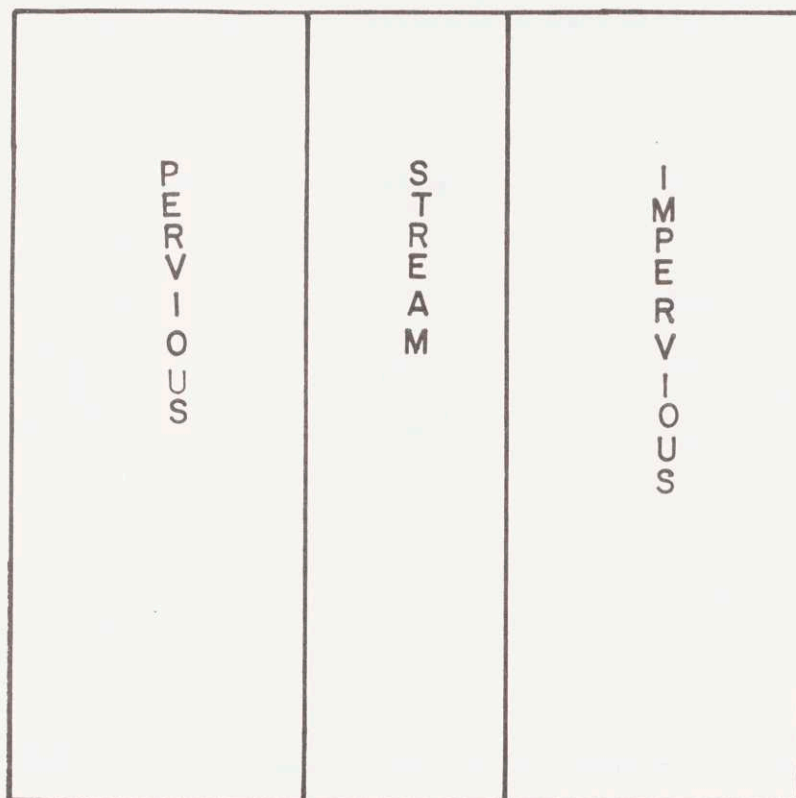
Figure 5-4: Non-Linear Hypothetical Catchment

are non-linear. The catchment parameters for this example appear in
Table 5-5.

<div align="center">Table 5-5</div>

<div align="center">Data for the Non-Linear Hypothetical Catchment</div>

1. Catchment:

Name	Length (ft)	α	m
Pervious	200.	0.5	2.0
Impervious	100	2.0	2.0
Stream	1000	0.1	1.33

2. Infiltration:

        Constant rate of 1.0 in/hr.

An "observed" storm was simulated by applying a rainfall of
constant intensity at 4.0 in/hr for 2 hours to this model. Measured run-
off was simulated by adding to the computed runoff rate a random noise
component, N.

This example was created to test whether the correct infil-
tration rates could be estimated by the FTM from measurements of rainfall
and runoff and from information derived from a model of the catchment.
The fact that (i) the real catchment is non-linear, and (ii) the catch-
ment model is non-linear raises the question of how best to approximate
the linear catchment response functions H_1 and H_2 that appear in the

FTM.

In principle there are numerous ways to derive linear response functions H_1 and H_2 that approximate the behavior of the non-linear catchment. Different values of H_1 and H_2 would "best" approximate the response to different storms. In this case, the measured rainfall, P, is known so the estimation of H_1 and H_2 should apply to this particular storm.

Matrices H_1 and H_2 are needed by the FTM to compute the vector

$$F = P(H_1 + H_2) - Q \qquad (5-6)$$

and we now wish to devise a procedure for using the kinematic wave catchment model to estimate certain terms that appear on the rhs of this equation.

Consider first the term PH_1. According to Eq. (5-1), $PH_1 = Q_1$ (See also Fig. 5-2) which is the runoff from the impervious area. One way to estimate Q_1 is to apply P to a kinematic wave model of the catchment in which the infiltration rates over the pervious area are set greater than P. The response of the model will be $\hat{Q}_1$, an estimate of Q_1. Now it would be possible to use $\hat{Q}_1$ together with P to estimate H_1. But H_1 was introduced originally because of the need to estimate Q_1. Since we can estimate Q_1 directly there is no need to introduce H_1. Moreover, the fact that the actual response of the impervious area is non-linear is also accounted for by the non-linear catchment model used to estimate Q_1. In other words, the non-linearities of the impervious parts of the catchment are fully accounted for in the

filter calculations. The revised form of Eq. (5-6), up to the point, is

$$F = \hat{Q}_1 + PH_2 - Q \qquad (5-58)$$

The next problem is to estimate the term PH_2. The procedure to estimate this term will lead to a modified definition for F (i.e., Eq. (5-58) will be changed). The term PH_2 is equal to the runoff that would occur from the pervious area if there were no infiltration. One way to estimate this using the catchment model would be (i) apply P to the catchment model with all infiltration rates set to zero and observe the response $\hat{Q}_T$. Then (ii) estimate PH_2 as

$$\widehat{PH}_2 = \hat{Q}_T - \hat{Q}_1 \qquad (5-59)$$

From $\widehat{PH}_2$ and $\hat{P}$ it would be possible to compute the elements of H_2 by multiple regression. This procedure was actually tried, but different values of P led to different values of H_2. It seemed then if ψ were large compared to P that the non-linear response of the pervious area would not be properly accounted for by this linearization.

A better approach seemed to be to assume an initial value for ψ_* and then to use the FTM to compute corrections ψ_{*_r} to the initial assumption. Let ψ_{o_*} denote the initially assumed values of the infiltration parameters. Then, the initial values of the infiltration rates are

$$\psi_o = \psi_{o_*} B \qquad (5-60)$$

Now, use the catchment model to apply P to the impervious area and

the effective rainfall $P - \psi_o$ to the pervious area. Observe the response $\hat{Q}$ from the catchment model. We seek H_2 so that

$$(P - \psi_o) \, H_2 \approx \hat{Q} - \hat{Q}_1 \tag{5-61}$$

Regression techniques may be used to compute the elements of H_2. (The details of this calculation are not presented here).

Define

$$F' = \hat{Q}_1 + (P - \psi_o) \, H_2 - Q \tag{5-62}$$

This vector can now be computed from the available information. Also assume that any differences between Q_1 and $\hat{Q}_1$ are included in N so that Eq. (5-4) may be rewritten

$$Q = \hat{Q}_1 + Q_2 + N \tag{5-63}$$

Assume further that Q_2 in Eq. (5-63) is defined as

$$Q_2 = (P - \psi_o - \psi_r) \, H_2 \tag{5-64}$$

Substituting Eqs. (5-63) and (5-64) into (5-62) gives

$$F' = \psi_r \, H_2 + \tilde{N} \tag{5-65}$$

or

$$F' = \psi_* \, G + \tilde{N} \tag{5-66}$$

where $G = BH_2$ (Eq. (5-7)).

It follows that the estimate of the corrections is

$$\hat{\psi}_{*_r} = F' L \qquad\qquad (5\text{-}67)$$

and that the estimated infiltration parameters are

$$\hat{\psi}_* = \psi_{*_o} + \hat{\psi}_{*_r} \qquad\qquad (5\text{-}68$$

To test the FTM, the given values of P and Q for the hypothetical catchment in Fig. 5-4 were used to estimate the infiltration parameters ψ_*. Different initial values, ψ_{*_o} were used to estimate H_2. The values of Q, $\hat{Q}_1$ and $\hat{Q}(\psi_{*_o})$ appear in Table 5-6. Since the true ψ is 1.0, the values of Q differ from $\hat{Q}(\psi_o = 1.0)$ by the noise term N.

The estimated infiltration parameters for different values of ψ_{*_o} appear in Table 5-7. The total storm period was divided into 3 periods of 60 minutes each. $\hat{\psi}_{*_1}$ is an estimate of the average infiltration rate during the first period; ψ_{*_2}, during the second; etc. The true values of ψ_{*_1} and ψ_{*_2} were 1.0. The true value of ψ_{*_3} is unknown but lies somewhere between 0 and 1.0. ψ_{*_3} is unknown because the catchment model is programmed to continue the infiltration process as long as there is water on the surface. After rainfall ceases the infiltration continues until there is no more water to infiltrate. The actual infiltration rates are not printed out by the model. Only the potential infiltration rate is known.

Table 5-6

Hydrograph Data for the Non-Linear Hypothetical Catchment

(Units of Q are cfs)

Storm: Intensity — 4.0 in/hr

         Duration — 2.0 hrs.

True Infiltration Rate = 1.0 in/hr.

Time Min.	Q	Impervious $\hat{Q}_1$	Total $\hat{Q}$			
			$\psi_o = 0.$	0.5	1.0	1.5
2	0.0	0.0	0.00	0.00	0.0	0.00
4	0.0	0.0	0.00	0.00	0.0	0.00
6	0.0	0.01	0.01	0.01	0.01	0.01
8	0.0	0.03	0.05	0.04	0.04	0.04
10	0.11	0.09	0.12	0.11	0.11	0.10
12	0.13	0.19	0.26	0.25	0.23	0.22
14	0.42	0.35	0.49	0.45	0.43	0.40
16	0.67	0.56	0.78	0.73	0.68	0.64
18	0.77	0.79	1.15	1.06	0.99	0.93
20	2.09	1.05	1.59	1.46	1.35	1.25
22	1.46	1.32	2.10	1.91	1.75	1.62
24	2.23	1.61	2.69	2.43	2.20	2.02
26	1.92	1.92	3.37	3.01	2.71	2.46
28	2.86	2.23	4.15	3.68	3.28	2.95
30	3.56	2.56	5.04	4.42	3.90	3.48
32	5.26	2.90	6.03	5.26	4.60	4.06
34	5.81	3.25	7.14	6.18	5.37	4.69
36	6.68	3.60	8.35	7.20	6.21	5.39
38	6.39	3.97	9.65	8.31	7.14	6.14
40	8.09	4.35	11.02	9.48	8.13	6.95
42	9.51	4.73	14.44	10.72	9.19	7.82
44	10.86	5.12	13.91	12.02	10.30	8.76
46	10.84	5.52	15.41	13.35	11.46	9.74
48	12.77	5.93	16.90	14.71	12.66	10.76
50	14.29	6.34	18.37	16.06	13.88	11.82
52	15.17	6.76	19.77	17.38	15.09	12.90
54	16.22	7.19	21.07	18.63	16.26	13.97

(Continuation)

56	17.28	7.62	22.26	19.77	17.35	14.98
58	17.29	8.03	23.30	20.79	18.33	15.90
60	19.04	8.41	24.20	21.68	19.18	16.70
62	19.42	8.70	24.97	22.43	19.90	17.38
64	20.04	8.92	25.60	23.07	20.52	17.94
66	21.33	9.06	26.11	23.60	21.04	18.44
68	20.81	9.15	26.53	24.03	21.48	18.85
70	22.15	9.20	26.85	24.38	21.85	19.22
72	22.23	9.22	27.10	24.66	22.15	19.54
74	22.74	9.24	27.29	24.87	22.40	19.82
76	22.61	9.25	27.43	25.04	22.60	20.05
78	22.48	9.25	27.53	25.16	22.75	20.24
80	22.84	9.25	27.60	25.25	22.87	20.40
82	23.10	9.26	27.66	25.31	22.95	20.52
84	22.00	9.26	27.69	25.36	23.01	20.61
86	22.98	9.26	27.72	25.39	23.05	20.68
88	23.66	9.26	27.74	25.41	23.08	20.43
90	22.92	9.26	27.75	25.43	23.10	20.76
92	23.13	9.26	27.76	25.44	23.12	20.79
94	22.85	9.26	27.77	25.45	23.13	20.80
96	23.23	9.26	27.77	25.45	23.13	20.81
98	23.21	9.26	27.77	25.46	23.14	20.82
100	23.47	9.26	27.77	25.46	23.14	20.82
102	22.75	9.26	27.78	25.46	23.14	20.83
104	22.71	9.26	27.78	25.46	23.15	20.83
106	23.86	9.26	27.78	25.46	23.15	20.83
108	23.03	9.26	27.78	25.46	23.15	20.83
110	23.47	9.26	27.78	25.46	23.15	20.83
112	23.37	9.26	27.78	25.46	23.15	20.83
114	22.79	9.26	27.78	25.46	23.15	20.83
116	22.78	9.26	27.78	25.46	23.15	20.83
118	22.84	9.26	27.78	25.46	23.15	20.83
120	22.31	9.26	27.78	25.46	23.15	20.83
122	22.94	9.23	27.70	25.39	23.08	20.77
124	22.96	9.12	27.42	25.12	22.83	20.54
126	23.21	8.90	26.89	24.62	22.35	20.11
128	22.24	8.62	26.17	23.94	21.71	19.52
130	20.40	8.31	25.32	23.14	20.96	18.83
132	20.27	7.97	24.38	22.25	20.13	18.06
134	18.86	7.63	23.37	21.30	19.24	17.25
136	18.85	7.28	22.32	20.31	18.31	16.41
138	16.95	6.93	21.24	19.29	17.37	15.51
140	16.26	6.56	20.15	18.27	16.41	14.59
142	14.88	6.21	19.05	17.23	15.45	13.71

(Continuation)

144	14.50	5.87	17.96	16.21	14.50	12.84
146	13.02	5.55	16.89	15.20	13.57	11.99
148	12.29	5.23	15.84	14.22	12.65	11.16
150	10.67	4.92	14.82	13.26	11.76	10.35
152	10.57	4.62	13.84	12.33	10.91	9.57
154	9.81	4.33	12.90	11.45	10.09	8.83
156	9.78	4.05	12.02	10.60	9.30	8.13
158	8.67	3.79	11.18	9.81	8.56	7.46
160	6.41	3.54	10.39	9.06	7.87	6.83
162	6.28	3.30	9.66	8.36	7.22	6.25
164	5.52	3.07	8.98	7.71	6.62	5.71
166	5.96	2.85	8.35	7.11	6.06	5.21
168	5.74	2.65	7.78	6.56	5.55	4.76
170	4.69	2.46	7.24	6.05	5.08	4.34
172	4.21	2.28	6.75	5.59	4.65	3.96
174	4.86	2.12	6.30	5.16	4.26	3.62
176	3.92	1.96	5.89	4.77	3.91	3.31
178	3.62	1.82	5.51	4.41	3.59	3.03
180	2.99	1.68	5.16	4.08	3.30	2.78

Table 5-7

Results (Non-Linear Hypothetical Catchment)

Estimated Infiltration Rates

ψ_o	$\hat{\psi}_{*1}$	$\hat{\psi}_{*2}$	$\hat{\psi}_{*3}$	$\hat{\sigma}_1{}^2$	$\hat{\sigma}_2{}^2$	$\hat{\sigma}_3{}^2$
0.0	1.1434	1.0525	0.5550	0.0006	0.0007	0.0025
0.5	1.0833	1.0188	0.5334	0.0006	0.0007	0.0026
1.0	.9578	.9971	.6572	0.0007	0.0008	0.0027
1.5	.8917	.9450	.5927	0.0006	0.0007	0.0031

5.4 Infiltration Rates at Gray Haven.

The FTM is used to compute the apparent rates of infiltration experienced at Gray Haven. Three storms (June 10, 1963; June 14, 1963; August 1, 1963) are presented to illustrate the application of the FTM to a gaged catchment. Infiltration is assumed to occur according to the model

$$\phi(t) = f_c + (f_o - f_c) e^{-kt} \qquad (5-70)$$

where f_o and $f_o - f_c$ are the parameters to be estimated. It is assumed that $k = .0233$ minutes^{-1}.

The estimates obtained for storm June 10, 1963, were

$$\hat{f}_c = -0.3476 + 1.5 = 1.1524 \text{ in/hr}$$

$$\hat{f}_o = 0.5333 + 1.1524 + 0.5 = 2.1857 \text{ in/hr.}$$

Figure 5.5 compares the observed and simulated ($f_o = 2.1857$ in/hr.; $f_c = 1.1524$ in/hr) hydrographs. The goodness of the fit is better than the one illustrated in Figure 4-28 where the simulated hydrograph is computed for $f_o = 2.0$ in/hr and $f_c = 1.5$ in/hr.

The estimator for this storm performs very well; the estimates of the infiltration parameters are physically sound and the simulated hydrograph is an improved solution over the results previously achieved in Chapter 4.

The estimates obtained for storm August 1, 1963, are

STORM JUNE 10,1963

OBSERVED
UPDATED

DISCHARGE (c.f.s.)

TIME (MINUTES)
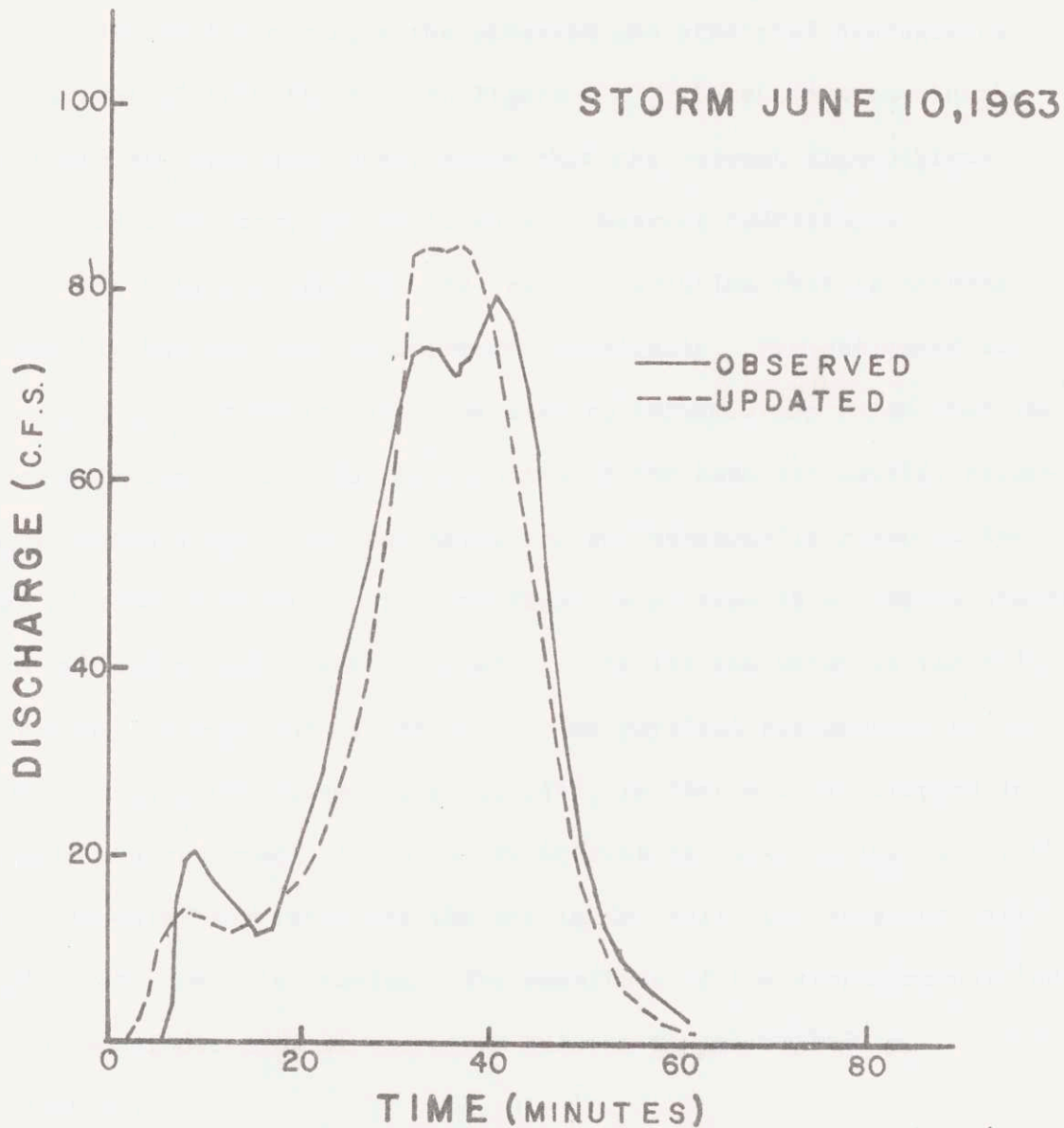
Figure 5-5: Comparison of Observed and Simulated (with $\hat{\psi}_*$) Hydrographs: Storm of June 10, 1963.

$$\hat{f}_c = 0.8193 + 1.5 = 2.3193 \text{ in/hr}$$

$$\hat{f}_0 = -1.3643 + 2.3193 + 0.5 = 1.4550 \text{ in/hr}.$$

Figure 5-6 compares the observed and simulated hydrographs. A comparison of this figure with Figure 4-27, where the same storm had previously been simulated, shows that the current figure gives an improved match between simulated and observed hydrographs.

In this case the FTM has led to a solution that is mathematically feasible but not easy to interpret physically. The estimated infiltration parameters in this case lead to infiltration rates that increase with time, which is the opposite of the behavior usually expected of Horton's law. The estimates are not necessarily rejected because of this difficulty; the infiltration process is a complex process where two media (air - water) interact. To let the water in the soil, the air has to move out of the soil. One physical explanation of the results derived for storm August 1, 1963, is that air was trapped in the soil and was gradually but at an increasing rate, moving out of the soil. As water was replacing the air in the soil, the apparent infiltration rates were increasing. The magnitude of the storm intensities and the short duration of the storm enhance the plausibility of the explanation.

The estimates obtained for the storm of June 14, 1963, are:

$$\hat{f}_c = 1.5 - 0.1278 = 1.3722 \text{ in/hr}$$

$$\hat{f}_0 = 1.3722 + 0.2607 + 0.5 = 2.1329 \text{ in/hr}.$$
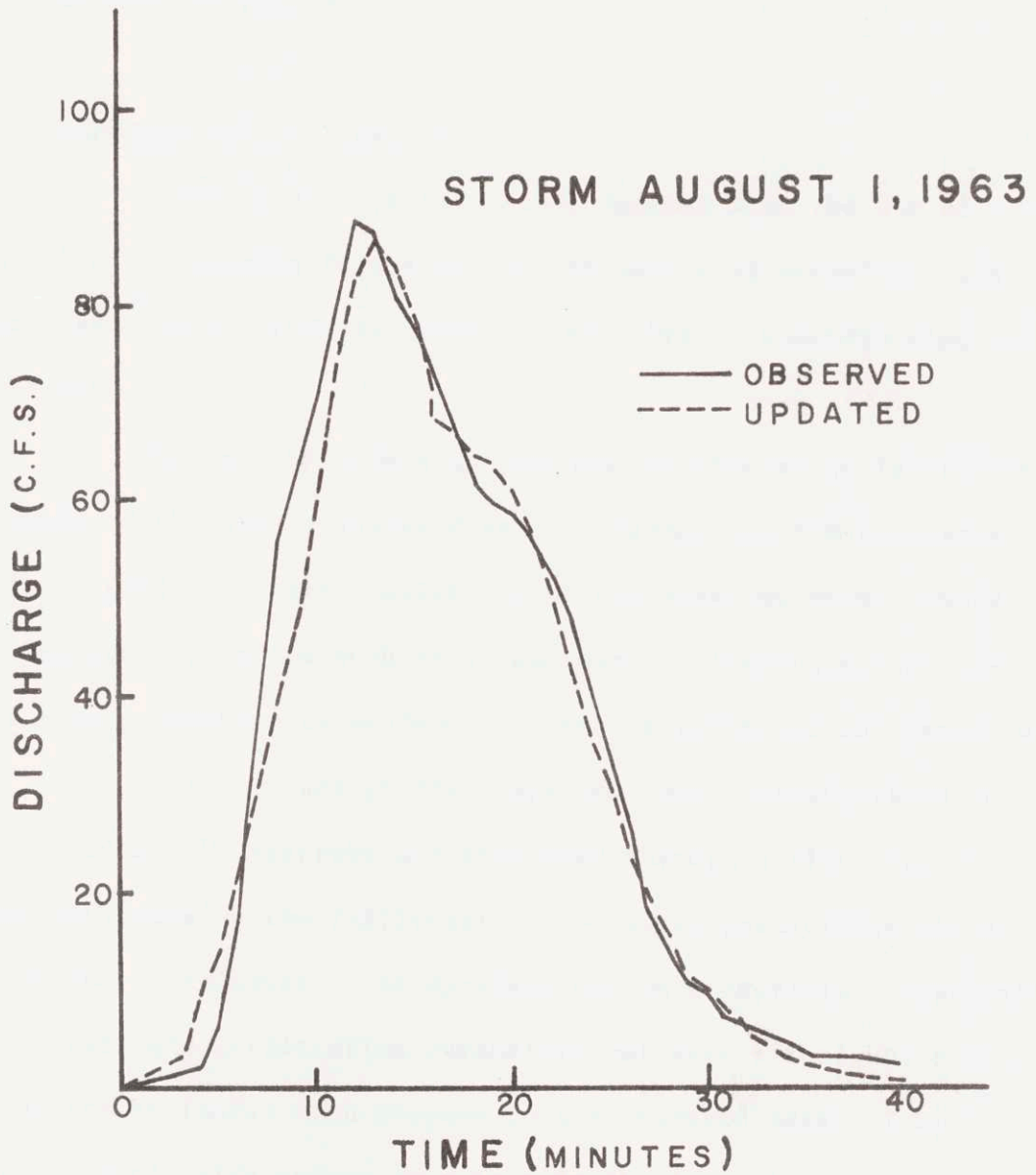
Figure 5-6: Comparison of Observed and Simulated (with $\hat{\psi}_*$)
Hydrographs: Storm of August 1, 1963

These estimates are well behaved in terms of their physical inter-
pretation but, when used to simulate the runoff hydrograph, they

do give an improved match over the results previously achieved in

Chapter 4. A comparison of the simulated and observed hydrographs

is illustrated in Figure 5-7.

5-5 Discussion and Conclusions

        The results of this study suggest that the use of filter

theory has a promising future in the estimation of hydrologic param-

eters. Additional study is needed to gain better understanding and

experience.

        One of the promising outcomes of this study is that in

all three of the storms analyzed at Gray Haven, the FTM estimates

led to as good or better simulations of the observed storm events

than was obtained after much trial and error adjusting to the in-

filtration parameters to achieve the results presented in Chapter 4.

        The proposed general approach where the simulated and

observed runoff hydrographs are processed through a filter to ge-

nerate estimates of the infiltration process is potentially attrac-

tive to the hydrologist. The approach not only provides a systematic

tool to estimate infiltration parameters but also a tool which op-

timizes the estimates with respect to the observed data. The

approach should also reduce or eliminate the iterations required to

find good estimates of infiltration parameters.

        In this study, the general estimation problem has been
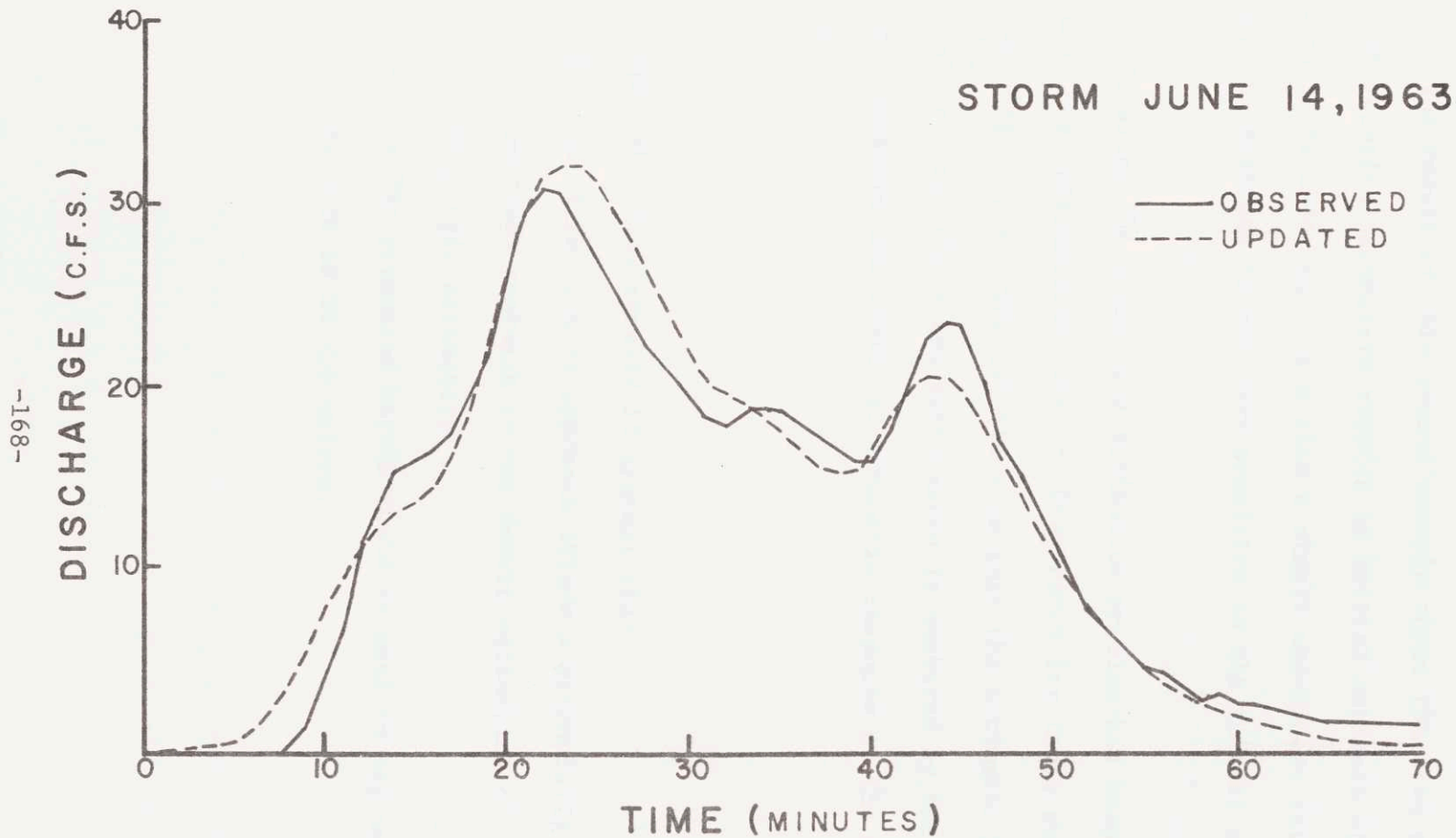
Figure 5-7: Comparison of Observed and Simulated (with $\hat{\psi}_*$) Hydrographs: Storm of June 14, 1963

greatly simplified; the approach is relatively simple to solve and has been shown to perform well for a linear catchment. The approach has also been verified for a non-linear catchment subject to intense rainfall. The result of this second example shows that the estimates of the infiltration parameters require an initial estimate of these parameters to be made, but tests with a simple non-linear catchment show that the estimate is not very sensitive to the initial assumptions.

Finally, the simplified estimation problem has been used to estimate the infiltration rates of Gray Haven for three observed rainfall-runoff events. The results show that the estimator performs well for all storms, where the performance is measured by the match between the observed and simulated kinematic response of the catchment.

From all these results it appears that

1- The filter theory approach offers a potentially important approach to the future estimation of hydrologic parameters;

2- The FTM presented herein could be used in engineering practice as it now exists.

CHAPTER 6

DERIVED FREQUENCY CURVES FOR GRAY HAVEN

6.1 Introduction

The preceding chapters presented material developed to derive runoff frequency curves directly from the rainfall. In Chapter 2 the theoretical concepts were presented. In Chapter 3 a model of rainfall as a stochastic process was presented. In Chapter 4 procedure to model urban catchments was presented. In Chapter 5 a procedure for estimating infiltration parameters was proposed.

In this chapter, the information presented in these earlier chapters is applied to the derivation of runoff frequency curves for the Gray Haven urban catchment. Runoff frequency curves for two runoff variables, the peak runoff rate and the excess runoff volume when the runoff rate exceeds a given threshold are derived.

6.2 Data for the Case Study.

Frequency curves were derived for the Gray Haven catchment. This catchment is illustrated in Figure 4-7. The frequency curves were derived for the peak runoff rate, Q_{max}, and for the exceedance volume $V(QTH)$ defined as the volume of runoff which occurs when the runoff rate exceeds a given flow threshold, QTH. A graphical illustration of $V(QTH)$ appears in Figure 6-1.

The rainfall at Gray Haven, Md., is described by (i) the rainfall exterior variable as derived from U.S.W.B. data for Baltimore City, and (ii) by the rainfall interior variables, estimated from rainfall observations made by the Johns Hopkins Storm Drainage Research
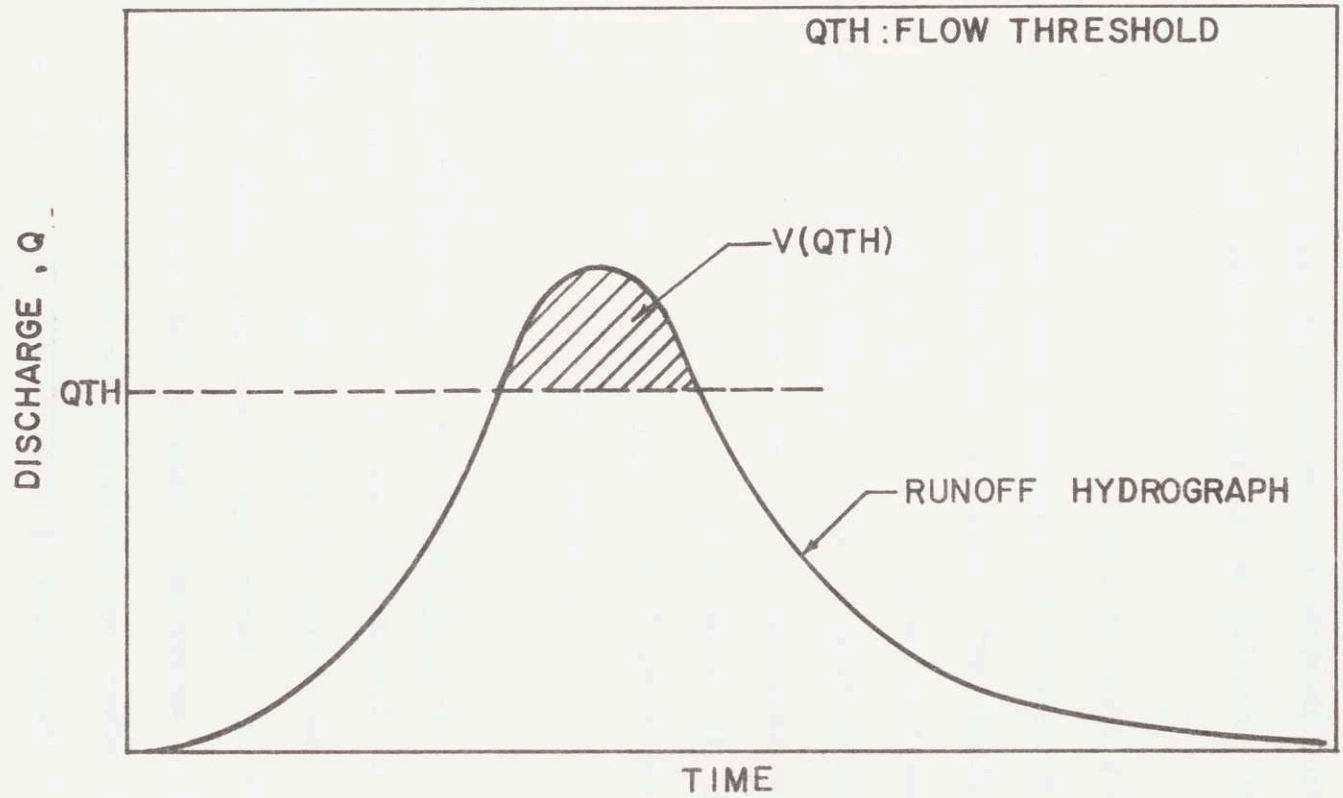
Figure 6-1:   Exceedance Volume, V(QTH)

Projects at Gray Haven and at Northwood (another urban catchment located in Baltimore). The statistical properties of the rainfall exterior variables are estimated on a monthly basis and the statistical properties of the interior variables were assumed constant during the year. The quantitative information on rainfall at Baltimore is presented in Chapter 3.

The kinematic wave model was used to route storms through the catchment. The simplified configuration IV described in Section 4.5.6 was selected to model the catchment. The infiltration parameters were assumed constant from storm to storm (not enough storm data were available to make inferences of the variability of the infiltration parameters from storm to storm). The infiltration rate was modeled by Horton's Law of infiltration (Equation 4-12) where $f_o = 2.0$ in/hr, $f_c = 1.5$ in/hr, and $k = 0.0233$ min.$^{-1}$ which are the same parameter values as used throughout Chapter 4.

6.3 Computational Methods for Solution of Eq. 2-1

A method of solution of Eqs. 2-1 to 2-10 is needed in order to derive the runoff frequency curves for Gray Haven. These equations are intractable analytically and so some combination of analytical and numerical approximations must be made. The issues involved in developing alternative solution procedures are too complex to be dealt with in depth in this report. In Appendix B, four possible solution methods are presented. One of these, stochastic/deterministic simulation

was selected because it appeared to be the least expensive alternative in this case.

The alternative solution methods presented in Appendix B demonstrate that solution procedures other than simulation do exist and to suggest the possibility that future research may lead to computational schemes that are less expensive than the simulation procedure used in this study.

6.4 Stochastic/Deterministic Simulation Procedure.

A seven-step procedure was followed to derive the frequency curve of the runoff variable V. This procedure is illustrated in Figure 6-2.

The first step is the selection of a runoff variable V. Examples of possible definitions of V include the peak flow, the exceedance volume, the duration of these exceedances at a given location, etc. Other variables, related to the runoff, could also be selected. An example is the concentration of a substance either at the outlet of the site or in the receiving body of water; another example is the erosion due to the runoff from the site at a downstream location.

The second step is the adoption of a routing model and the estimation of the parameters of this model.

The third and fourth step are respectively the modeling of rainfall as a stochastic process and the use of this model to generate a long rainfall trace.
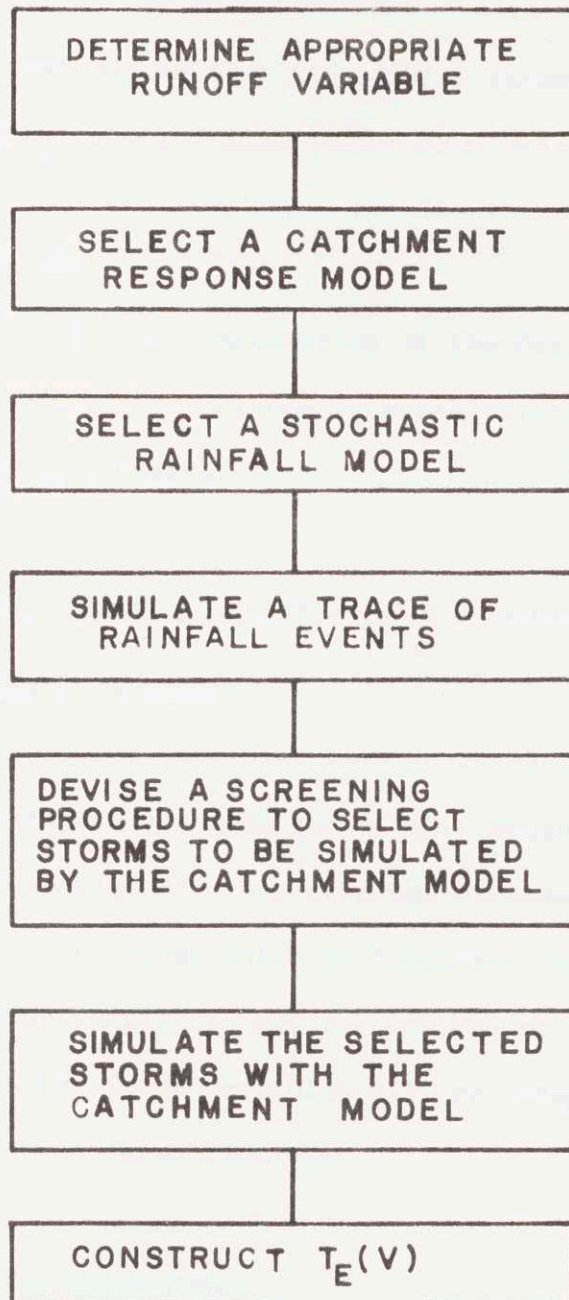
Figure 6-2: Stochastic Deterministic/Simulation Procedure
for $T_E(V)$

The fifth step is the selection from the generated rainfall trace of those storms that may be significant with respect to $F_V(v)$.

The sixth step is the simulation of each selected storm with the catchment model. From the simulation results the runoff variable for each storm is determined.

The final step is the construction of the derived frequency curve, $F_V(v)$. From this the recurrence interval relation $T_E(V)$ may be obtained as explained in Chapter 2.

6.5 Application of the Stochastic/Deterministic Simulation Procedure.

6.5.1 Selection of Runoff Variables

Two different runoff variables were selected for investigation. The first of these was the peak runoff rate because this variable is commonly used in the design of urban sewerage systems. The second of these was the exceedance volume which is important in the selection of detention storage facilities for the control of urban runoff. Runoff frequency curves for these variables will be presented in Section 6.5.7 for the Gray Haven catchment.

6.5.2 Selection of a Catchment Model

In Chapter 4, several alternative models of the Gray Haven catchment were presented. These included a detailed configuration and four simplified configurations which were developed to reduce the computational costs. Since it is now proposed to simulate a number

of storm events, the computational cost enters as an important factor to be considered in model selection. In this particular case, simplified configuration IV of Gray Haven was selected.

6.5.3 Selection of a Stochastic Rainfall Model.

The stochastic rainfall model used is described in Chapter 3.

6.5.4 Simulation of Rainfall Events

The rainfall model was used to simulate a trace of rainfall events. An important question at this point is the required duration of this trace. As the duration of the trace increases, the accuracy of the derived frequency curve increases but also the simulation costs increase as well. Therefore, there is a trade-off between cost and accuracy. This trade-off should be evaluated in view of the fact that the historical rainfall data which underlie the analysis have a limited record length. In this particular application the historical rainfall record was 23 years and the generated rainfall trace was for 200 years.

It may appear at first that the generated trace is unnecessarily long. Nevertheless, 200-yr. generated trace was created to reduce the simulation errors of the solutions to Eqs. 2-1 to 2-10 in the range $10 \leqslant T_E \leqslant 50$ yr.

6.5.5 Select Storms to be Simulated by the Catchment Model

The rainfall generator produced a 200 yr. trace of rainfall events. In each year, many events occurred. Typically, there would

be more than 100 events per year or more than 20,000 events over the period of generation. Since the 20-th largest event in the 200 yr. period corresponds to the 10-yr. event, only a small number of storms need to be simulated.

Since only a few events are of interest and since the generation of storm interiors is costly, storm interiors were not generated for all storms. Instead, a selection procedure was employed to sort out a relatively small number of storms for further study. This selection procedure made a tentative assumption that the rainfall in each storm was distributed according to a triangular pattern. Then, the maximum depth of rain, DMAX, during a given critical time, AVGTIM, was determined. The storms were ranked in decreasing order according to DMAX with AVGTIM = 30 min. (The time of concentration of Gray Haven is about 30 min.). Storm interiors were then generated for the largest 48 and these were retained for subsequent study.

6.5.6 Simulate Selected Storms

The selected storms consisted of a set of 48 events. Each event consisted of a hyetograph of block shaped rainfall intensities at 5 minute intervals. Each of these storms was routed through the catchment model and values of the peak runoff rate Q_{max} and the exceedance volume V(QTH) for 4 different values of QTH between 60 and 120 cfs were determined. The results are tabulated in Table 6-1 where the storm number corresponds to the rank of the storm among the 48 events selected in the previous step.

Table 6-1

Results of Catchment Simulation of Selected Rain-
fall Events

Storm No.	Q_{max}	V(QTH)			
		QTH = 60	QTH = 80	QTH = 100	QTH = 120
1	135.78	72234	33705	12502	2649
2	209.11	104168	80862	60927	43847
3	106.74	33870	14001	1817	0
4	121.90	23131	12201	4424	110
5	111.37	40047	19187	4243	0
6	108.64	34234	12827	1667	0
7	197.26	59452	44896	32502	22021
8	91.33	14823	3081	0	0
9	86.97	17864	2027	0	0
10	79.12	4991	0	0	0
11	82.70	12767	484	0	0
12	73.60	4445	0	0	0
13	99.01	21416	6760	0	0
14	99.66	15503	5404	0	0
15	66.24	2762	0	0	0
16	113.65	17788	8141	1924	0
17	48.54	0	0	0	0
18	96.95	19193	6250	0	0
19	98.54	12040	3671	0	0
20	139.91	66476	40887	21270	7150
21	71.74	3663	0	0	0
22	55.23	0	0	0	0
23	74.03	6871	0	0	0
24	73.49	6788	0	0	0
25	42.03	0	0	0	0

(Table 6-1, continued)

Storm No.	Q_{max}	V(QTH)			
		QTH = 60	QTH = 80	QTH = 100	QTH = 120
26	34.95	0	0	0	0
27	36.67	0	0	0	0
28	48.67	0	0	0	0
29	68.33	4829	0	0	0
30	63.07	426	0	0	0
31	78.26	5965	0	0	0
32	43.16	0	0	0	0
33	53.40	0	0	0	0
34	30.08	0	0	0	0
35	30.76	0	0	0	0
36	27.15	0	0	0	0
37	28.12	0	0	0	0
38	141.71	56812	36901	20661	8009
39	53.77	0	0	0	0
40	28.53	0	0	0	0
41	77.53	9252	0	0	0
42	28.96	0	0	0	0
43	33.17	0	0	0	0
44	78.69	11545	0	0	0
45	60.69	45	0	0	0
46	86.87	11781	1315	0	0
47	64.44	1473	0	0	0
48	40.77	0	0	0	0

6.5.7 Construction of the Derived Frequency Curves

Separate frequency curves were constructed for each of the runoff variables that appear in Table 6-1. The first step in constructing each frequency curve was to rank the events in decreasing order, and this was done for each variable. The resulting ranks of the events appear in Table 6-2.

If the rank of an event is m, an estimate of the average recurrence interval, T_E, between events that equal or exceed that event is

$$T_E = \frac{N+1}{m} \qquad\qquad (6-1)$$

where N is the total number of years of data (in this case N = 200).

The frequency curve for Q_{max} which appears in Fig. 6-3 was created by plotting the values of Q_{max} in Table 6-1 as function of T_E which was computed by Eq. (6-1) from the data in Table 6-2. Through these points was drawn a fitted curve which represents the derived frequency curve for Q_{max}.

Similarly, the data for V(QTH) was plotted in Fig. 6-4 for each of the four different values of QTH. Four different frequency curves appear in this figure. The uppermost curve gives the frequency with which different runoff volumes occur when the flow rate is at or above 60 cfs. In other words, this is the volume that would be required in an overflow storage facility to prevent spillage of combined waste water under the condition that the interceptor

Table 6-2

Rank of Runoff Variables

Storm Number	Rank of Storm according to Rain-fall Selection Algorithm	Rank of Storm according to Peak Runoff Rate	Rank of Storm according to Exceedance Volume			
			QTH=60	QTH=80	QTH=100	QTH=120
1	1	5	2	5	5	5
2	2	1	1	1	1	1
3	3	10	8	7	9	–
4	4	6	9	9	6	6
5	5	8	6	6	7	–
6	6	9	7	8	10	–
7	7	2	4	2	2	2
8	8	15	15	15	–	–
9	9	16	12	16	–	–
10	10	19	24	–	–	–
11	11	18	16	18	–	–
12	12	24	25	–	–	–
13	13	12	10	11	–	–
14	14	11	14	13	–	–
15	15	28	28	–	–	–
16	16	7	13	10	8	–
17	17	36	–	–	–	–
18	18	14	11	12	–	–
19	19	13	17	14	–	–
20	20	4	3	3	3	4
21	21	26	27	–	–	–
22	22	32	–	–	–	–
23	23	23	21	–	–	–

(Table 6-2, Continuation)

24	24	25	22	–	–	–
25	25	38	–	–	–	–
26	26	41	–	–	–	–
27	27	40	–	–	–	–
28	28	35	–	–	–	–
29	29	27	26	–	–	–
30	30	30	30	–	–	–
31	31	21	23	–	–	–
32	32	37	–	–	–	–
33	33	34	–	–	–	–
34	34	44	–	–	–	–
35	35	43	–	–	–	–
36	36	48	–	–	–	–
37	37	47	–	–	–	–
38	38	3	5	4	4	3
39	39	33	–	–	–	–
40	40	46	–	–	–	–
41	41	22	20	–	–	–
42	42	45	–	–	–	–
43	43	42	–	–	–	–
44	44	20	19	–	–	–
45	45	31	31	–	–	–
46	46	17	18	17	–	–
47	47	29	29	–	–	–
48	48	39	–	–	–	–
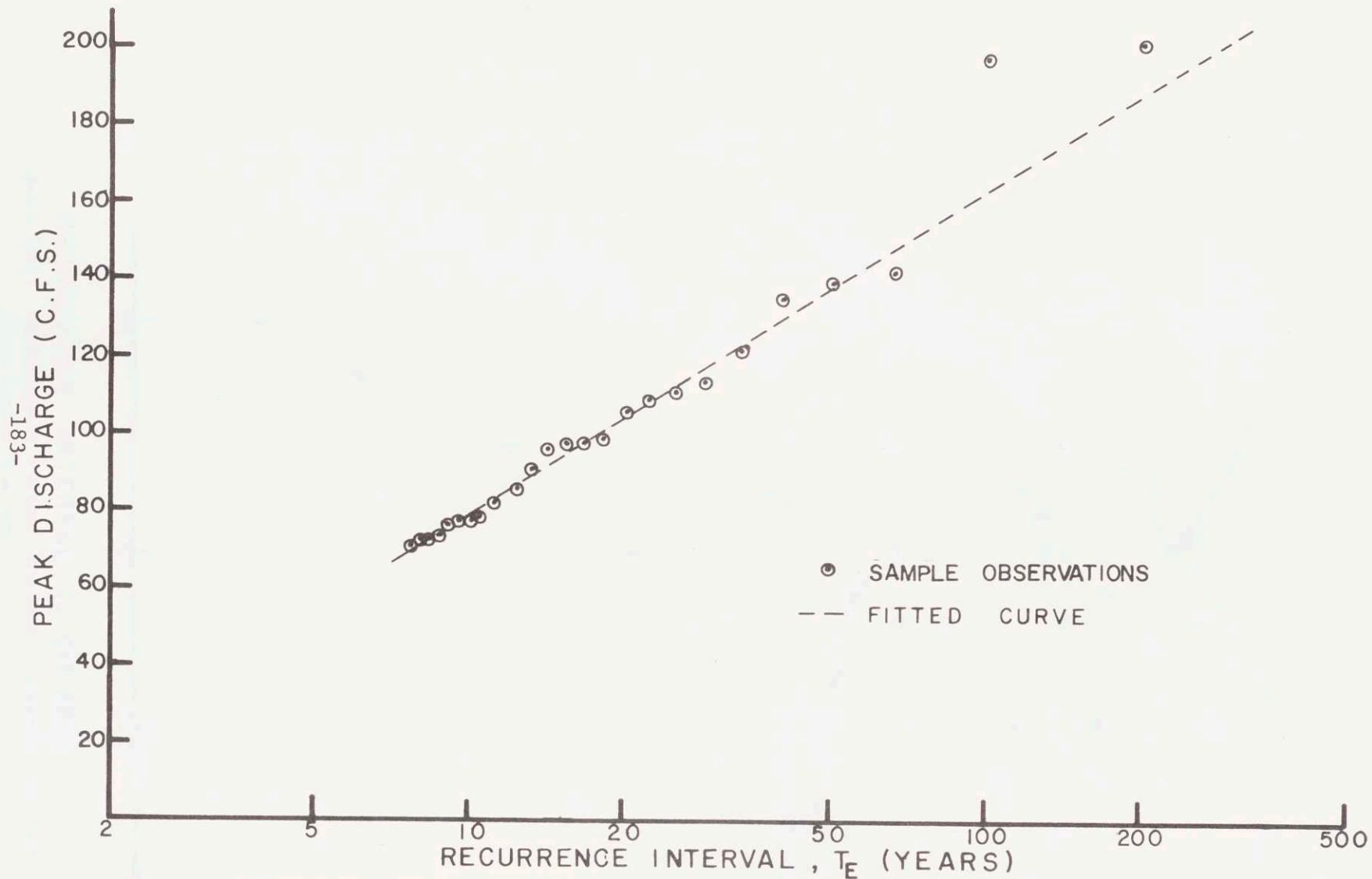
Figure 6-3: Peak Runoff Frequency Curve for the Gray Haven Catchment
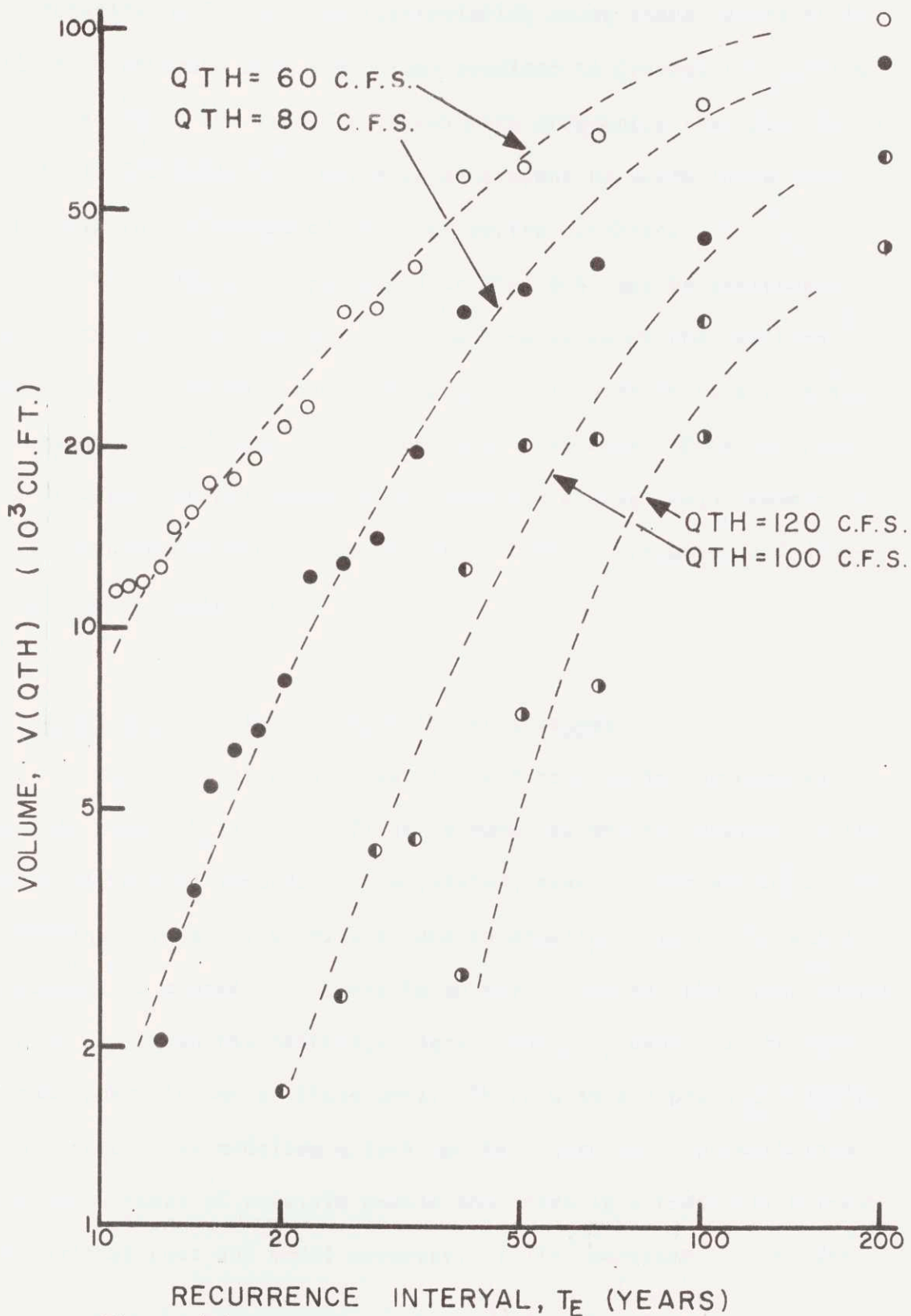
Figure 6-4:   Exceedance Volume Frequency Curves for the
Gray Haven Catchment

-184-

has a capacity of 60 cfs. By interpolating among these curves it is possible to estimate that the volume required to prevent the outflow from exceeding 70 cfs from Gray Haven more frequently than once in 20 years is 13,200 cubic feet which is equivalent to 0.156 inches of depth uniformly distributed over the entire catchment.

The information presented in Fig. 6-4 may be rearranged as shown in Fig. 6-5. In Fig. 6-5 each curve shows the relation between overflow storage and maximum allowable outflow rate to reduce spillage events to occur at the indicated frequency. From the viewpoint of flood control these curves show the storage requirements to prevent flooding downstream as function of flood frequency and downstream channel capacity.

6.6 Accuracy of the Derived Runoff Distributions

There are three sources of error present in the derived frequency curve $T_E(V)$. The first is sampling errors inherent in the limited historical records of the rainfall events. The second is due to modeling errors. The third is due to sampling errors inherent in the simulation procedure. There is no way to control the first source since we are given the historical data. Our only choice is to make the best possible use of these data. There also are practical limits on the extent that modeling errors can be controlled. Nevertheless there are a range of possible models and there is a trade-off between computational cost and model accuracy. It is important to consider
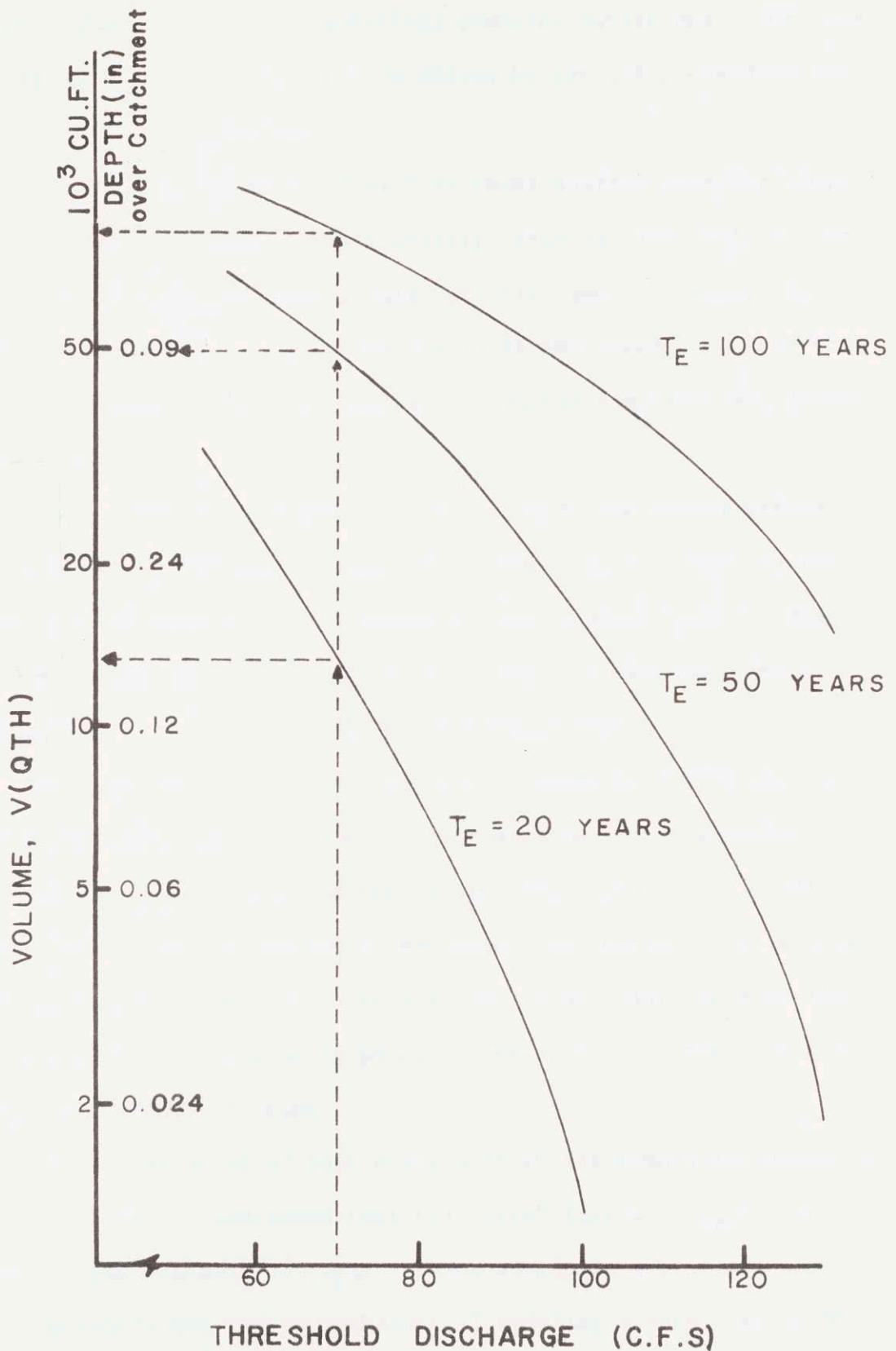
Figure 6-5: Overflow Storage and Maximum Allowable Outflow
Rate at Constant T_E

-186-

the trade-off in view of the historical sampling variations. The final source may be limited to any desired degree by extending the duration of the simulation calculations.

It would be desirable if each of these sources of error could be dealt with analytically. Unfortunately, this is very difficult and no fully satisfactory techniques exist at this time. Moreover, it is virtually impossible to separate the first two sources because the particular parameters that are estimated from the historic data depend upon the model.

It is possible to quantitatively analyze some of the errors introduced by the solution procedure to estimate $T_E(V)$. Each of the solution methods presented in Appendix B involves numerical or analytical approximations to the solutions of Eqs. 2-1 to 2-10. These approximations can often be analyzed quantitatively.

The particular solution procedure selected in this study was the stochastic/deterministic simulation procedure. This procedure introduces statistical sampling errors into the estimate of $T_E(V)$ and these errors may be limited by extending the length of the simulation. An important question to be answered is how many years of simulation are required and what is gained by extending the simulation for an additional period of years.

At the beginning of this discussion of the simulation sampling errors the reader is cautioned that the "true" function $T_E(V)$ is unknown and the estimate of $T_E(V)$ being sought is subject to historical sampling errors and to mathematical modeling errors that at this

point, cannot be controlled. In addition to these errors, however, are the additional simulation errors which are now to be discussed.

It would appear from the simulation results shown in Fig. 6-3 that peak runoff rate from Gray Haven is exponentially distributed according to

$$f(Q_{max}) = ke^{-kQ_{max}} \qquad (6-2)$$

where the parameter k, estimated from the fitted curve in Fig. 6-3 is equal to .0274. Now, the data shown in Fig. 6-3 comprise a sample from a 200-yr. simulation. Therefore, k is a random variable and is distributed according to a sampling PDF.

In Appendix C it is shown that the sampling distribution of k (when it is known that x is exponentially distributed and when k is estimated according to the estimator given in Appendix C) is a Gamma PDF with parameters

$$\alpha = n \qquad (6-3)$$

and

$$\beta = \frac{n+1}{n^2} k \qquad (6-4)$$

where

$$\hat{k} = \frac{n}{\sum_i x_i} \qquad (6-5)$$

In general the simulation run will be long enough to neglect the difference between n and n+1 so that

$$\beta \approx \frac{\hat{k}}{n} \tag{6-6}$$

Additionally, n will be large enough so that the normal distribution is a good approximation to the Gamma Distribution. The mean and variance of the PDF for k is

$$\mu_k = \hat{k} \tag{6-7}$$

and

$$\sigma_k^2 = \frac{\hat{k}^2}{n} \tag{6-8}$$

or

$$\sigma_k = \frac{\hat{k}}{\sqrt{n}} \tag{6-9}$$

Now the CDF for the exponential distribution is

$$F_{Q_{max}}(Q_{max}) = 1 - e^{-kQ_{max}} \tag{6-10}$$

which may be re-written in terms of the recurrence interval as

$$T_E(Q_{max}) = \frac{1}{e^{-kQ_{max}}} \tag{6-11}$$

At a given value of $T_E(Q_{max})$, confidence intervals for Q_{max} may be found as follows. Eq. (6-11) may be rearranged to read

$$Q_{max} = \frac{\ln[T_E(Q_{max})]}{k} \tag{6-12}$$

where k now is a random variable which is approximately normally dis-
tributed with mean and variance given by Eq. (6-7) and (6-8.) Con-
fidence limits at the 95% level for Q_{max} were derived using Eqs.
(6-12), (6-7) and (6-8). These appear in Fig. 6-6 for simulation
durations of 50, 200 and 1000 years. Since these confidence limits
were derived on the basis of the sampling distribution of k they
apply to entire distributions not to individual sample points which
may be plotted as shown in Fig. 6-3. Similarly, confidence limits
at the 50% level appear in Fig. 6-7.

Figs. 6-6 and 6-7 give some approximation of the possible
computational errors inherent in the simulation process. These Figures
show clearly that it is necessary to simulate a long period of rain-
fall events. Because of the computational costs, it is desirable
to process only a few of the many generated rainfall events through
the catchment model. A possible screening procedure was presented
in Section 6.5.5.

On the basis of this screening procedure, the generated storms
were ranked according to the maximum rainfall depth in any 30 minute
period. The largest 48 storms were routed through the catchment model.
Then, the largest 23 values of Q_{max} were ranked and used to construct
$T_E(Q_{max})$. A less costly procedure would have been simply to simulate
the top ranked 20 of the original 48 storms. But this would have
introduced an error into the estimates of T_E in the neighborhood of
$T_E = 10$ to 20 years. This is illustrated in Fig. 6-8 where an estimate
of $T_E(Q_{max})$ based on these 20 storms is compared to $T_E(Q_{max})$ from
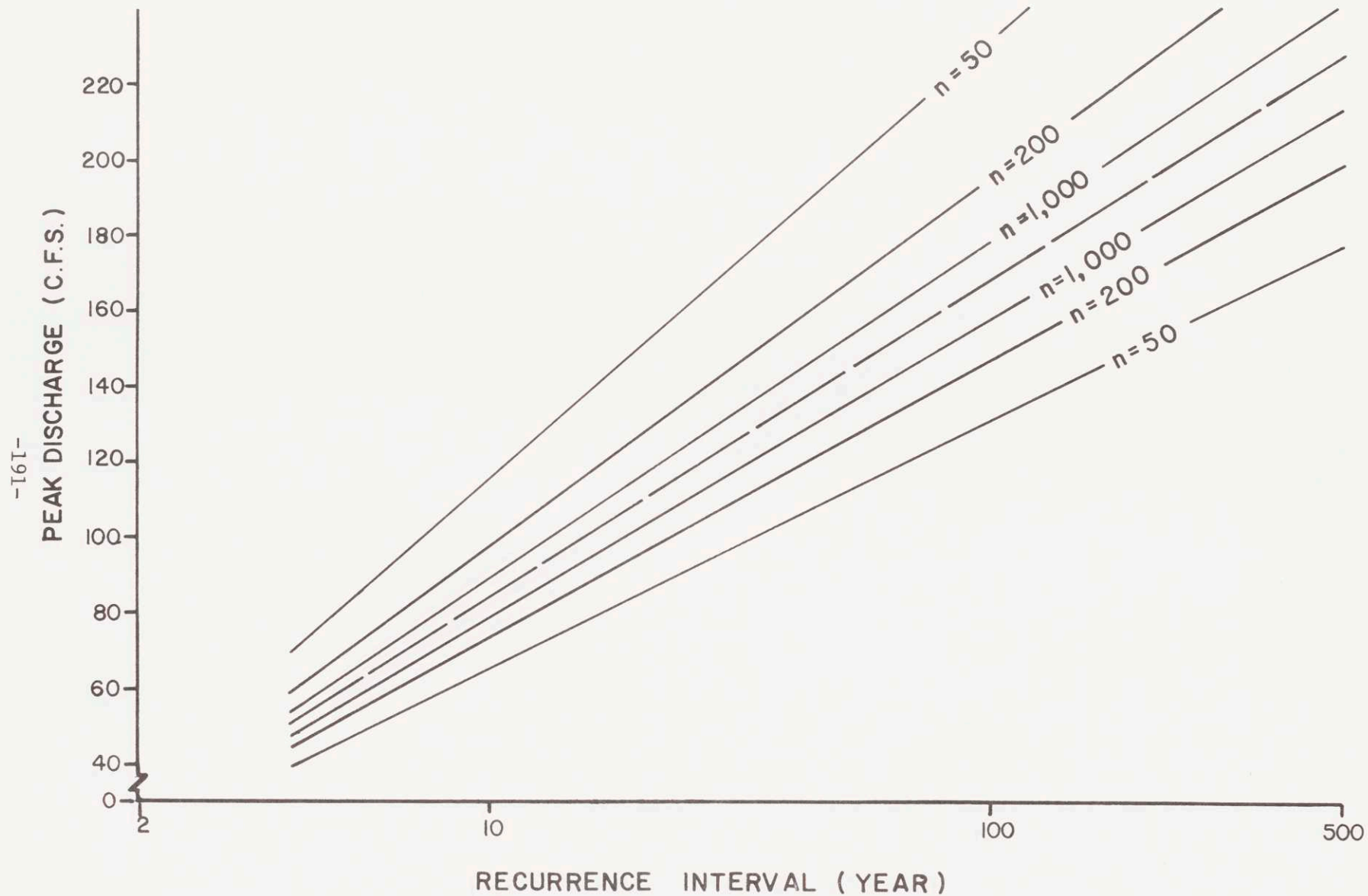
Figure 6-6: 95% Confidence Limits for $T_E (Q_{max})$
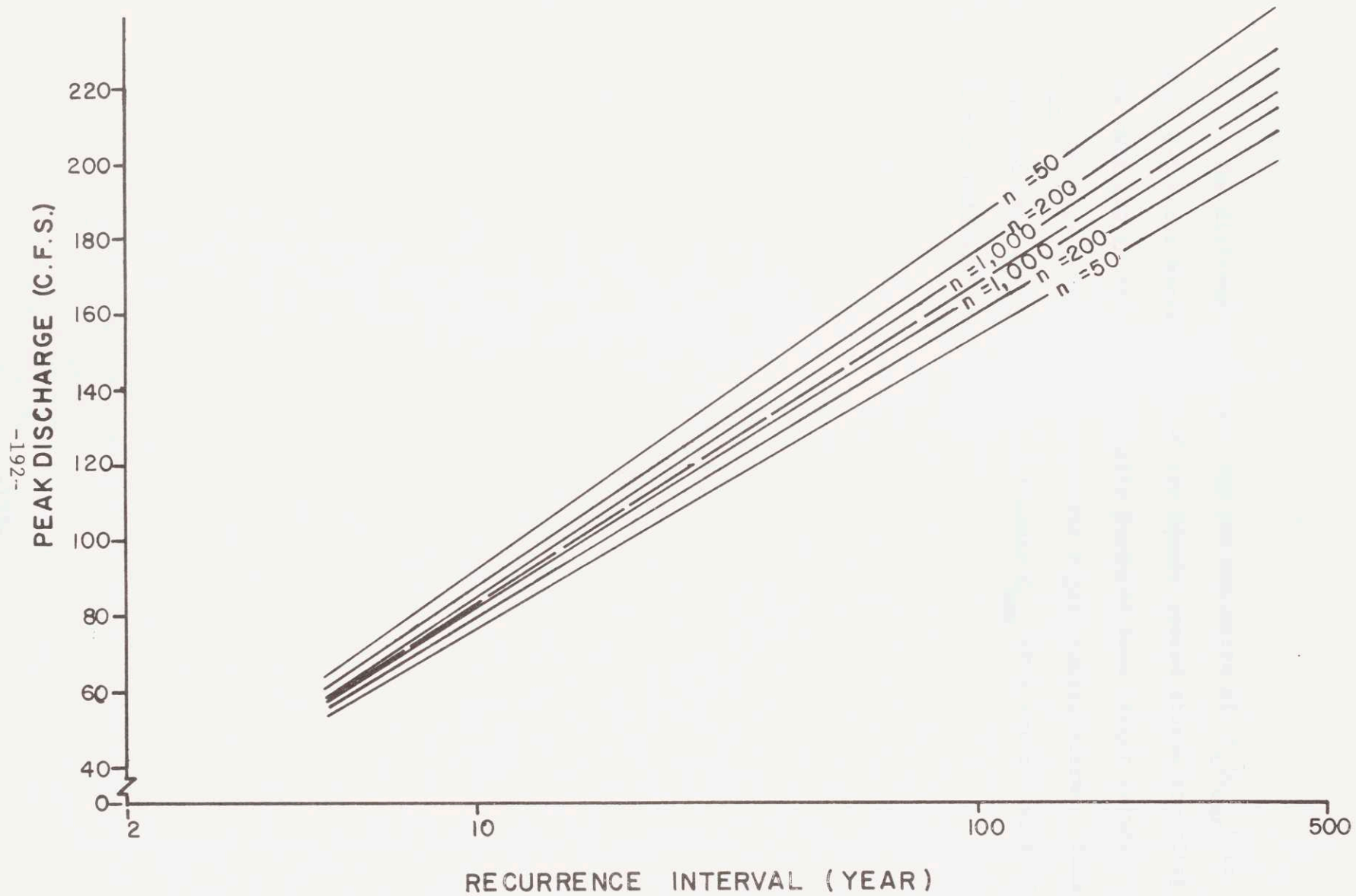
Figure 6-7: 50% Confidence Limits for T_E (Q_{max})

Fig. 6-3.

The differences between the two estimates of $T_E(Q_{max})$ in Fig. 6-8 occur because some of the lesser ranked storms according to the DMAX-AVGTIM criterion actually produced some larger values of Q_{max} than was produced by some of the higher ranked storms. This occurred because more factors influence Q_{max} than are accounted for in the DMAX-AVGTIM criterion.
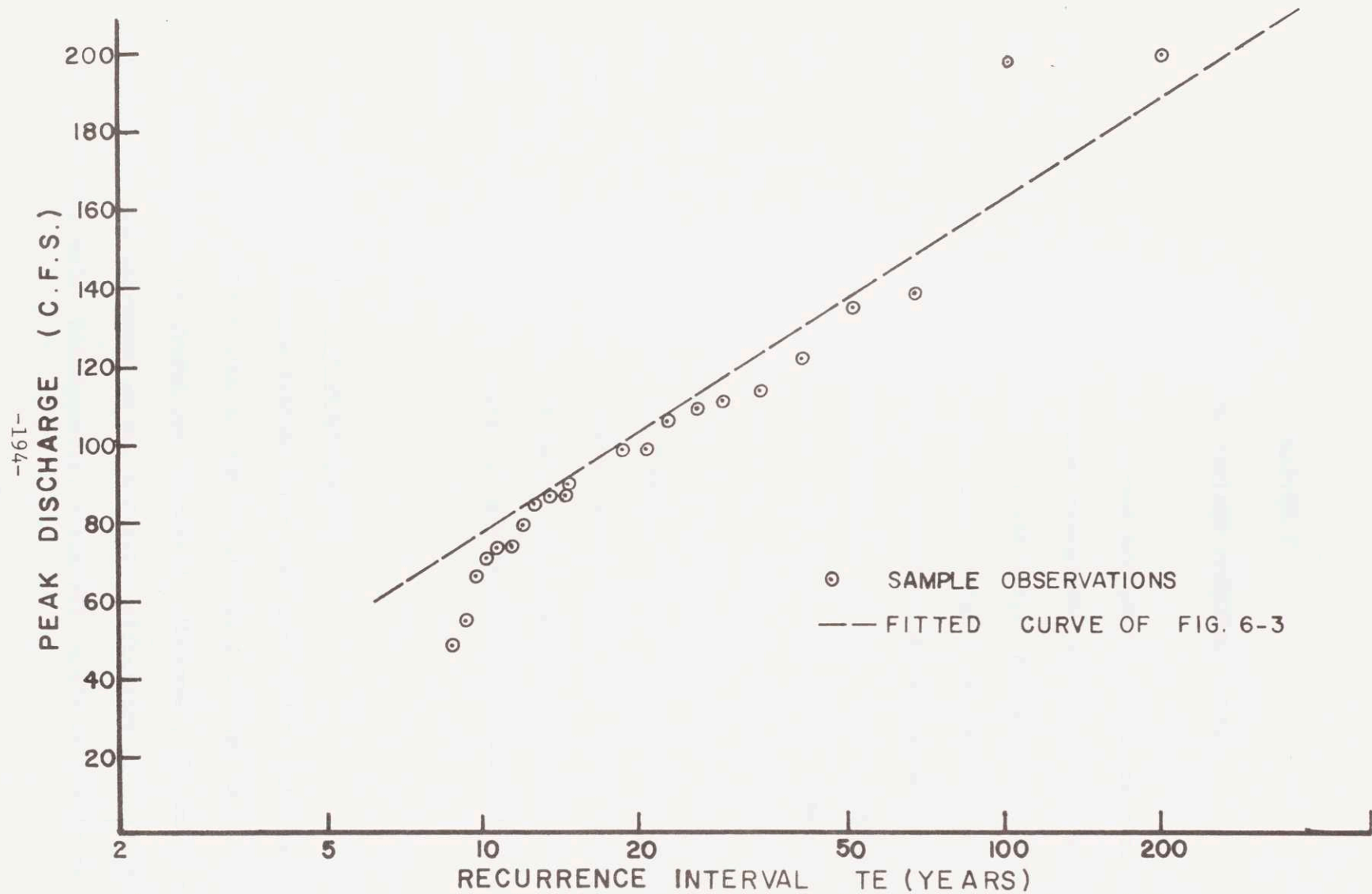
Figure 6-8: Peak Runoff Frequency Curves derived with the first 23 storms, ranked according to the DMAX-AVGTIM criterion.

CHAPTER 7

APPLICATIONS OF DERIVED FREQUENCY CURVES

Hydrologic frequency curves are used in water resources engineering because water resources management and investment schemes must deal with natural hydrologic variability. Frequency curves offer a valuable means to describe hydrologic variability and to give quantitative measure to the hydrologic impacts of environmental changes.

Considered in this chapter are several example problems where the techniques presented in this report may apply. The specific problem areas are (i) the impact of urbanization on the runoff from a small watershed, (ii) the relative hydrologic impacts of alternative strategies for urban development, (iii) the relative efficiency of different runoff control alternatives, and (iv) the hydrologic basis for establishing drainage charges(which are analogous to effluent charges) for the costs of controlling downstream hydrologic impacts.

7.1 Hydrologic Impacts of Urbanization

Urban drainage systems have been designed to dispose quickly of urban runoff. The volume of this runoff is increased as the pervious areas of the catchment are decreased. Moreover, the rates of urban runoff are increased as the hydraulic efficiency of the drainage network is improved. Consequently, urbanized runoff is likely to reach

Table 7-1

Characteristics of Hypothetical Catchment

Characteristic	Undeveloped	Developed (Shopping Center)
A (acres)	10	10
L_c (ft)	500	50
S (ft/ft)	.01	.01
n	.50	.10
N(storms/yr)	30	110

apply to the undeveloped and the developed states of the catchment. The effect of the development is to decrease typical overland flow length (L_c) from 500 ft to 50 ft by the construction of drainage works such as gutters and swales. The impervious surfaces increase the number of runoff producing storms each year (N) and also reduce the surface roughness coefficients (n).

The runoff frequency curves for this 10-acre catchment could be derived by the stochastic/deterministic simulation technique that was used in the previous chapter. Nevertheless, for the purpose of illustrating the potential utility of other solution procedures the analytical solution for $T_E(Q)$ developed in Appendix D will be applied to this problem.

The catchment is furthermore assumed to be located in Boston

greater magnitudes faster than was observed before development occurred, both due to the increase in the direct runoff volume and the reduced timing of each branch of the drainage network.

To date, analysis of the impacts of urbanization on runoff has been primarily conducted in a deterministic framework in terms of changes in the physical parameters of the catchment or in terms of changes in certain properties of runoff hydrographs.

Knapp and Glasby [1972] prepared a bibliography with abstracts that gives a complete set of references to previous theoretical and experimental investigations of this topic. More recent studies have also been reported by Kadoya [1972] and McCuen [1973]. These previous studies generally are not strongly founded in the theories of probability and fluid mechanics of how specific physical changes in the urban environment influence the magnitude and frequency of urban runoff events. These studies do speak of the effects of channelization or of the effects of impervious surfaces, but these mainly are general observations that do not necessarily apply to specific circumstances such as the potential impacts of the lining of a given stream channel or the construction of a shopping center at some particular location. Nevertheless, these previous studies certainly may provide valuable insights and information to the use of the techniques presented herein in dealing with such specific problems.

The application of the techniques investigated in this study may be illustrated by considering the urbanization of a hypothetical 10 acre catchment. Let the conditions given in Table 7-1

where $\beta = 30$ (hr/in), $\lambda = 0.13$ (hr^{-1}), and the average number of rainfall events per year is 110.

The computation of the frequency curves for the developed and undeveloped cases appear in Table 7-2. The frequency curves are plotted in Fig. 7-1 and show that increased peak flows would occur more frequently after developments. Fig. 7-1 shows that any structure that had a design capacity to handle the 20-yr event under natural conditions would be adequate to handle only the 3 year event under developed conditions.

This simple example illustrates a very important application of frequency curves. Of course, this procedure can be used for complex urban catchments to predict the impact of proposed changes in land use. The frequency curves at any stage of development can be derived as they were in Chapter 6 for Gray Haven. The results of the derived frequency curves could be presented exactly as those derived for this example.

This example was constructed to illustrate in principle the use of derived frequency curves to assess the hydrologic impacts of urbanization. This particular example of a hypothetical 10-acre area led to the frequency curves in Fig. 7-1. A careful examination of these curves by an experienced drainage engineer would suggest that these curves might actually underestimate the runoff rates to be expected, particularly in the developed catchment case. The most plausible explanation for this is that the storm interior pattern is generally not rectangular as assumed in this example.

Table 7-2

Frequency Curve Calculations for the Hypothetical 10-acre Catchment

Undeveloped   Developed

1. Compute α_c from Eq. (D-8)

$$\alpha_c = \frac{1.49}{0.5}(.01)^{1/2} = .298 \qquad \alpha_c = \frac{1.49}{.1}(.01)^{1/2} = 1.49$$

2. Compute t_c for different values of Q from Eq. (D-9a)

$$t_c = .0156\left[\frac{(.5)(500)(10)^{2/3}}{(.01)^{1/2}Q^{2/3}}\right]^{3/5} \qquad t_c = .0156\left[\frac{(.1)(50)(10)^{2/3}}{(.01)^{1/2}Q^{2/3}}\right]^{3/5}$$

$$= 4.28\, Q^{-2/5} \qquad\qquad\qquad = .410\, Q^{-2/5}$$

Q(cfs)	t_c(hr)	t_c(hr)
.5	5.65	.541
1	4.28	.410
2	3.24	.311
3	2.76	.264
4	2.46	.235

3. Compute B from Eq. (D-25) for each Q

$$B = \frac{t_c}{2}\sqrt{\left[\frac{Q}{(871.2)(.298)}\right]^{3/5}\left(\frac{24}{t_c}\right) - \frac{Q}{10}} \qquad B = \frac{t_c}{2}\sqrt{\left[\frac{Q}{(871.2)(1.49)}\right]^{3/5}\frac{24}{t_c} - \frac{Q}{10}}$$

Table 7-2   (Continued)

$$= \frac{t_c}{2} \sqrt{\frac{.854Q^{3/5}}{t_c} - \frac{Q}{10}} \qquad\qquad = \frac{t_c}{2} \sqrt{\frac{.0817Q^{3/5}}{t_c} - \frac{Q}{10}}$$

Q	B	B
.5	.630	.060
1	.675	.065
2	.724	.069
3	.754	.072
4	.776	.074

4. Compute σ from Eq. (4-23) for each Q

$$\sigma = 30 \left[(.5)(.13)B/30\right]^{2/3} = .502 \, B^{2/3}$$

Q	σ	σ
.5	.369	.077
1	.386	.081
2	.405	.084
3	.416	.087
4	.424	.088

(Table 7-2 (Continued)

5. Compute I_o from Eq. (D-22) for each Q

Q	I_o	I_o
.5	.614	1.0
1	.593	1.0
2	.569	1.0
3	.556	1.0
4	.546	1.0

6. Compute T_E from Eq. (D-27)

$$T_E = \frac{e^{3Q}}{30 \, I_o} \qquad\qquad T_E = \frac{e^{3Q}}{110 \, I_o}$$

Q	T_E	T_E
.5	.24	.01
1	1.13	.18
2	23.6	3.67
3	486.	73.7
4	--	1480.
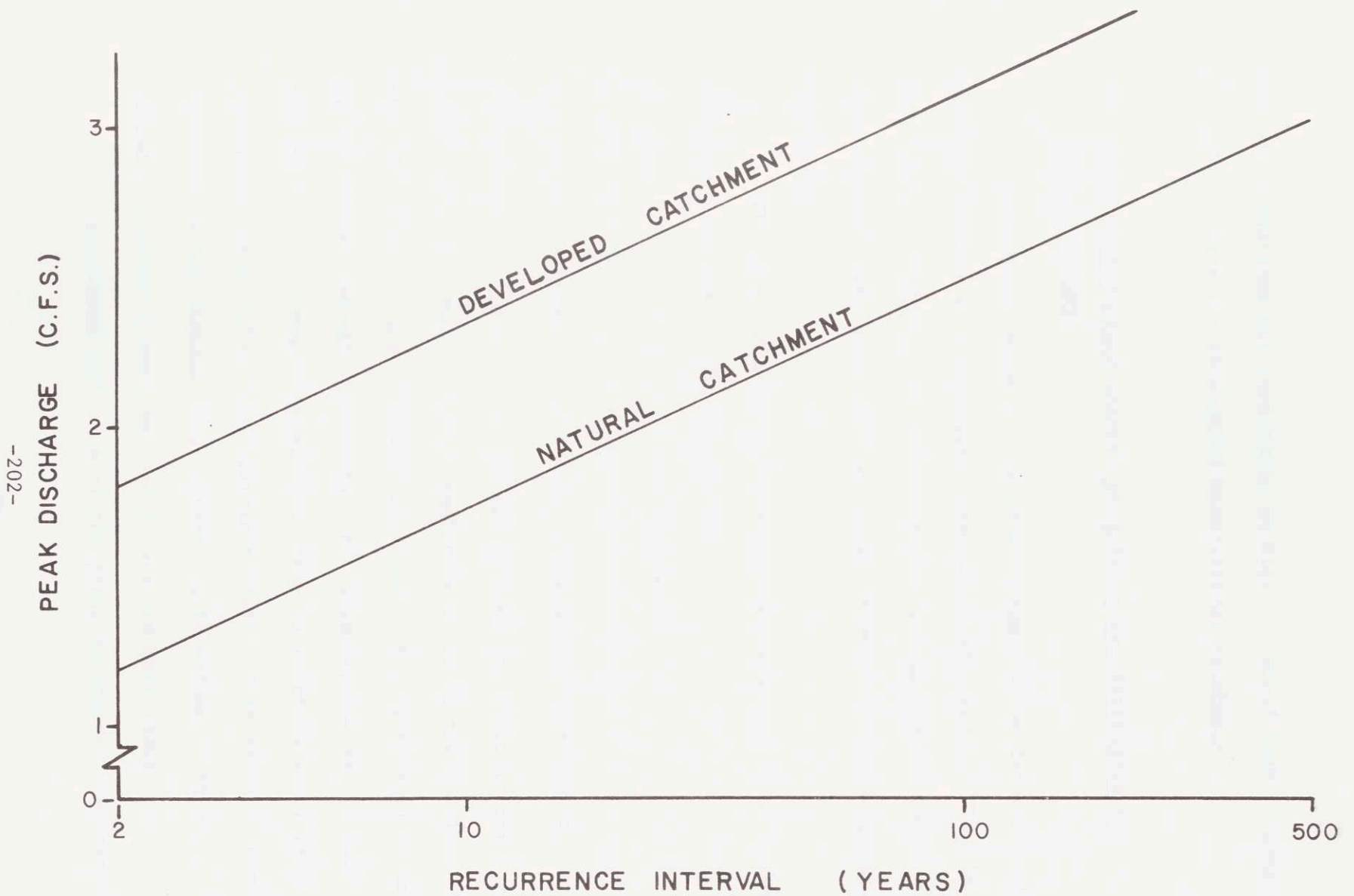
Figure 7-1: Peak Runoff Frequency (developed and undeveloped stages) for the Hypothetical 10 Acre Catchment

Temporal variations not considered in Fig. 7-1 would lead to greater peak runoff rates for this small hypothetical catchment.

7.2 Relative Hydrologic Impacts of Alternative Strategies for Urban Development

Frequency curves can be used to compare the impacts on the runoff of an area of alternative development strategies. This is achieved by determining the sensitivity of the frequency curve to variations in those parameters which may be modified by the proposed development.

The three main physical changes accompanying urban development that have hydrologic impacts are:

(i) increases of impervious area

(ii) reductions of overland flow lengths

(iii) reductions of surface roughness of flow paths.

The effects of some of these changes as they may occur in any development strategy, may be modeled analytically as in the previous example. In addition, a much deeper assessment of a wide range of impacts may be studied through simulation. For example, one way to reduce the impacts of increased impervious areas is to route water from the impervious areas across other pervious areas. This permits increased infiltration and reduces total direct runoff volume. The model presented in Chapter 4 could be used to analyze this issue.

Associated with each of the physical changes that cause

hydrologic impacts are well defined, physically meaningful parameters
in the present model to account for the physical change.

7.3 Analysis of the Relative Efficiency of Urban Runoff Control
     Alternatives

        The Denver Regional Council of Governments (1969) enumerates
several alternatives to control the runoff from urbanized areas;
these alternatives range from restoration of natural channels to con-
struction of small reservoirs. Anderson [1970] reported that the
efficient use of the available storage of the main components of com-
bined sewers reduces the magnitude and frequency of overflows.
Devenis (1968) described the combined sewage overflow detention and
chlorination station which is operated by the Metropolitan District
Commission, serving over 40 cities and towns in the Metropolitan
Boston area. The dual objective City of Chicago underflow project
to control runoff and to generate hydroelectric power is another
well documented experiment. Marks et al [1971] proposed small
storage tanks located at critical points in the combined sewer net-
work of the city of Cambridge, Ma. to alleviate overflows to the
Charles River and to reduce the frequency of street and basement
flooding. Recent work at Resource Analysis Inc. (1973) investigated
detention storage reservoirs as measures for controlling the developed
runoff from small sites.

7.3.1 Analysis of Detention Storage Ponds

Bauer [1969] argued that urban drainage problems should be regarded as volume control problems rather than as peak runoff rate control problems. One of the important alternatives for controlling runoff volumes is the use of detention storage ponds. Such ponds would remain empty (unless there is some other reason to have standing water) except during brief periods when storms occur. The hydraulic function of such ponds is to store runoff during peak runoff periods for release during subsequent off-peak periods.

Derived runoff frequency curves offer a valuable means to analyze detention storage ponds because a wide range of storm conditions need to be controlled. Individual storms have different depths, durations and interior rainfall patterns. One of these potential storms could be selected as a "design storm" and used to evaluate the effectiveness of the pond in controlling the runoff from that particular "design" storm. Because of the wide range of possible storm conditions, there is no reliable way to select such a "design storm". One relatively simple way to evaluate such ponds, however, would be based on the derived frequency curves of the response characteristics of different pond designs.

If detention storage ponds are to be used for runoff control, it is important to evaluate not only the outflow characteristics from the pond itself but also to consider other impacts downstream. For example, such ponds in the upstream regions of a catchment may delay the upstream runoff and reduce peak flow rates downstream. On

the other hand, such ponds on downstream tributaries would delay the downstream runoff which could cause the downstream peak runoff rate to occur at the same time as the peak from upstream and this would undesirably increase the downstream peak runoff rates.

In order to illustrate some of the issues in evaluating storage detention ponds only the response characteristics of the ponds at the pond outlet are considered in this section. The illustrated approach would also be used to examine the downstream impacts.

7.3.2 Detention Storage Control of a Given Inflow Hydrograph

A detention storage pond discharges water as a function of the hydraulic head on its outlets. The pond introduces a time delay between the inflow and outflow hydrographs because of the time required to create this hydraulic head. This time delay and consequent attenuation in outflow peak runoff rate depends upon the type of outlets, their number and their size . Figure 7-2 illustrates this for four different outlet designs for a hypothetical pond. The pond is assumed to be a rectangular box of area, 20,000 square feet (for instance, 200'x100') and for the present discussion, of infinite height. The pond is empty at the beginning of the storm. Table 7-3 summarizes the physical characteristics of the pond, and Table 7-4 gives the discharge elevation curves for each design.

It is interesting to observe in Figure 7-2 that the controlled outflow hydrographs are single-peaked even though the inflow hydrograph had two peaks. Note also that the time to the controlled
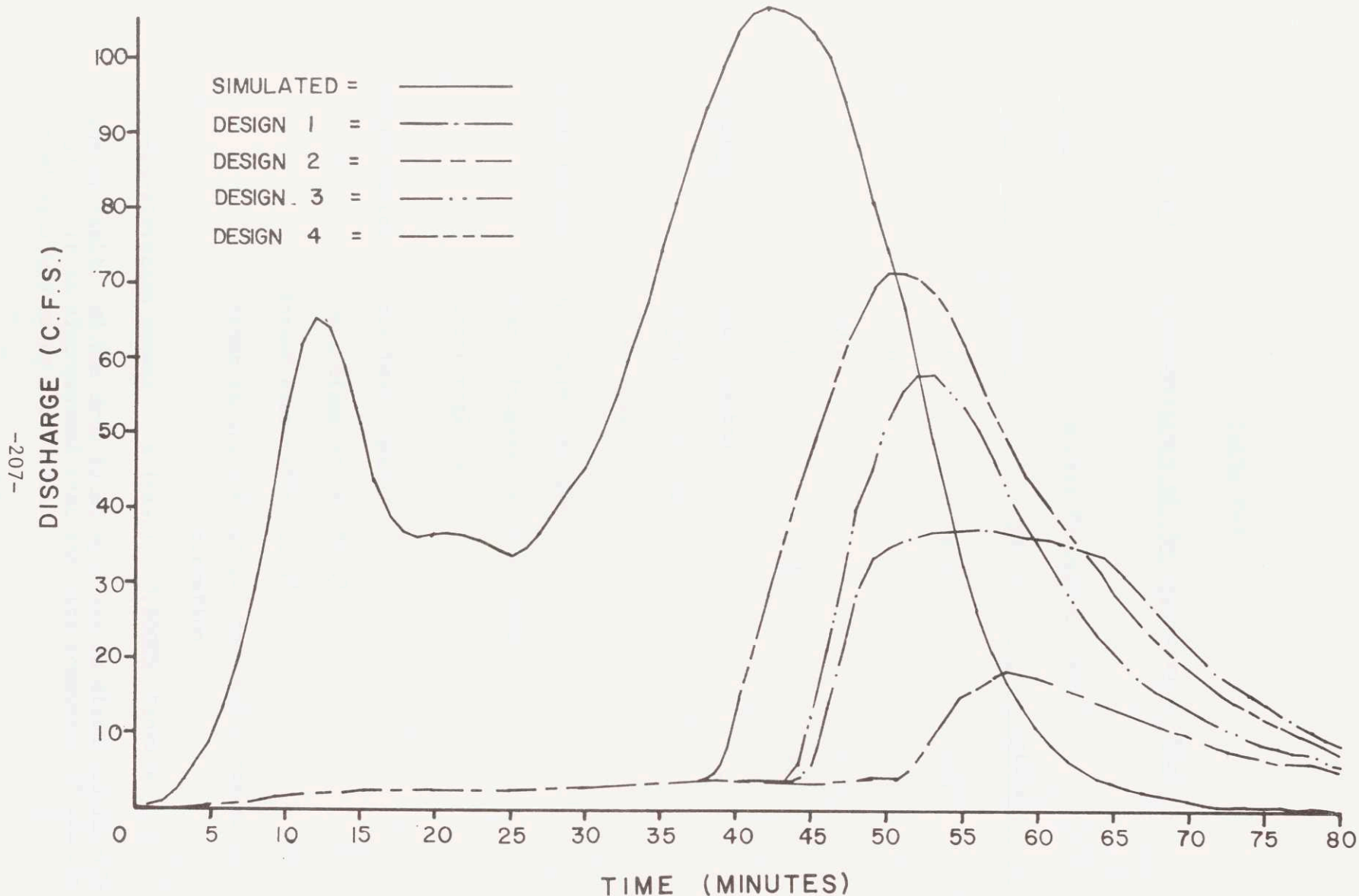
Figure 7-2: Controlled Outflow Hydrographs from the Hypothetical Pond, for four different outlet designs.

Table 7-3

Physical Characteristics of the Hypothetical Pond

Design	Outlet Elevation (feet)		
	Lower	Upper	Spillway
1	0.0	6.0	8.0
2	0.0	-	8.0
3	0.0	-	6.0
4	0.0	4.5	6.0

Spillway   Broad-crested

              Length: 20 feet

              c_d = 3.09

Lower Outlet: Drop inlet spillway[*]

              Crest diameter = 6.0 inches

              throat neglected

Upper outlet: drop inlet spillway[*]

              crest diameter = 36.0"

              throat diameter = 21.0"

              throat location = at 1.0 foot below the crest
                                    elevation

Storage-elevation curve: h (feet) = 0.00005 Storage

* The hydraulic of the drop inlet spillway is discussed in reference 36. It is also assumed that the pipe component of the drop inlet spillway never flows full.

Table 7-4

Discharge Elevation Curves for each Combination of Outlets

Elevation (feet)	Discharges (cfs)			
	DESIGN 1	2	3	4
0.0	0.00	0.00	0.00	0.00
0.5	1.50	1.50	1.50	1.50
1.0	1.84	1.84	1.84	1.84
1.5	2.12	2.12	2.12	2.12
2.0	2.37	2.37	2.37	2.37
2.5	2.60	2.60	2.60	2.60
3.0	2.81	2.81	2.81	2.81
3.5	3.00	3.00	3.00	3.00
4.0	3.18	3.18	3.18	3.18
4.5	3.36	3.36	3.36	3.36
5.0	3.52	3.52	3.52	15.85
5.5	3.68	3.68	3.68	31.01
6.0	3.83	3.83	3.83	46.61
6.5	16.30	3.97	14.89	69.28
7.0	31.44	4.11	35.01	97.67
7.5	36.11	4.25	61.02	130.66
8.0	38.79	4.88	91.77	167.65
8.5	48.21	15.42	126.64	208.20

(Continuation, Table 7-4)

9.0	74.55	35.53	165.19	252.02
9.5	102.65	61.52	207.08	298.85
10.0	135.40	92.26	252.07	348.50

peak runoff is delayed and that the peak discharge, not only is reduced in all cases but that the amount of reduction is sensitive to the design of the outlets.

This reduction of the runoff rates is achieved by a redistribution of the incoming water over time since no water losses are experienced. Figure 7-2 may be misleading because it reflects only the volume of water discharged from the reservoir during the storm and does not indicate the volume of water stored in the reservoir at the end of the storm. Table 7-5 demonstrates that the water balance is preserved and shows the magnitude of the volume stored at time t = 80.0 minutes.

The information presented in this example suggests that there is a definite relationship between the maximum storage utilized, the peak outflow rate and the characteristics of the inflow hydrograph. Note for this particular inflow hydrograph that the volume stored at the end of the storm (see Table 7-5) was greatest for the designs that gave the smallest peak outflow rates. Nevertheless, certain outlet designs would appear to be superior to others. For example, compare designs 1 and 3. In Table 7-5 the volume stored at the end of the storm was about the same for both designs, but the peak reduction for design 1 was substantially greater than for design 3.

A more careful comparison shows that the maximum storage utilized at any time during the storm was a little greater for design 1 (153,000 ft^3) than for design 3 (148,800). But the ratio of peak outflows (design 1/design 3) was 0.64 whereas the ratio of

Table 7-5

Water Balance of the Pond for Hydrographic Storm in Fig. 7.5

Inflow Volume (ft^3) :   188,549.25

Pond Initial Volume (ft^3):   0.00

Total (ft^3) :   188,549.25

	Design 1	Design 2	Design 3	Design 4
Outflow volume (ft^3)	64214.17	27223.55	65462.54	94555.19
Volume stored at time 80 minutes (ft^3)	124336.62	161324.42	123085.19	93991.94
Total	188550.79	188547.97	188547.73	188547.13

maximum storage requirements was 0.97.

7.3.3   Comparison of Detention Storage Designs for the Control of Gray Haven Runoff

Each of 4 pond designs in Tables 7-2 and 7-3 were analyzed as a means to control the direct runoff from Gray Haven. The pond was located at the downstream end of the catchment and was assumed to be empty at the beginning of each storm. Each design was also assumed to have a finite storage capacity (in the previous section no storage capacity was assumed). Since the limited storage capacity in effect, changes the design, the four designs will now be referred to as A, B, C, D rather than 1, 2, 3, 4. The spillway elevation of each design is given in Table 7-6. (The spillway width was assumed to be infinite so that the outflow was equal to the inflow rate whenever there was flow over the spillway).

Each design was analyzed in terms of its response to each of the 48 hydrographs which were presented in Chapter 6. These storms were selected from the 200-yr record of generated events at Gray Haven. The maximum outflow rates computed for these 48 storms were then used to construct the peak outflow frequency curve for each pond design.

The frequency curves for designs A and B appear in Fig. 7-3 together with the frequency curve for the uncontrolled peak from Gray Haven. It is immediately obvious that both pond designs greatly reduced the peak runoff frequency curve. Owing to the random fluc-

Table 7-6

Spillway Elevation for each Outlet Design

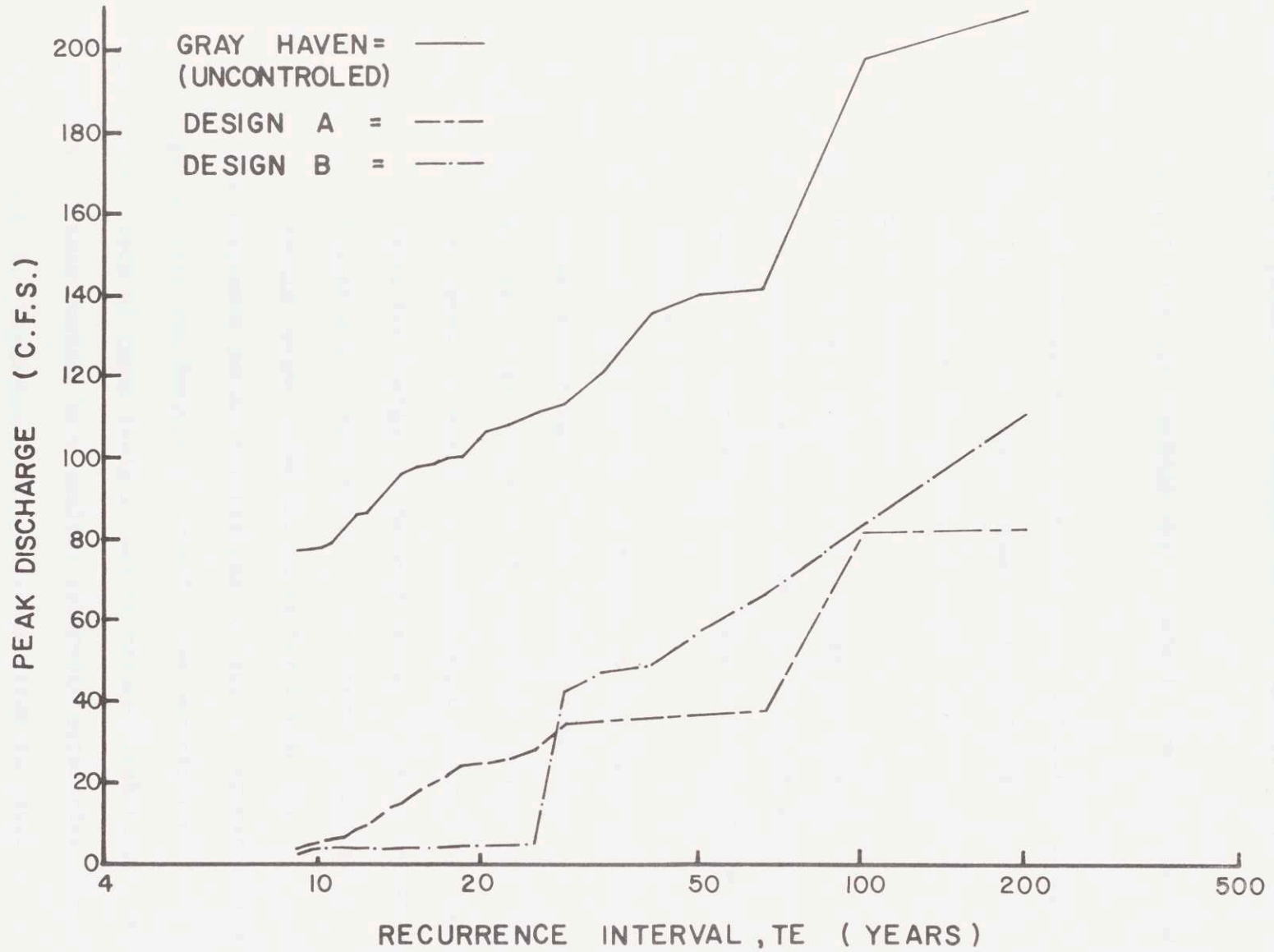| Design	Spillway Elevation feet
A	8.0
B	8.0
C	6.0
D	6.0

Figure 7-3: Peak Runoff Frequency Curves for Reservoir Outlet Designs A and B

tuations inherent in the simulation procedures, it is too risky to make relative judgements at or beyond the 100-year recurrence interval.

The following observations may be made in comparing designs A and B.

(1) The main physical difference is in the outlet design. Design B had only a lower outlet. Design A had a lower outlet plus a second outlet 3/4 of the distance up to the spillway.

(2) Both designs had the same storage capacity.

(3) For the more frequent events (up to T_E = 25 yrs), design B gave better reductions in peak outflow rates than did design A

(4) Beyond T_E = 25 yrs in design B the spillway was over-topped and design A gave better reductions.

(5) At very large values of T_E it might be expected that the curve for design A would begin to approach the curve for design B because design A will be over-topped also. Nevertheless, the curve for design A should remain below the curve for design F.

The frequency curves for designs C and D appear in Fig. 7-4 together with the frequency curve for the uncontrolled peak from Gray Haven. Both of these designs lead to reduced peak runoff rates. But both of these designs have smaller reservoir capacities than designs A and B. Consequently the peak reduction is less.
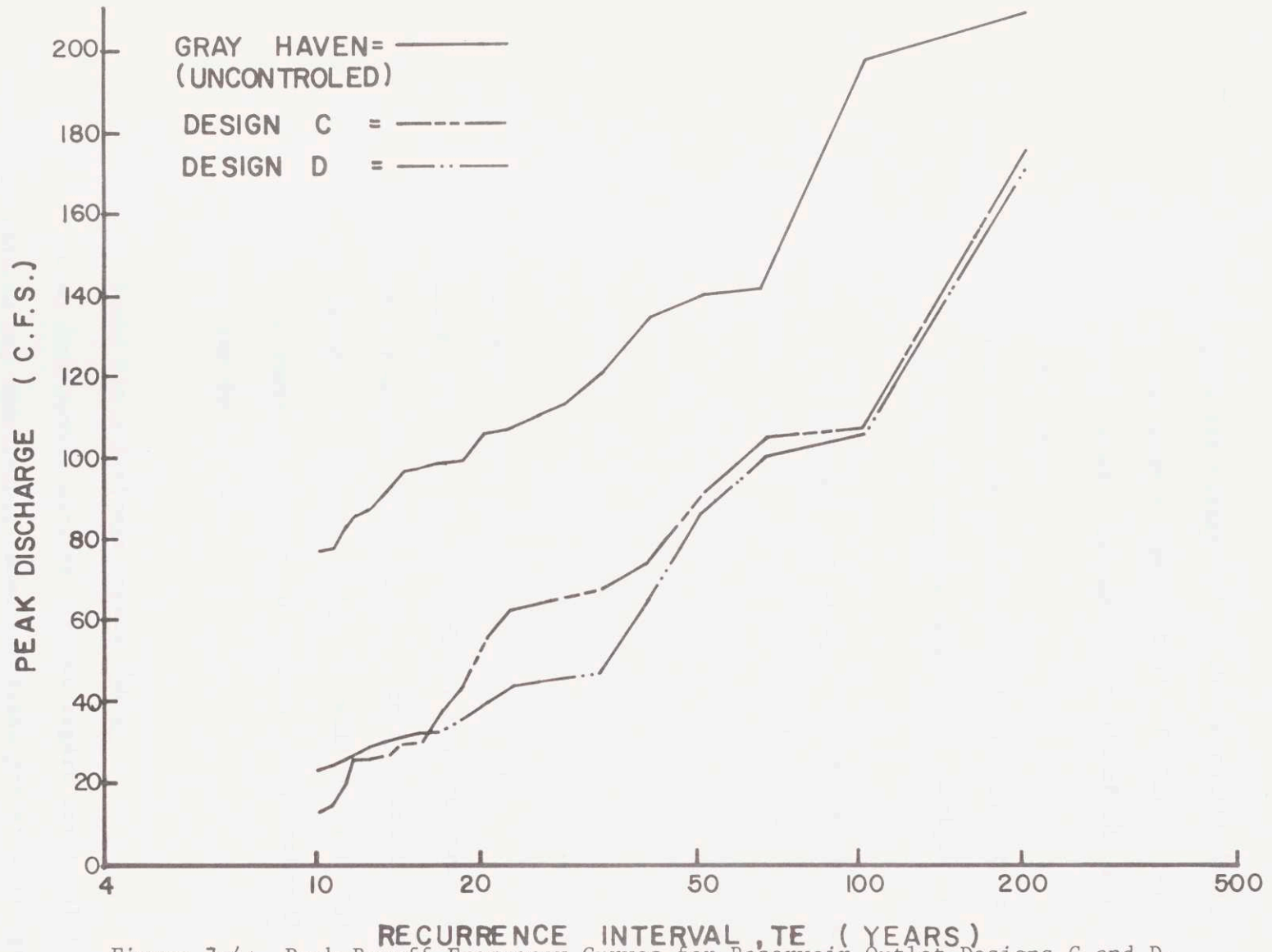
Figure 7-4:   Peak Runoff Frequency Curves for Reservoir Outlet Designs C and D.

The following observations may be made in comparing designs C and D.

(1) The main physical difference is in the outlet design. Design C had only a lower outlet. Design D had a lower outlet plus a second outlet 3/4 of the distance up to the wpillway.

(2) Both designs had the same storage capacity; it is equal to 75% of the storage capacity of designs A and B.

(3) Beyond T_E = 10 years, in design C, the spillway was overtopped. Design C was better than design D (overtopped when T_E = 35 years) up to T_E = 15 years because design C was overtopped late in the storm when the inflows to the pond were small.

(4) Beyond T_E = 15 years, design D gave better reduction in the peak runoff rates than design C.

(5) At large value of T_E it might be expected that the curve for design D would begin to approach the curve for design C because design D will be overtopped also. But the curve for design D should remain below the curve for design C.

7.4 Hydrologic Basis for a Drainage Impact Charge

Urban development pursued without regard for possible downstream impacts may undesirably cause increased property damages

and loss of life; districts once relatively free of flood hazard
may frequently be flooded unless expensive and unsightly projects
to convert natural streams into concrete channels are undertaken.
Unfortunately, these channel "improvements" also increase the flood
hazard further downstream.

Because the human perception to the flood hazard greatly
underestimates the true hazard, and because upstream development may
occur in between important flood events, the true downstream effects
may not become apparent to the public until some crisis occurs. By
that time the least costly alternatives to deal with the problem
will have been foregone.

Control of the urban flood hazard involves a maze of
social, economic, legal and hydrologic issues. Many values are
involved and some conflict with others. For example, upstream pro-
perty owners are interested in the maximum economic development of
their properties. Downstream property owners may be adversely
affected. But the actual impact of any single upstream property
owner on any one downstream property owner is too small to measure.
It is also difficult to establish in a court of law the total
extent of the burden on those adversely affected.

Among the alternatives for controlling the urban flood
hazard is the regulation of land use by zoning, the regulation of
urban drainage practice through drainage codes, and the assessment
of drainage impact fees on new construction. Perhaps the most direct
approach through drainage codes would be to prohibit any change in

the hydrologic response of any drainage area. Such a code, if applied
literally, would preclude any development and would thereby take away
individual property rights. Alternatively, drainage codes could be
written with the intention of minimizing hydrologic changes and assess-
ing a reasonable fee to compensate for the impacts of the changes
that do occur. Such drainage fees could be collected by a responsible
public authority and used to offset the remaining downstream impacts
by the construction of detention storage facilities on public lands
that could be purchased with these fees or by constructing channel
improvements whenever that is the best remaining alternative. De-
tention storage facilities might be used to regulate the flow from
certain tributaries in order to increase the capacity of the main
stem to handle increased flows from other tributaries. This would
require close coordination of land planning, zoning and master drain-
age planning agencies. The objective would be to make the best total
use of land, water and other natural resources. This would also
require appropriate hydrologic techniques to assess the hydrologic
impacts of different strategies and to serve as a basis for establish-
ing drainage impact fees.

The hydrologic technology to permit such planning and to
establish such fees now exists. In fact, the technique described
in this report are already being applied and eventually will be used
to help in the establishment of reasonable drainage impact fees.
One suggested approach would be first to estimate at different loca-
tions $F_V(v)$ for the most urbanized state. Then, some of the un-

desirable effects might be reduced through appropriate modifications in the drainage code. Other undesirable effects might also be reduced through zoning changes. Finally, the remaining impacts (due to undesirable changes in $F_V(v)$) could be reduced through publicly constructed facilities. Drainage impact fees would be assessed on a share basis of the cost of these facilities.

The final assessment of the possible impacts of future development is properly made in terms of changes in $F_V(v)$ (or more precisely in terms of economic weighted changes in $F_V(v)$). Moreover, planning control alternatives to eliminate these impacts also is properly done in terms of changes in $F_V(v)$. Planning procedures that fail to properly recognize both the magnitude and frequency of runoff events may lead to desirable changes of frequent events at the expense of undesirable increases in infrequent events or the converse could occur.

Once a fee structure is established on the basis of a master drainage plan to control changes in the magnitude and frequency of runoff events, the fee for a individual development can be computed. The individual developer would have the option of paying this fee or of revising his plans to reduce his impacts and to thereby reduce his fee.

CHAPTER 8

CONCLUSIONS AND RECOMMENDATIONS FOR FUTURE WORK

The runoff process was treated as a stochastic process. The characteristics of the runoff process were described by runoff frequency curves which were derived directly from the rainfall process.

Solution to Equation 2-1

The multiple integral (Equation 2-1) introduced in Chapter 2 defines the probability distribution of an individual event and, after further transformations, defines the runoff frequency curve. This multiple integral is difficult to solve. The best procedure, at this stage, appears to be stochastic/deterministic simulation, which may be an expensive method of solution. It is therefore important to look for ways which can reduce the cost of the simulation. Identification and elimination of unnecessary computations is one possible way. Development of procedures which integrate Equation 2-1 numerically is another way. The linear-numerical integration is such a procedure. These methods of solution also eliminate the sampling variability from $F_V(v)$ but when seasonal variations are observed in the random variables, the cost of solution will increase because then an integral must be solved for every season.

It is not clear at this time how many random variables must be used to derive $F_V(v)$; it may not be necessary to have

more than 2 or 3 random variables. More work needs to be done to analyse this question to which the cost of the solution is sensitive.

Rainfall Generator

The general structure of the rainfall generator seems to be a useful tool for engineering practice at the present time. It is possible to simulate rainfall samples that resemble the historical sample; the statistical properties of individual events are preserved. Moreover, the intensity duration frequency curves (IDF) an important statistical property of the sample, are preserved. The latter characteristic is significant because the IDF are not used as inputs to the rainfall generator.

There is a need for additional research on stochastic rainfall interiors. Studies should be oriented towards the determination of fixed rainfall interior patterns in terms of the climatic properties, the size of the catchment and its stage of development, the runoff variable V, etc.

The present model does not look at stochastic spatial variability; there is a need to find ways to describe it, to assess its importance so that it would be modeled only when it affects $F_V(v)$.

Catchment Model

The detailed segmentation gives excellent representation of the response of Gray Haven. In the interest of reducing cost of

simulation, the detailed segmentation was simplified from 42 to 8 segments. The simplified segmentation is a model of the detailed segmentation and gives very good representation of the response of the detailed segmentation. It is also understood why the simplified segmentation works so well.

The principal contribution made in Chapter 4 was to show that a simplified segmentation of a small urban catchment can be achieved. Experience gained in modeling Gray Haven and experience gained by others [Wooding, 1965a, 1965b, 1966], Harley et al [1970], Perkins and Harley [1971] shows that the kinematic wave model and the modular description of the catchment lead to a physically sound catchment model. Moreover, the parameters of the model are derived from the physical characteristics of the catchment.

The non-linear characteristics of the catchment model are important for the timing of the runoff events; good simulated hydrographs were achieved because these non-linearities were represented.

Additional work is needed to achieve simplified segmentation of urban areas larger than Gray Haven. These simplified segmentations are required if the methodology presented herein is to be applied economically to regional drainage problems.

Application of Filter Theory

Filter theory concepts were applied successfully to the estimation of the parameters of the infiltration process. Not only

the estimation effort gave accurate estimates $\hat{\psi}_*$, but lead to as good as or better parameters, than the trial and error search used in Chapter 4.

The estimator is the first application in hydrology of filter theory; and it appears that the estimator developed in Chapter 5 has the potential to become a practical engineering tool.

Because hydrologic models have many parameters, the technique promises to become a widely used technique in hydrology during the next decade.

Two possible applications of filter theory may be:

i) reformulation of the estimation problem to eliminate the dependence of the solution on the decay parameter k in the Horton's law of infiltration.

ii) use of the theory to help construct simplified models of the catchment. Such models will have a small number of non-linear differential equations. The parameters of this simplified model would be identified by filter theory. Such models can greatly reduce the cost of simulating individual events while preserving the non-linearities of the catchment response. Such an application would not replace the catchment model but might become a substitute to the catchment model, once calibrated for a particular catchment.

Two filter theory models and a regression model were compared. Under certain conditions the three models have the same

error variance. The second filter model should be explored in future work because it would generally have the smallest error variance of the three models presented.

Methodology and its Applications

The applications of the solution procedure illustrated in Chapter 6 demonstrate that the procedure works. Future efforts should be oriented towards the development of some curves that would determine for design purposes the location of the 5 or 10 year, Q_{max}, Vol(QTH) etc., as a function of the physical characteristics of the catchment.

The procedure developed may also be used to assess present design practices. The procedure presented may also be used to develop simplified procedures that may become substitutes to present drainage practices.

Since frequency curves give a complete description of the rainfall-runoff process, they are strongly recommended to assess the hydrologic impact of urban development and to evaluate the relative efficiency of runoff control alternatives. The applications presented in Chapter 7 are important applications of the proposed methodology.

A complete case study (possibly at the county level) is strongly recommended not only to show that the proposed methodology can be used advantageously in the planning of urban drainage systems but also to suggest standard procedures to analyse large urban drainage systems.

REFERENCES

1. Anderson, J.J., "Real-Time Computer Control of Urban Runoff,"
            Journal of the Hydraulics Division, ASCE, HY1,
            January, 1970.

2. Bauer, W.J., "Urban Hydrology", *presented at the International
            Seminar for Hydrology Professors*, University of
            Illinois, Urbana, Illinois, July 13-25, 1969.

3. Benjamin, J.R., and Cornell, C.A., *Probability, Statistics and
            Decision for Civil Engineers,"* McGraw-Hill Book Co.,
            1970.

4. Chow, V.T., (Editor), *Handbook of Applied Hydrology*, McGraw-Hill
            Book Co., pp. 8-19, 8-22, 1964.

5. Denver Regional Council of Governments, "Urban Storm Drainage
            Criteria Manual, prepared by *Wright-McLaughlin En-
            gineers*, Denver, Colorado, 1969.

6. Devenis, P.K., "Combined Sewage Overflow Detention and Chlorina-
            tion Station near Boston University Bridge," *presen-
            ted at a Spring Meeting of New England Water Pollution
            Control Ass.,* June 11, 1968.

7. Eagleson, P.S., Optimum Density of Rainfall Networks," *Water
            Resources Research*, Vol. 3, No. 4, pp. 1021-1033,
            1967.

8. Eagleson, P.S., *Dynamic Hydrology*, McGraw-Hill Book Co., 1970.

9. Eagleson, P.S., "Dynamics of Flood Frequency," *Water Resources
            Research*, Vol. 8, No. 4, pp. 878-898, 1972.

10. Fleming, G., and Franz, D.D., "Flood Frequency Estimating Tech-
            niques for Small Watersheds, *J. Hydraul. Div.*,
            Amer. Soc. Civil Eng., 97 (HY9) pp.1441-1460, 1971.

11. Franz, D.D., "Hourly Rainfall Synthesis for a Network of Stations,"
            Dept. of Civil Eng., Stanford Univ., Technical Report
            126, Stanford, Calif., 1970.

12. Grace, R.A., and Eagleson, P.S., "A Model for Generating Synthetic
            Sequences of Short-Time-Interval Rainfall Depths,"
            Proc. Int. Hydrology Symposium, Fort Collins,
            pp. 268-276, September 1967.

13. Grayman, W.M., and Eagleson, P.S., "Streamflow Record Length for Modeling Catchment Dynamics," *M.I.T., Dept. of Civil Engineering, Hydrodynamics Laboratory,* Report 114, February, 1969.

14. Grayman, W.M., and Eagleson, P.S., "Evaluation of Radar and Raingages Systems for Flood Forecasting," *M.I.T. Dept. of Civil Eng., Ralph M. Parsons Laboratory,* Report 138, Cambridge, Ma., 1971.

15. Harley, B.M., Perkins, F.E., and Eagleson, P.S., "A Modular Distributed Model of Catchment Dynamics," *M.I.T. Dept. of Civil Engineering, Ralph M. Parsons Laboratory,* Report No. 133, December 1970.

16. Holtan, H.N., "A Concept for Infiltration Estimates in Watershed Engineering," *United States Department of Agriculture, Agricultural Research Survey,* pp. 41-51, 1961.

17. Horton, R.E., "An Approach to the Physical Interpretation of Infiltration Capacity," *Proc. Soil Sci. Soc. Amer. 5:* 399-417, 1940.

18. Huggins, L.F., and Monke, E.J., "The Mathematical Simulation of the Hydrology of Small Watersheds," Technical Report 1, *Purdue University Water Resources Center,* Lafayette, Ind., August 1966.

19. Jazwinski, A.H., *"Stochastic Processes and Filtering Theory,"* Academic Press, 1970.

20. Kadoya, M., "Predictive Study on Urbanizing Effect of Drainage Basin on Flood Runoff," *Second Intern. Symposium in Hydrology,* Fort Collins, Sept. 1972.

21. Knapp, G.L., and Glasby, J.P., "Urban Hydrology - A Selected Bibliography with Abstracts," *Water Resources Investigations 3-72,* 1972.

22. Leclerc, G., and Schaake, J.C.,Jr., "Derivation of Hydrologic Frequency Curves," *M.I.T. Dept. of Civil Eng., Ralph M. Parsons Laboratory,* Report 142, Cambridge, Ma., 1972.

23. Leclerc G., and Schaake, J.C.,Jr., "Digital Urban Catchment Model - A User's Manual, Unpublished report, 1973.

24. Leclerc, G., and Schaake, J.C. Jr., "Derivation of Hydrologic Frequency Curves from Rainfall, *Forthcoming*.

25. McCuen, R.M., "Hydrologic Impact of Land-Use Intensity Zoning in a Watershed Subjected to Urban Development," presented at 54th Annual Meeting, *Amer. Geophs. Union*, Washington, April 18, 1973.

26. McKay, G.A., "Precipitation," in *Handbook on the Principles of Hydrology*, edited by D.M. Gray, Section II, Canadian National Committee for the International Hydrologic Decade, Ottawa, 1970.

27. Marks, D.H., Cohon, J.L., Leclerc, G., Marlay, R., Harley, M., "Cambridge Municipal Services Study," *M.I.T. Dept. of Civil Engineering, Systems Laboratory*, 1971.

28. Pattison, A., "Synthesis of Hourly Rainfall Data, *Water Resources Research*, Vol. 1, no. 4, pp, 489-498, 1966.

29. Perkins, F.C., "Flood Plain Modeling," *Water Resources Bulletin*, 6(3) pp. 375-383, 1970.

30. Perkins, F.E., and Harley, B.M., "Hydrologic Study of the Rio Piedras," prepared for *Flavio Acaron & Assoc.*, Santurce, Puerto Rico, 1971.

31. Randkivi, A.J., and Lawgun, N., "Synthesis of Urban Rainfall," *Water Resources Research*, Vol. 6, No. 2, 1970.

32. Resource Analysis Inc., "The Site Detention Efficiency Study," *prepared for Parsons, Brinckerhoff, Quade and Douglas, Inc.*, 1973.

33. Ross, D., "The Canonical Communication Channel," *The Johns Hopkins Univ*. Dept. of Electrical Eng., Baltimore 18, Md., 1971.

34. Schaake, J.C.,Jr., Ganslaw, M.J., Fothergill, J.W., and Harbaugh, T.E., "Multivariate Rainfall Generator for Annual, Seasonal, Monthly and Daily Events," presented at *International Symposium of Mathematical Modeling Techniques in Water Resources Systems*, Ottawa, Ontario, May 9-12, 1972.

35. Tucker, L.S. "Availability of Rainfall-Runoff Data for Sewered Drainage Catchments," *ASCE Urban Water Resources Research Program*, Technical Memorandum No.8, ASCE, 1969.

36. U.S. Dept. of the Interior, "Design of Small Dams," A Water Resources Technical Publication, Bureau of Reclamation, U.S. Govt. Printing Office, Washington, 1965.

37. Valencia, D.R., and Schaake, J.C.Jr., "Disaggregation Processes in Stochastic Hydrology," *Water Resources Research*, Vol. 9, No. 3, p.580-585, 1973.

38. Wooding, R.A., "A Hydraulic Model for Catchment-Stream Problem. I. Kinematic-Wave Theory," *J. Hydrol. Vol. 3, Nos. 3/4*, pp. 254-267, 1965a).

39. Wooding, R.A., "A Hydraulic Model for Catchment-Stream Problem, II. Numerical Solutions," *J. Hydrol. Vol. 3, Nos. 3/4*, pp. 268-282, 1965b).

40. Wooding, R.A., "A Hydraulic Model for Catchment-Stream Problem. III. Comparison with Runoff Observations," *J. Hydrol. Vol. 4*, pp. 21-37, 1966.

Biographical Resume

Guy Leclerc was born on August 12, 1945, in Montréal, Canada.

He is married to Lucie Brodeur Leclerc, (1968) and is the father of Eric, born on August 26, 1970.

He attended College André-Grasset (1957-1965) where he received a Bachelor of Arts (BA) degree. He was an undergraduate at Ecole Polytechnique de Montréal (1965-1969) where he received a Bachelor of Applied Sciences (BScA.) in Civil Engineering. In 1969 he entered M.I.T. where he received a Master of Science (S.M.) and a Civil Engineer (C.E.) Degree in 1972.

He received a scholarship from the Ministère des Richesses Naturelles, Gouvernement du Québec, while attending M.I.T. He was a Research Assistant at M.I.T. from September 1969 to September 1972 and was on practical training since then with Resource Analysis, Inc.

He is a registered member of the Corporation des Ingenieurs du Quebec. He is also a member of the American Society of Civil Engineers, of the American Geophysical Union, of the Association Québecoise des Techniques de l'Eau and of the Chi Epsilon Fraternity.

His publications include:

1. Leclerc, G., "Crues de Printemps sur la Rivière Chaudière," *Ministère des Richesses Naturelles*, Gouv. de Québec, T.P.25, 1969.

2. Marks, D.H., Cohen, J.L., Leclerc, G., Marley, R., Moore, H., "Cambridge Municipal Services Study," Civil Engineering Systems Laboratory, M.I.T., 1971.

3. Marks, D.H., and Leclerc, G., "Water Re-Use Systems Analysis: Discussion of a Paper by Bishop and Hendriks," Journal of the Sanitary Engineering Division, American Society of Civil Engineers, August 1971.

4. Leclerc G. and Schaake, J.C. Jr., "Derivation of Hydrologic Frequency Curves," Report 142, *Ralph M. Parsons Laboratory*, Dept. of Civil Engineering, M.I.T., 1972.

5. Leclerc, G., and Marks, D.H., "Determination of the Discharge
    Policy for an Existing Reservoir Network under Differing Ob-
    jectives," accepted for publication in Water Resources Research.

6. Leclerc, G., Régularisation à Fins Multiples par un Système de
    Réservoirs," presented at the Congrès Annuel de l'Association
    Québecoise des Techniques de l'Eau, 30 April 1973, Québec, Qué.

APPENDIX A

PROOF THAT EQUATION 5-32 MINIMIZES TRACE OF $\mathbb{E}$.

The following proof may be found in Ross [1961]. Equation 5-32 becomes

$$L = \mathbb{N}^{-1} G^T [G \mathbb{N}^{-1} G^T]^{-1} \tag{A-1}$$

when z is replaced by $\mathbb{N}^{-1}$.

$$\text{Let} \quad L_o = \mathbb{N}^{-1} G^T (G \mathbb{N}^{-1} G^T)^{-1} \tag{A-2}$$

$$\text{and} \quad \mathbb{E}_o = [G \mathbb{N}^{-1} G^T]^{-1} \tag{A-3}$$

where L_o is the 'optimum' filter and $\mathbb{E}_o$ is the 'optimum' error covariance matrix.

It will now be shown that the trace of $\mathbb{E}_o$ is the minimum trace of $\mathbb{E}$.

Suppose L_o is not the optimal filter. Let the optimum filter be

$$L = L_o + L_1 \tag{A-4}$$

where L_1 is any $m \times n$ matrix with

$$GL = I \tag{A-5}$$

$$\text{Then} \quad G(L_o + L_1) = I \tag{A-6}$$

$$\text{and} \quad G(L_o + L_1) - G L_o = I - I = 0 \tag{A-7}$$

Therefore $\quad G\, L_1\ =\ 0$ $\hspace{4cm}$ (A-8)

Now

$$\mathbb{E}\ =\ (L_o^{\ T}+L_1^{\ T})\quad (L_o+L_1) \hspace{3cm} \text{(A-9)}$$

$$\mathbb{E}\ =\ L_o^{\ T}\,L_o+L_1^{\ T}\,L_o+L_o^{\ T}\,L_1+L_1^{\ T}\,L_1 \hspace{2cm} \text{(A-10)}$$

$$\mathbb{E}\ =\ {}_o+L_1^{\ T}\ {}^{-1}G^T\,(G\ {}^{-1}G^T)^{-1}$$

$$+\ (G\ {}^{-1}G^T)^{-1}\,G\ {}^{-1}\,L_1+L_1\ L^T \hspace{2cm} \text{(A-11)}$$

Since $\ G\, L_1\ =\ 0$

$$\mathbb{E}=\mathbb{E}_o+L_1^{\ T}N\,L_1 \hspace{3cm} \text{(A-12)}$$

Thus $\mathbb{E}$ can be written as the sum of two Hermitian non-negative definite matrices, one of which is constant and the other is zero if and only if $L_1=0$. Thus, $\mathbb{E}_o$ is the minimum error covariance matrix and L_o is the optimum filter.

APPENDIX B

Conceptual Framework and Methods of Solutions for the

Derived Frequency Curves, $T_E(Q_{max})$

This appendix first presents a general conceptual framework
for the theoretical derivation of a runoff frequency curve, and
secondly presents four (4) possible methods of solution.

B.1   Conceptual Framework

The frequency curve of a runoff parameter such as the peak
runoff rate or the runoff volume occurring when the flow rate ex-
ceeds a given level may be derived from rainfall. Let the variable
Q denote the particular runoff variable of interest and let Θ de-
note the vector of hydrological variables upon which Q depends.
The functional relationship

$$Q = Q(\Theta) \qquad\qquad (B-1)$$

between Θ and Q is a model of catchment response to rainfall and
to antecedent conditions. This model is usually sufficiently complex
to require a digital computer for solution, although simple models
may also be useful.

For illustration, it will be convenient to consider the
vector Θ containing as elements only two hydrological variables.
Accordingly, let the two variables be storm duration, t_{re}, and
average excess rainfall intensity, $\bar{i}_e$, during an individual storm.

-235-

Additionally, it will be convenient for illustration to select the runoff parameter, Q, as the peak runoff rate, although other parameters could have been used.

The function $Q(\bar{i}_e, t_{re})$ may be displayed in the $\bar{i}_e - t_{re}$ plane in terms of the contours of the function, as illustrated in Figure B-1. The contour for any particular value of Q, say Q_{max}, divides the $\bar{i}_e - t_{re}$ plane into two regions, one where $Q \geq Q_{max}$ which lies to the northeast of the contour and the other where $Q < Q_{max}$ which lies to the southwest.

Let the first-order density function of the stochastic process generating the hydrologic variables $\bar{i}_e$ and t_{re} be $f(\bar{i}_e, t_{re})$. This density function also may be displayed in the $\bar{i}_e - t_{re}$ plane in terms of the contours of $f(\bar{i}_e, t_{re})$ as illustrated in Figure B-2. According to the definition of $f(\bar{i}_e, t_{re})$, the total volume under that function is equal to unity.

For this example, Equation 2-1 is rewritten as

$$F_Q(Q_{max}) = \iint_{R(Q_{max})} f(\bar{i}_e, \ t_{re}) \ d\bar{i}_e \ dt_{re} \qquad (B-2)$$

where Q_{max} replaces q and where Θ is replaced by $\bar{i}_e$ and t_{re}, the only random variables pertinent to $F_Q(Q_{max})$ for the present problem. $R(Q_{max})$ is the region of the $\bar{i}_e - t_{re}$ plane where $Q \leq Q_{max}$.

Graphically, Equation B-2 defines a volume as illustrated in Figure B-3. This volume is located under the surface defined by
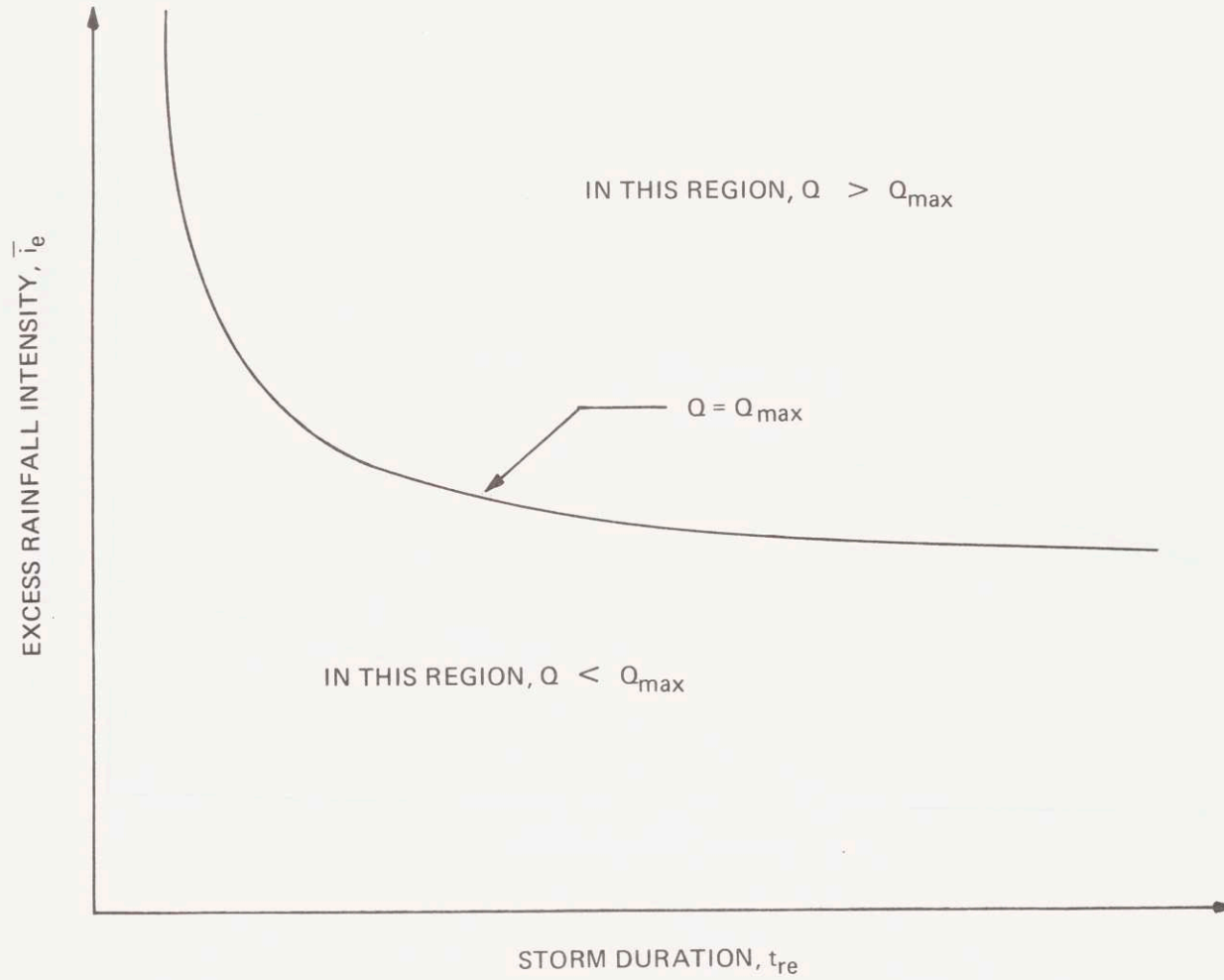
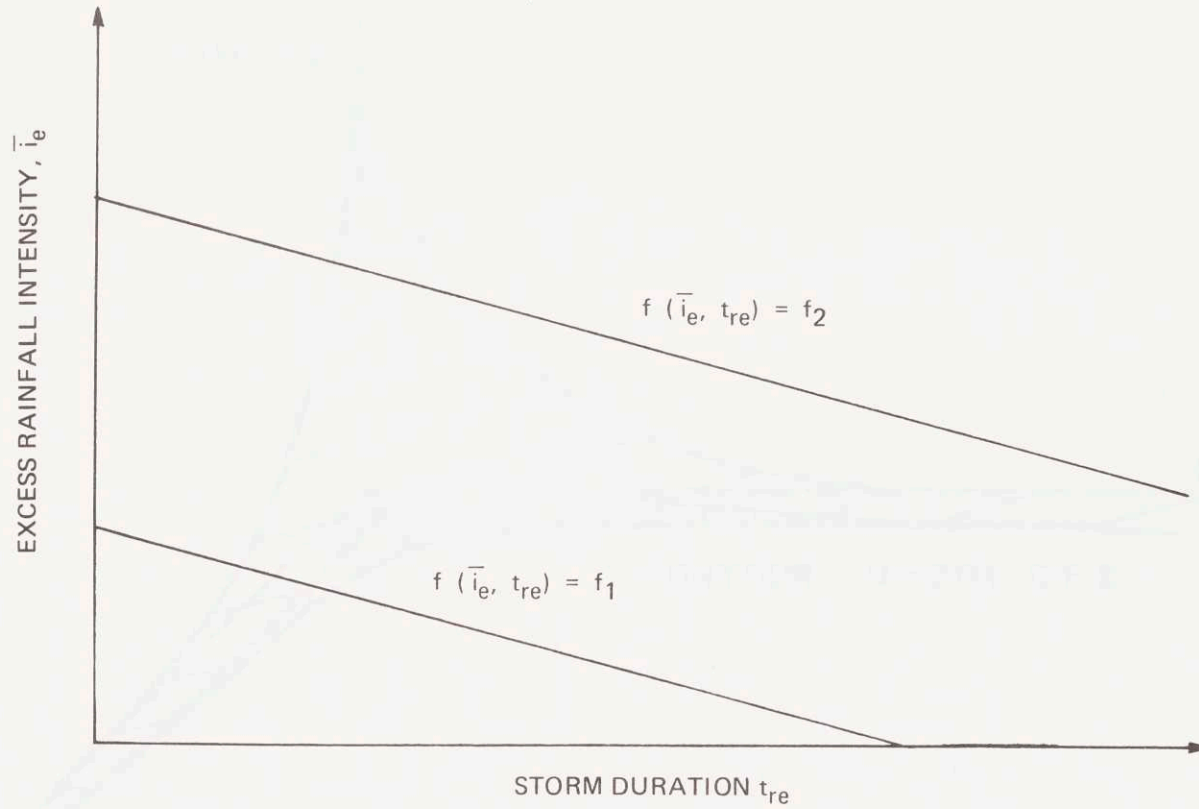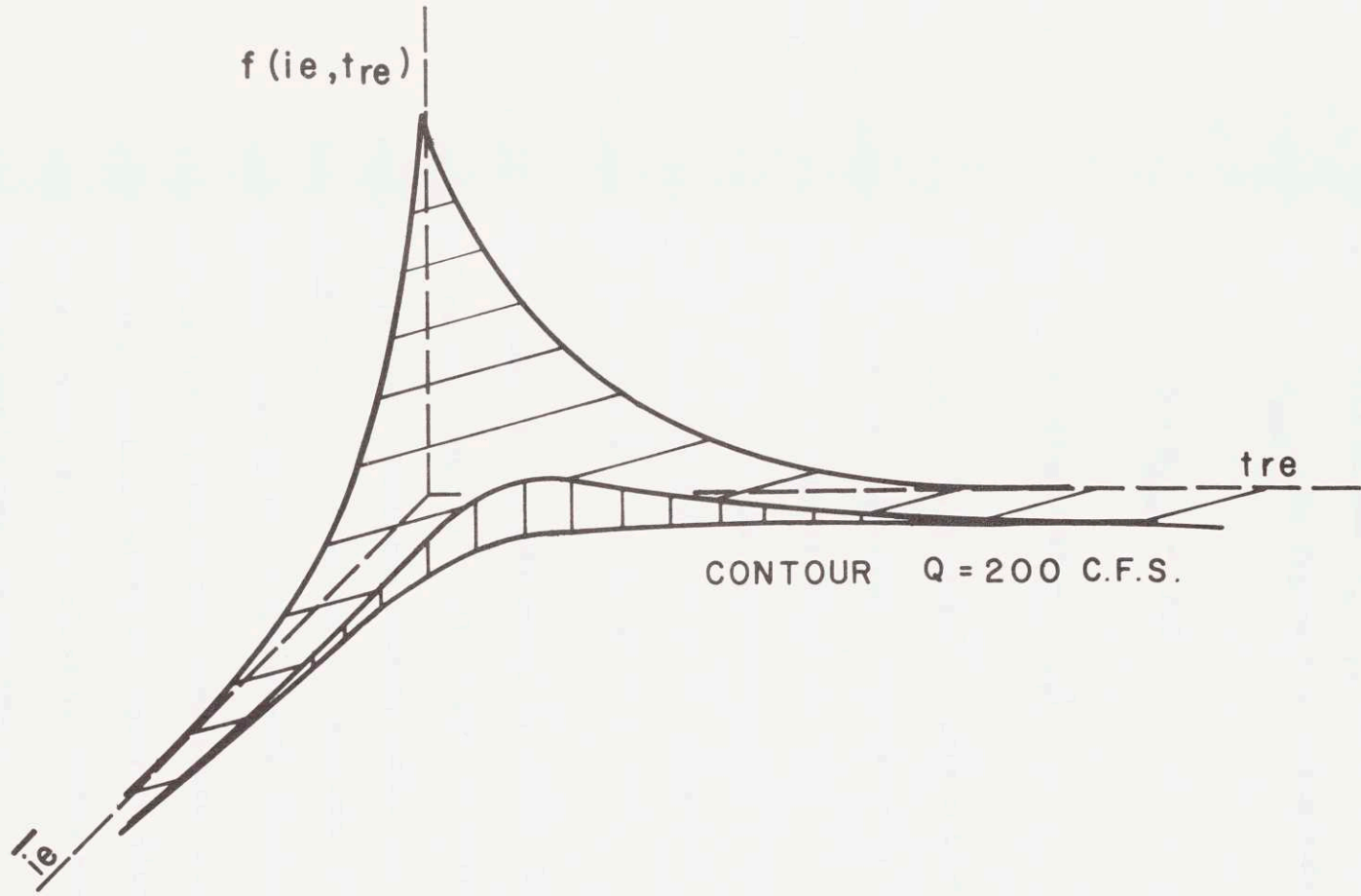Figure B-1: The Function $Q(\Theta) = Q(\bar{i}_e, t_{re})$

-238-

Figure B-2: CONTOURS OF THE JOINT PROBABILITY DENSITY FUNCTION $f(\bar{i}_e, t_{re})$

f (ie, t_{re})

tre

CONTOUR   Q = 200 C.F.S.

ie

B-3:   Graphical Representation of $F_Q(q)$

$f(\bar{i}_e, t_{re})$, within the axis of the $\bar{i}_e - t_{re}$ plane and to the south-west of the contour $Q = Q_{max}$. In Figure B-3, this volume is illustrated for

$$Q = Q_{max} = 200 \qquad \text{(B-3)}$$

and $\qquad f(\bar{i}_e, t_{re}) = \beta\lambda \exp(-\beta\bar{i}_e - \lambda t_{re}) \qquad \text{(B-4)}$

where $\beta = 30$ hr/in and $\lambda = 0.13$ hr^{-1}. This volume represents the probability that for any individual rainfall event the resulting peak runoff rate is smaller than or equal to Q_{max}.

If some other model of the rainfall-runoff process had been used, the integral (Equation B-2) would be written in the more general form of Equation 2-1. It is observed that

(1) The purpose of a runoff model in runoff frequency studies is to define the function $Q(\Theta)$ which, in turn, defines the region $R(q)$ over which the density function $f(\Theta)$ is to be integrated in order to find $F(q)$. Any runoff model can be accommodated. The runoff model not only defines $Q(\Theta)$ but it also defines the variables that constitute the vector Θ, different hydrological variables appear in different catchment models. However, only those variables that are stochastic variables need appear in the vector Θ. All other deterministic variables such as lengths, slopes, etc., are herein considered to be *parameters* of the functional part of $Q(\Theta)$.

(2) The purpose of the stochastic rainfall model is to de-
fine the statistical distribution of Θ, and this is given
by the density function $f(\Theta)$. Formally, $f(\Theta)$ is the so-
called first order density function of the multivariate
stochastic process that generates Θ .

(3) If variable antecedent conditions are to be treated
stochastically, then one or more elements of Θ must repre-
sent antecedent condition variables. Correspondingly, $f(\Theta)$
must account for the random variation in the antecedent con-
ditions.

Equation 2-1 applies to any catchment model and to any
model of the stochastic process that generates Θ .

Once $F_Q(q)$ is known, $T_E(Q)$ or $T_M(Q)$ can be constructed
using Equations 2-2 to 2-10.

B.2 Methods of Solution for $F_Q(q)$.

Several methods of solution to Equation 2-1 can be developed,
methods which embrace the full range between analytical and stochastic
simulation procedures; four methods were presented by Leclerc and
Schaake [1973]:

 * analytical

 * linear/numerical integration

 * discretization of Θ and $f(\Theta)$

 * stochastic/deterministic simulation.

The analytical solution was developed and fully documented by Eagleson [1972]. This method was developed for a standard catchment, (see Figure 4-4a), subject to a rainfall modelled with two independent rainfall variables, the average excess intensity, $\bar{i}_e$, and the storm duration t_{re}. Both variables are exponentially distributed. Under these conditions it was possible to derive the peak runoff frequency curve $T_E(Q_{max})$ although serious difficulties were encountered in the analytical derivation of an expression for Q_{max}, due to the adoption of the kinematic wave equations for the routing model.

The linear/numerical integration method replaces the kinematic wave routing model by an impulse response function which preserves the time of concentration of i) the overland flow segment t_c and of ii) the stream segment, t_s of a standard catchment, for each storm event considered. The linear model is used to construct an analytical expression for $Q_{max}(i_e, t_{re})$. Then, Eq. 2-1 is integrated numerically.

Discretization of Θ is a technique that should be generally applied to solve Equation 2-1. Let Θ_i be the ith value of Θ, $i = 1, \ldots, M$. The probability that Θ_i will occur is p_i where

$$\sum_{i=1}^{M} p_i = 1 \qquad (B-5)$$

The distribution $F_Q(q)$ is then computed as:

$$F_Q(q) = \sum_{i \in I} p_i \qquad (B-6)$$

where I is the set of indices such that

$$Q(\Theta_i) \leq q \qquad\qquad (B\text{-}7)$$

This technique is illustrated in Figure B-4 for the two-random variable case. In Figure B-4 the $\bar{i}_e - t_{re}$ plane is covered by a rectangular grid; at each grid point a value $Q(\Theta_i)$ may be computed.

If this $Q(\Theta_i)$ were assumed representative of the runoff variable of all the storms that are located inside the rectangle whose corners are mid-way between the grid intersections, the probability that $Q(\Theta_i)$ would occur is equal to the probability of occurrence of all the storms located inside that rectangle. In Figure B-4, the probability of $Q(\Theta_A)$ is thus equal to
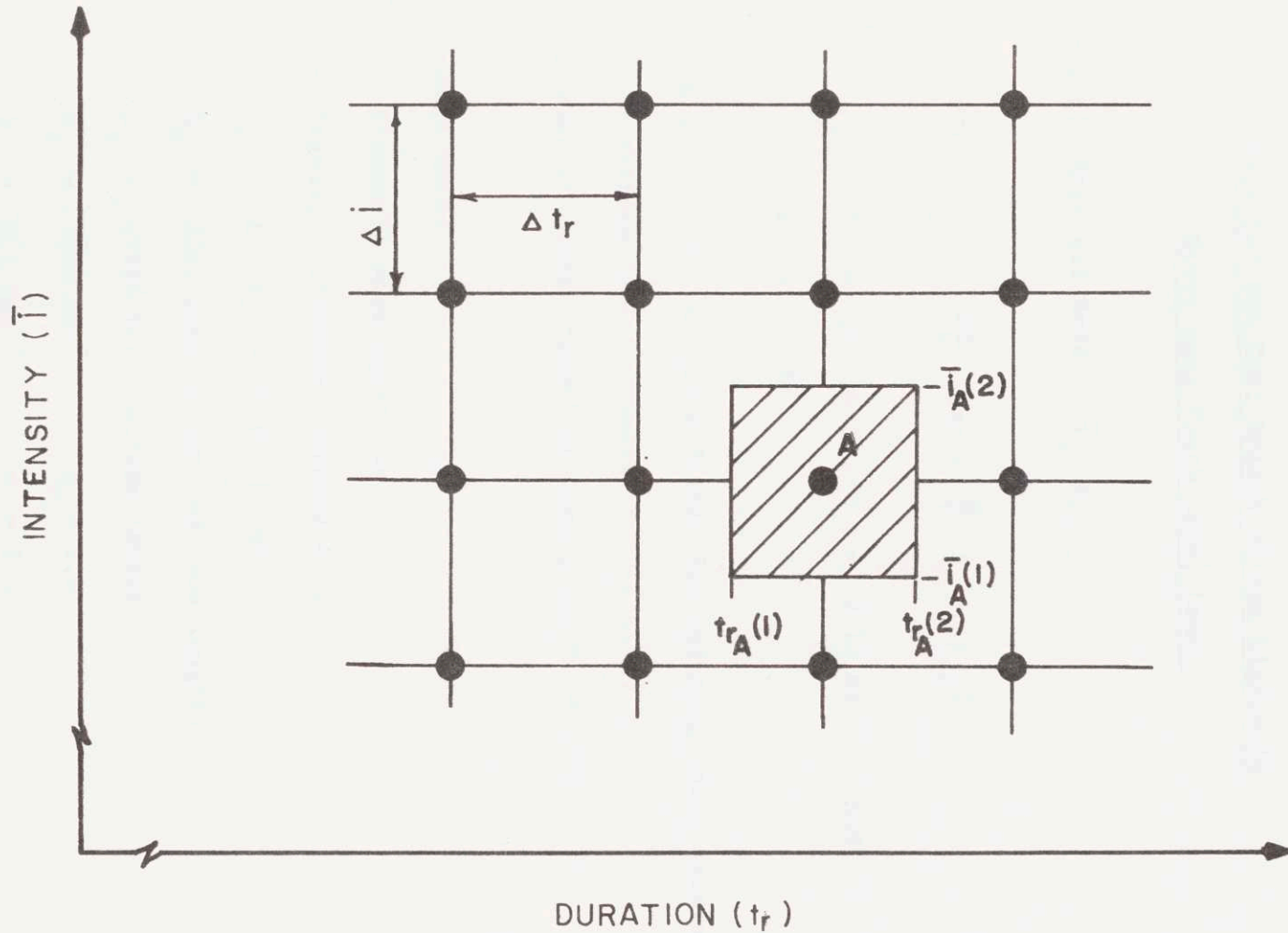
$$P_A = \int_{\bar{i}_A(1)}^{\bar{i}_A(2)} d\bar{i} \int_{tr_A(1)}^{tr_A(2)} f(\bar{i},tr)\, dtr \qquad\qquad (B\text{-}8)$$

Equation (B-6) is then used to compute $F_Q(q)$.

The stochastic/deterministic method of solution is documented in Chapter 6.

B-3: Numerical Example

The four methods of solution were used to derive the peak runoff frequency curve of the 22 sq.mi. catchment of the East Branch of the Eight mile River near North Lyme, Conn. Table B-1 presents

B-4: Discretization of the $\bar{i}_e$-t_{re} Plane

Table B-1

Data for the East Branch of the Eightmile

River near North Lyme, Conn.

1. Stochastic Rainfall Model, $\bar{i}_e - t_{re}$

$$f(\bar{i}_e, t_{re}) = \frac{\beta\lambda}{k} \exp\left[-\frac{\beta}{k}\bar{i}_e - \lambda t_{re}\right]$$

where β = 30. hr/in, λ = 0.13 hr^{-1}, and

k = 0.988

The parameter, k, is a factor for reducing point rainfall intensity to average over the direct runoff area.

Number of direct runoff producing storm = 30

2. Catchment Model

   - Kinematic wave equations

   - Standard catchment (Figure 4.4a)

   - A_r = 1/3 A_c = 7.333 sq.mi.

     R_c = 2381 feet (overland flow length)

     L_s = 42926 feet (stream length)

     α_c = 10.0 sec^{-1} m_c = 2.0

     α_s = 0.1 sec^{-1} m_s = 1.5

the data for this example.

Figures B-5 and B-6 illustrate the derived frequency curves, obtained by each of the four methods presented. These curves show that each method gives a reasonable $T_E(Q_{max})$. The differences observed between the curves are caused by the type of approximation made in developing each method.

B.4 Summary

The conceptual framework provides a theoretical basis for understanding the mechanics underlying the derivation of runoff frequency curves. Within this framework methods of solution may be developed and assessed, not only for the two random variable cases but also for cases where more random variables are required to appropriately describe the problem. These potential applications of the conceptual framework have been analyzed in the course of this study; they are not discussed herein even though they are interesting because they were not used in this study.
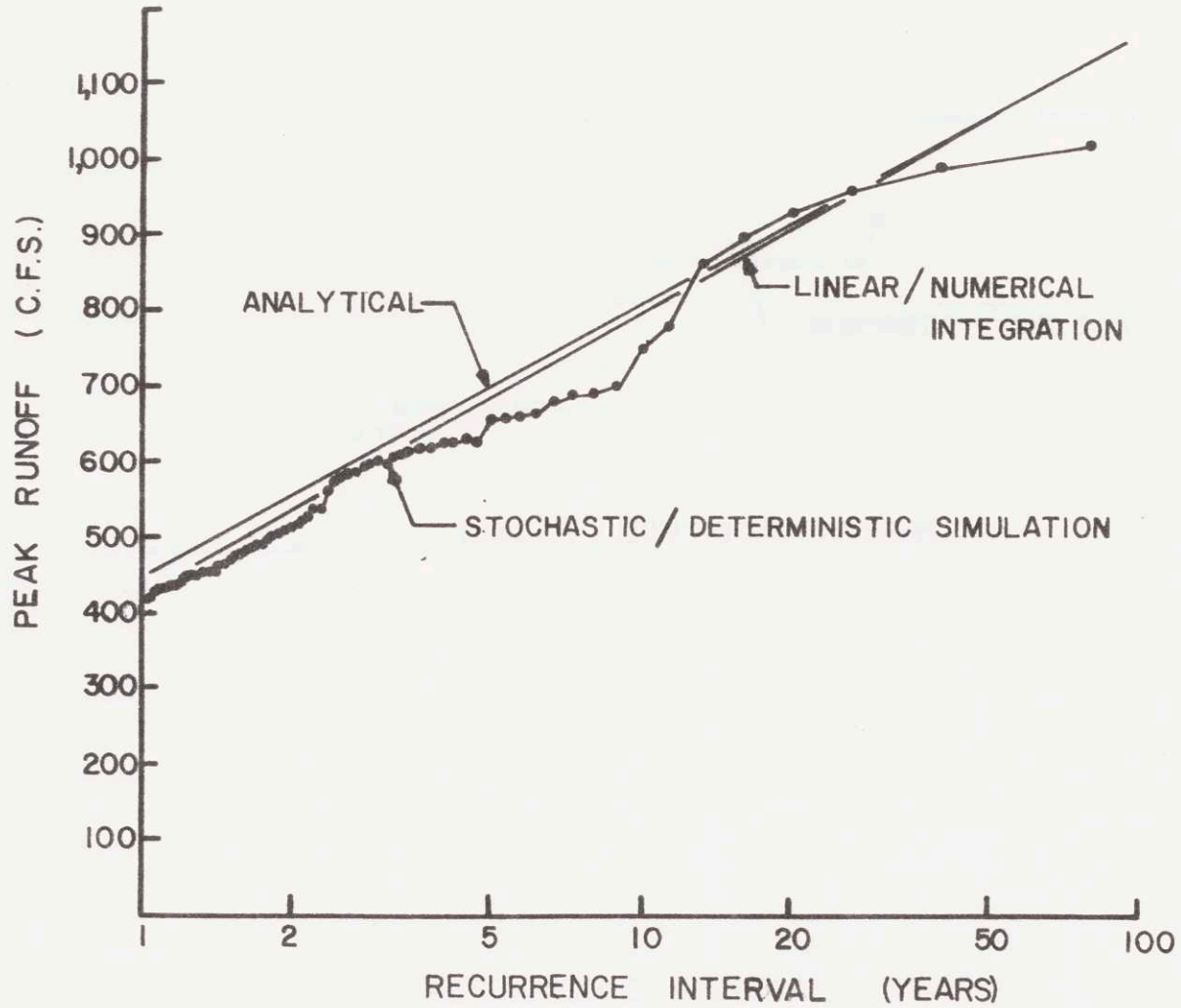
Figure B-5: Numerical Example: Analytical vs Linear/Numerical Integration vs Stochastic/Deterministic Simulation Solutions.
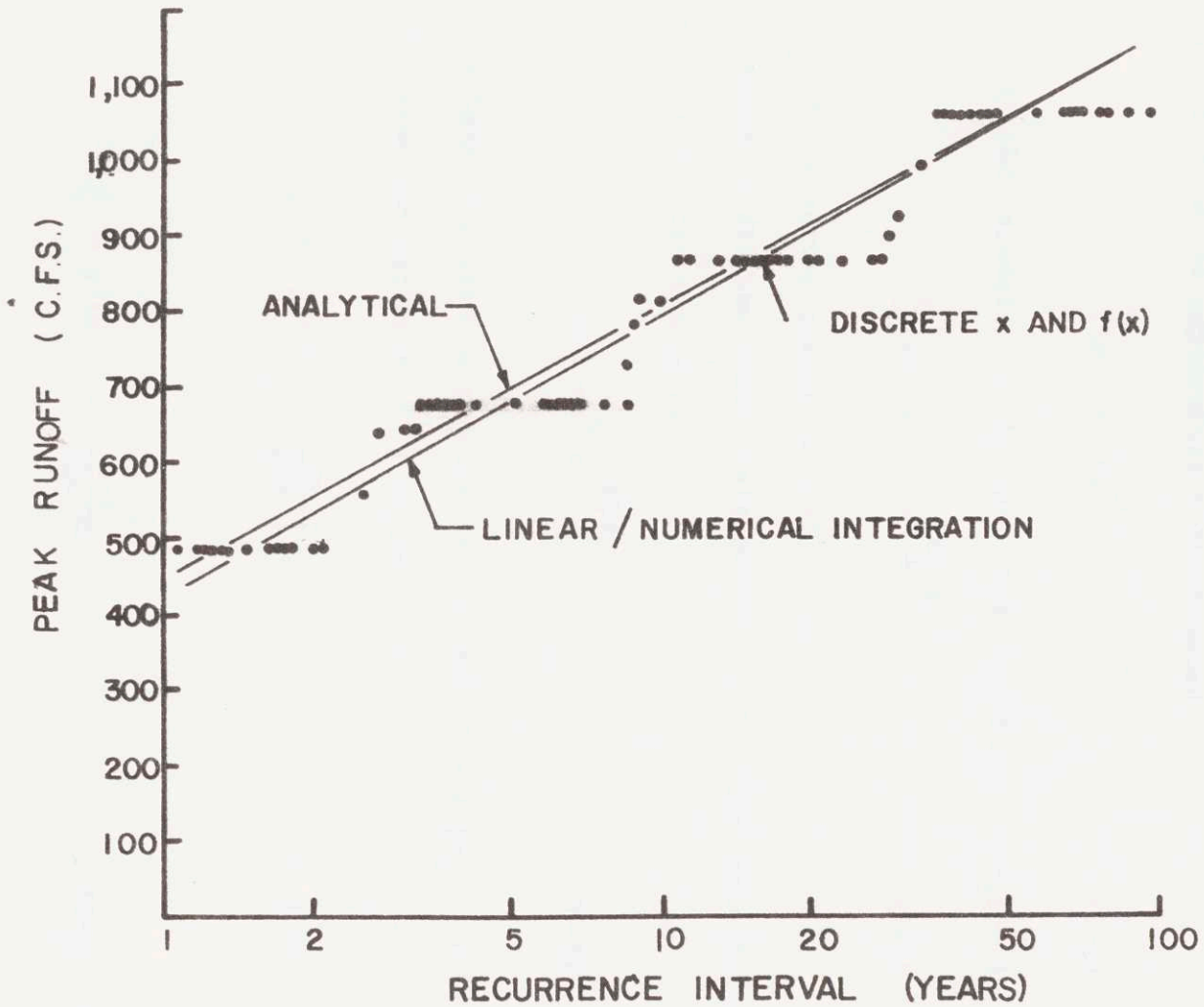
Figure B-6: Numerical Example: Analytical vs Linear/Numerical Integration
vs Discrete Θ and f(Θ) Solutions

Appendix C

Sampling Variance of the Parameter of an Exponential Distribution

Variable x is exponentially distributed

$$f(x) = ke^{-kx} \qquad (C-1)$$

where k is the parameter of the PDF. The likelihood function is

$$L(k) = k^n e^{-k\sum_i x_i} \qquad (C-2)$$

where x_i are observations of x (i=1,...,n).

Assuming a diffuse prior distribution on k, the posterior
PDF for k given the sample is

$$f(k) \propto k^n e^{-k\sum_i x_i} \qquad (C-3)$$

which is a Gamma PDF with parameters $\alpha = n$ and $\beta = 1/\sum_i x_i$ (C-4)

The mean and variance of f(k) are

$$\mu_k = \beta(\alpha+1) = \frac{n+1}{\sum_i x_i} \qquad (C-5)$$

and

$$\sigma_k^2 = \beta^2(\alpha+1) = \frac{n+1}{(\sum_i x_i)^2} \qquad (C-6)$$

The maximum likelihood estimate of k is

$$\hat{k} = \frac{n}{\sum_i x_i} = \frac{1}{\bar{x}} \qquad (C-7)$$

Assuming that n is large enough so that the difference between n and n+1 is inconsequential and asssuming that k is estimated according to (C-7), the sampling variance of k is, therefore.

$$\sigma_k{}^2 = \frac{k^2}{n} \qquad \qquad (C-8)$$

It is important to note that the value of n that appears in Eq. C-8 is the number of individual storm events that were used to estimate k. If, on the average, m events per year occur,

$$n = mN \qquad \qquad (C-9)$$

events may be expected to occur in N years.

APPENDIX D

ANALYTICAL DERIVATION OF THE FREQUENCY CURVE OF PEAK

RUNOFF FROM AN OVERLAND FLOW PLANE

This appendix presents the derivation of $T_E(Q_p)$, the frequency curve of the peak discharge of an overland flow plane. This derivation follows closely Eagleson's [1972] derivation of the flood frequency curve for a natural catchment.

Stochastic Model of the Rainfall.

Eagleson, [1972], modeled the rainfall during an individual storm event in terms of two random variables: the average rainfall intensity, $\bar{i}_o$ [in/hr], and the storm duration t_r [hr]. The first order joint density function (conditional on the occurrence of a storm event) is

$$f(\bar{i}_o, t_r) = \beta\lambda \exp [-\beta\bar{i}_o - \lambda t_r] \qquad (D-1)$$

where β and λ are parameters

For Boston, Ma., $\beta = 30$ hr/in

and $\lambda = 0.13$ hour^{-1} [Eagleson, 1972] .

The average rainfall excess intensity, $\bar{i}_e$ [in/hr] is assumed to be

$$\bar{i}_e = \bar{i}_o - \emptyset \qquad (D-2)$$

where $\emptyset$ is a constant rate of water loss [in/hr].

It can be shown, (conditional on the occurrence of a rainfall excess event) that the joint PDF of $\bar{i}_e$ and t_{re} is

$$f(\bar{i}_e, t_{re}) = \beta\lambda \exp [-\beta\bar{i}_e - \lambda t_{re}] \tag{D-3}$$

where t_{re} is the duration [hr] of the rainfall excess intensity. The total number of storms during a year is Θ but only $N \leq \Theta$ of these produce rainfall excess. Each storm is assumed to have a rectangular storm interior.

Mechanics of Overland Flow

Let the overland flow plane have a total area of A (acres) a slope of S [ft/ft] and a length of overland flow of L_c [ft]. The width [ft] of the plane is

$$w = \frac{43560\ A}{L_c} \tag{D-4}$$

The peak discharge [cfs] from the plane is

$$Q = \frac{w\ L_c\ \bar{i}_e}{(12)(3600)} \qquad t_r \geq t_c \tag{D-5}$$

or

$$Q = w\ \alpha_c \left[\frac{\bar{i}_e t_r}{12}\right]^{m_c} \qquad t_r < t_c \tag{D-6}$$

where α_c and m_c are given parameters which may be evaluated by the Manning formula as

$$m_c = 5/3 \tag{D-7}$$

$$\alpha_c = \frac{1.49}{n} S^{\frac{1}{2}} \tag{D-8}$$

The units of $\bar{i}_e$ are [in/hr] and t_r are [hr].

The time of concentration of the overland flow plane, in hr, is

$$t_c = .0156 \left[\frac{nL_c}{S^{\frac{1}{2}} \bar{i}_e^{\frac{2}{3}}} \right]^{\frac{3}{5}} \tag{D-9}$$

or

$$t_c = .0156 \left[\frac{nL_c}{S^{\frac{1}{2}} (Q/A)^{\frac{2}{3}}} \right]^{\frac{3}{5}} \tag{D-9a}$$

$F_Q(Q)$ for Individual Storms

From Chapter 2

$$F_Q(Q) = \iint\limits_{R} f(\bar{i}_e, t_{re}) \, d\bar{i}_e \, d_{tr} \tag{D-10}$$

where the region of integration is the region to the southwest of Curve A in Fig. D-1. The analytical structure of this region precludes an exact analytical integration of Eq. (D-10). An approximation, suggested by Eagleson (1972) is to approximate the region R to the southwest of curve A by the region R' to the southwest of curve B. These curves are illustrated in Figure D-1. Region R'

may be partitioned into two subregions R_1 and R_2. Eq. D-10 may be approximated by

$$F_Q(Q) = I_1 + I_2 \tag{D-11}$$

where

$$I_1 = \iint_{R_1} f(\bar{i}_e, t_{re}) \, d\bar{i}_e \, dt_r \tag{D-12}$$

and

$$I_2 = \iint_{R_2} f(\bar{i}_e, t_{re}) \, d\bar{i}_e \, dt_{re} \tag{D-13}$$

Eq. (D-12) may be replaced by the iterated integral

$$I_1 = \int_o^\infty dt_{re} \int_o^{Q/A} f(\bar{i}_e, t_{re}) \, d\bar{i}_e \, dt_{re} \tag{D-14}$$

which together with Eq. (D-1) gives

$$I_1 = 1 - \exp[-\beta Q/A] \tag{D-15}$$

Eq. (D-13) may be replaced by the iterated integral

$$I_2 = \int_o^\infty di \int_o^{g(i)} \beta\lambda e^{-\beta(i+Q/A)} e^{-\lambda t_{re}} \, dt_{re} \tag{D-16}$$

where

$$i = \bar{i}_e - Q/A \tag{D-17}$$

and

$$g(i) = t_{re} \tag{D-18}$$

defines curve B in Fig. D-1.

Eq.(D-16) reduces to

$$I_2 = \exp[-\beta Q/A] \left\{ 1 - \beta \int_0^\infty \exp[-\beta i - \lambda g(i)] \, di \right\} \tag{D-19}$$

Eagleson [1972] showed that if

$$I_o = \beta \int_0^\infty \exp[-\beta i - \lambda g(i)] \, di \tag{D-20}$$

and if

$$g(i) = t_{re} = B/i^m \tag{D-21}$$

that I_o is closely approximated by

$$I_o \simeq e^{-\sigma/m} \sigma^{-\sigma+1} \Gamma(\sigma) \tag{D-22}$$

where

$$\sigma = \beta(m\lambda B/\beta)^{1/(m+1)} \tag{D-23}$$

The idea now is to choose B so that Curve B closely resembles Curve A in the region of most probable values of $\bar{i}_e$ and t_{re}.

One approximation is to make curves A and B intersect at $t_{re} = \xi t_c$ where $0 < \xi < 1$. The equation for B is then

$$B = \xi t_c \left[\left(\frac{Q}{w\alpha_c} \right)^{3/5} \left(\frac{12}{\xi t_c} \right) - \frac{Q}{A} \right]^m \tag{D-24}$$
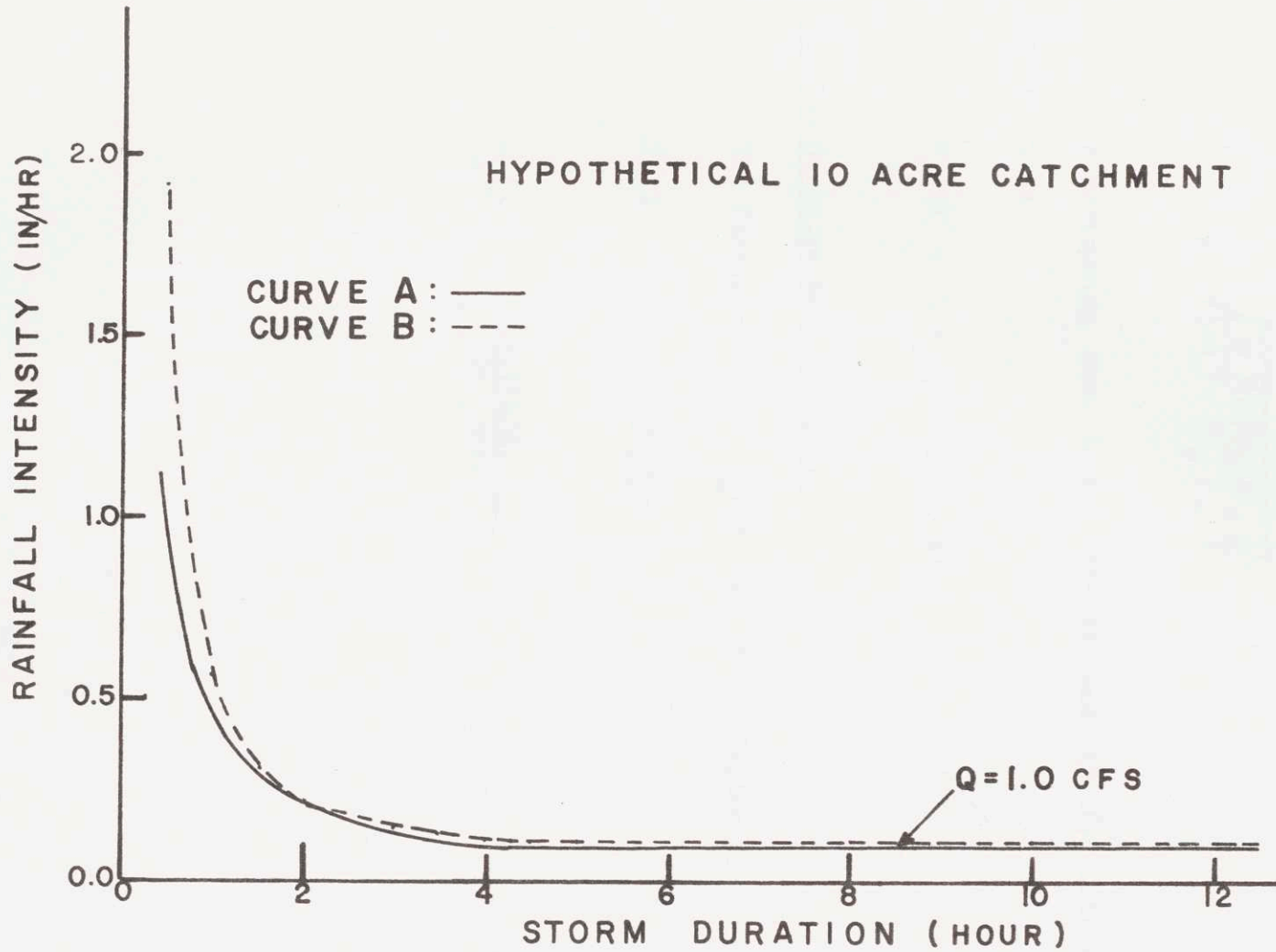
Figure D-1: $\bar{i}_e - t_{re}$ Plane for the Peak Runoff from an Overland Flow Plane

If $\xi = 1/2$ and $m = 1/2$ (Eagleson used $m = 1/2$), Eq. (D-24) becomes

$$B = \frac{t_c}{2} \sqrt{\left(\frac{Q}{w\alpha_c}\right)^{3/5} \left(\frac{24}{t_c}\right) - \frac{Q}{A}}$$

(D-25)

Substituting Eqs. (D-15), (D-19) and (D-20) into Eq. (D-11) gives

$$F_Q(Q) = 1 - I_o \exp\left[-\beta Q/A\right]$$

(D-26)

Partial Duration Series $T_E(Q)$

The frequency curve $T_E(Q)$ is (after Eagleson)

$$T_E(Q) = \frac{1}{N\, I_o \exp\left[-\beta Q/A\right]}$$

(D-27)

or

$$T_E(Q) = \frac{\exp\left[\beta Q/A\right]}{N\, e^{-2\sigma}\, \sigma^{-\sigma+1}\, \Gamma(\sigma)}$$

(D-28)